Nano Today 26 (2019) 57–97

Contents lists available at ScienceDirect

Nano Today

journal homepage: www.elsevier.com/locate/nanotoday

Review

Recent progresses in graphene based bio-functional nanostructures for advanced biological and cellular interfaces

Chuanxiong Nie[a,b,1], Lang Ma[c,1], Shuang Li[d,*], Xin Fan[a], Ye Yang[a], Chong Cheng[a,b,*], Weifeng Zhao[a], Changsheng Zhao[a,e,*]

[a] College of Polymer Science and Engineering, State Key Laboratory of Polymer Materials Engineering, Sichuan University, Chengdu, 610065, China
[b] Department of Chemistry and Biochemistry, Freie Universität Berlin, Takustrasse 3, 14195, Berlin, Germany
[c] Department of Ultrasound, West China School of Medicine/West China Hospital, Sichuan University, Chengdu, 610041, China
[d] Functional Materials, Department of Chemistry, Technische Universität Berlin, Hardenbergstraße 40, 10623 Berlin, Germany
[e] National Engineering Research Center for Biomaterials, Sichuan University, Chengdu, 610064, China

ARTICLE INFO

Article history:
Received 6 December 2018
Received in revised form 2 March 2019
Accepted 18 March 2019
Available online 5 April 2019

Keywords:
Bio-functional nanostructures
Graphene composites
Biointeractions and biocompatibilities
Biological and cellular interfaces
Biomedical applications

ABSTRACT

Currently, abundant efforts have been devoted to research on graphene in interdisciplinary applications due to their unique physicochemical, electronic and biological properties. Accompanying the rapid developments of graphene, it is highly important to explore graphene based bio-functional nanostructures (G-BFNs) to bridge the gap between the fundamental advantages of graphene and the requirements in designing hybridized biomaterials. Here, this review aims to outline and summarize the recent advancements in fabricating G-BFNs for advanced biological and cellular interfaces. We first discuss the general protocols for the synthesis of G-BFNs, especially diverse facile and eco-friendly strategies. Then, we carefully summarize the current developed G-BFNs based on their nanostructures and biofunctionalities, such as physiologically-stability, stimuli-responsibility, graphene-inorganic nanohybrids, functional nano-inks, nacre-like layered composites, macroporous scaffolds, 3D printed microlattices, and injectable hydrogels. Moreover, biointeractions at the interfaces of G-BFNs with viruses, bacteria and stem cells, and the relevant biocompatibilities are also highlighted. Furthermore, the emerging applications and future perspectives of G-BFNs in nanotherapeutics, anti-pathogens, tissue regeneration, and monitoring biosensors are carefully discussed. We envision that such a timely and cutting-edge review will not only take a step towards the development of G-BFNs but also inspire new opportunities by using emerged nanomaterials for biological and cellular interfaces.

Contents

* Corresponding authors.
E-mail addresses: shuang.li@campus.tu-berlin.de (S. Li), chong.cheng@fu-berlin.de (C. Cheng), zhaochsh70@scu.edu.cn, zhaochsh70@163.com (C. Zhao).
[1] These two authors contributed equally to this article.

https://doi.org/10.1016/j.nantod.2019.03.003
1748-0132/

Introduction

Graphene, an atomic layered 2D nanomaterial in the broad family of carbon nanoallotropes [1], consists of sp^2-bonded carbon atoms [2,3], has become one of the most promising nano-platforms in the horizons of material, chemical, physical and biological science [4]. In addition to single- and multi-layer graphene, the family of graphene nanostructures (GNs) that has established broad biomedical applications includes graphene oxide (GO), reduced graphene oxide (RGO), graphene nanoribbons (GNRs), graphene quantum dots (GQDs), and corresponding organic molecular/inorganic compounds functionalized nanostructures [5,6]. Owing to the unique chemical structures and outstanding electrical, mechanical, optical, and thermal properties [7–10], recent rapid studies of diverse GNs have demonstrated their revolutionary roles in the energy [11–13], electronic [14–16], and environmental fields [17,18]; meanwhile, combining their atomic 2D morphology, high surface area, strong biomolecules and nano-biological interactions, the graphene and GNs have also established manifold new opportunities in diverse biomedical and biological applications, such as drug/gene delivery vehicles [19–23], photo-thermal treatment reagents [24–26], cellular and tissue imaging nanoagents [27,28], stem cell and tissue regeneration scaffolds [29,30], and monitoring biosensors [31,32].

Accompanying the rapid developments of graphene and GNs in diverse physical and chemical fields, it is of great importance to explore graphene based bio-functional nanostructures (G-BFNs) to bridge the gap between the fundamental advantages of graphene/GNs and the application requirements in designing advanced hybridized biomaterials. Meanwhile, bare graphene and GNs also exhibit potential adverse bioeffects and unsatisfied biointeractions at the biological and cellular interfaces, which may inhibit their biomedical applications [33–36]. By implementing biofunctional/bioactive molecules and nanomaterials, there are rapidly increased investigations on tailoring the interfacial characteristics of graphene and GNs [37–41]. Currently, researchers are able to allow the development of highly bio-adaptable G-BFNs to satisfy the requirements at biological and cellular interfaces, such as nano-sized carriers, physiologically-stable and biocompatible nanoagents, stimuli-responsive nano-bio-system, graphene-inorganic nanohybrids, functional nano-inks for bioelectronics, nacre-like layered composites, superstructures and macroporous composites, 3D printed porous microlattices, and 3D injectable hydrogels [30,42–45]. Notably, the bioinspired strategies to synthesize G-BFNs have received increased interests in recent years, such as mussel protein-inspired nanointerfacial decoration, nacre-like structures, biomineralization processes, and nanoenzyme systems [46–51].

In recent years, abundant studies and efforts have been dedicated to the exploration of highly bio-adaptable G-BFNs with diverse favorable biological and cellular characteristics, such as hazardous by-product free synthesis, “intelligent” nanosystem, and manipulative or programmable functionalities [5,52]. However, we have noticed that the current review articles for graphene and GNs in biological aspects are generally based on their biomedical applications, such as in drug/gene delivery, cancer nanotherapeutics, bioimaging, tissue engineering, and bioelectronics [8,53–61]; a featured and cutting-edge review article focuses on the biological and cellular interfaces of G-BFNs that covers the fabrications, achievements in functionalities, interfacial biointeractions, and future perspectives related to G-BFNs was still absent.

Here, we outline and summarize recent advancements in fabricating G-BFNs for advanced biological and cellular interfaces, as shown in Scheme 1. We first discuss the general protocols for the synthesis of G-BFNs, especially diverse facile and eco-friendly synthetic and decorating strategies. Then, we carefully summarize the current developed G-BFNs based on their nanostructures and biofunctionalities rather than the used materials for graphene

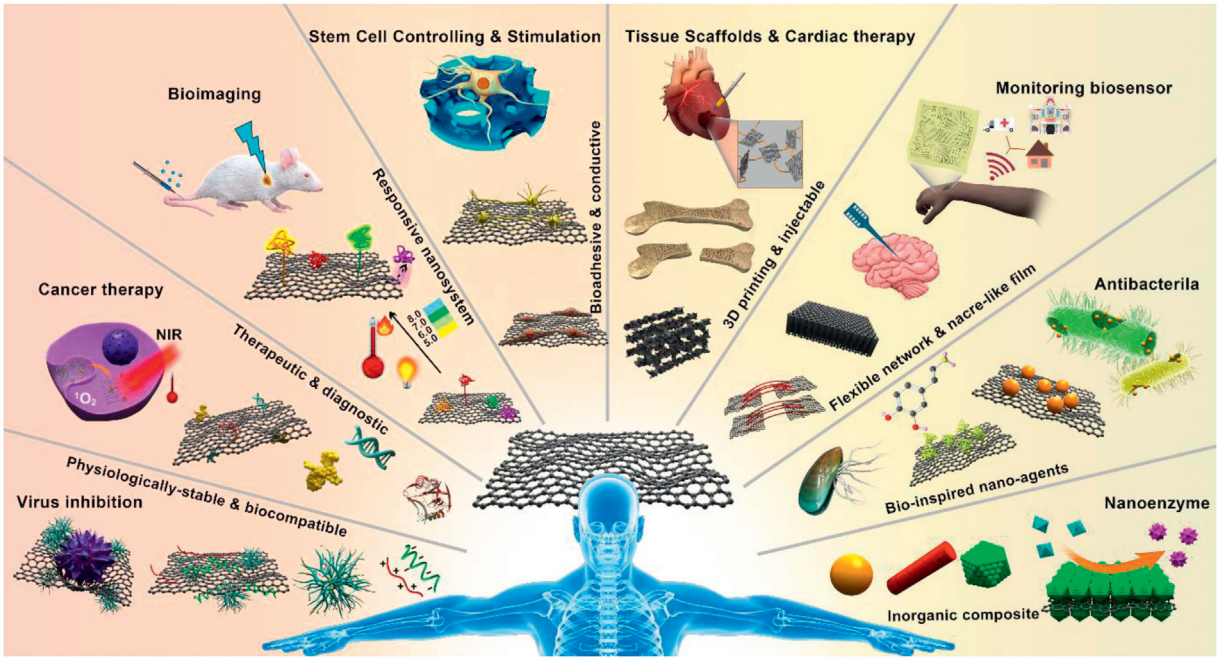

Scheme 1. Illustrations of the current advancements of bio-adaptable G-BFNs with diverse functional characteristics at the interfaces of G-BFNs for applications in nanomedicines, biocomposites, and biomedical devices.

functionalization. Moreover, biointeractions at the interfaces of G-BFNs with viruses, bacteria and stem cells, and the relevant biocompatibilities are also highlighted. Furthermore, the emerging applications and future perspectives on G-BFNs in nanotherapeutics, anti-pathogens, regenerative medicine, and monitoring biosensors are carefully discussed.

General protocols for fabrications and synthesis of G-BFNs

Graphene derivatives and G-BFNs from green synthetic methods

Subjected to size and surface functional groups, the family of graphene derivatives that has established broad biomedical applications for the fabrication of G-BFNs includes GO, RGO, GNRs and GQDs [1]. GO is the most frequently used graphene derivative and an ideal scaffold for the design of different G-BFNs for nanomedicines and biocomposites [5]. On one hand, GO can be reduced to RGO to achieve enhanced mechanical performance and electric conductivity [5]. Additionally, GO can also be cut into GNRs and GQDs; the former is a linear ribbon that has been made into semiconductors and field effect transistors due to its unique carrier mobility; and the latter consists of nano-sized quantum dots with excellent optical properties for bioimaging and phototherapies [8].

In general, GO is usually prepared by exfoliation of graphite via the Hummer's method using $KMnO_4$ as the oxidant [31]. However, it has shown clear drawbacks for large-scale biomedical usages, such as sophisticated purification and collection processes, for which a fraction of residual oxidants may cause severe cytotoxicity. Therefore, green approaches to produce GO have been pursued to produce more G-BFNs to fulfill the extensive needs of GNs in biological, clinical and human healthcare systems [31]. Recently, it was discovered that the K_2FeO_4 can serve as a strong yet green oxidant for the exfoliation of GO, as illustrated in Fig. 1a [62]. The intercalation, oxidation and exfoliation proceeded extremely rapidly, with 100% mono-layered GO being obtained within 1 h at room temperature. The side products from K_2FeO_4, K^+ and Fe^{3+}, could be easily removed by washing and centrifugation. The electrochemical exfoliation of GO, which employs electrons for graphite oxidation, has also been reported. In this process, the anodic electrocatalytic oxygen evolution reaction of water reacts with the carbon lattice of graphite, as shown in Fig. 1b [63]. Under optimized conditions, the productivity reaches 12 g/h, and the yielded GO shows similar chemical and mechanical properties to those of GO obtained using Hummer's methods.

Normally, RGO is obtained by the reduction of GO using hydrazine, dimethyl hydrazine, or $NaBH_4$ as reductive agents [5]. However, these chemical agents are usually highly toxic, and trace amounts will cause detrimental effects in humans; therefore, green reduction of GO by biomolecules is highly needed. In addition, reduction with biomolecules have another advantage, abundant biofunctional molecules would attach to the RGO surface simultaneously after chemical reduction, namely, "one-step" reduction and modification [64–66]. For example, gelatin, a polypeptide composed of multiple amino acids, can convert GO to RGO mildly and adhere to the RGO surface via hydrophobic interactions, yielding a stable RGO/gelatin dispersion for multiple biomedical applications [67]. The reductive sugars have also been used as capping and reductive agents to synthesize water-soluble RGO composites, such as glucose, fructose and sucrose [68]. GO-to-RGO conversion occurred by simply heating the mixture of GO/sugars; simultaneously, the sugars were oxidized and served as capping agents, resulting in water-soluble RGO/sugar composites. Other biomolecules, including vitamin C [64], serum proteins [65], tea polyphenols [69], cellulose [70] and natural plant extracts [66], have also been used for the synthesis of water-soluble RGO nanosheets through the "one-step" process. Being facile, low-cost and eco-friendly, these novel approaches have opened up new possibilities for the large-scale production of GO and RGO for G-BFNs.

Though, GO and RGO provide low-cost possibility for manufacturing G-BFNs on a large scale, the structures of GO and RGO consist of highly oxidized and disordered sp^3-bonded carbon layers, there will always be a large number of defects in the graphitic structure, thus leading to unsatisfied electrical conductivity to the G-BFNs [71]. Directly electrochemical exfoliation of graphite to produce slightly oxidized graphene has drawn abundant attention as a potential method to produce high quality graphene and

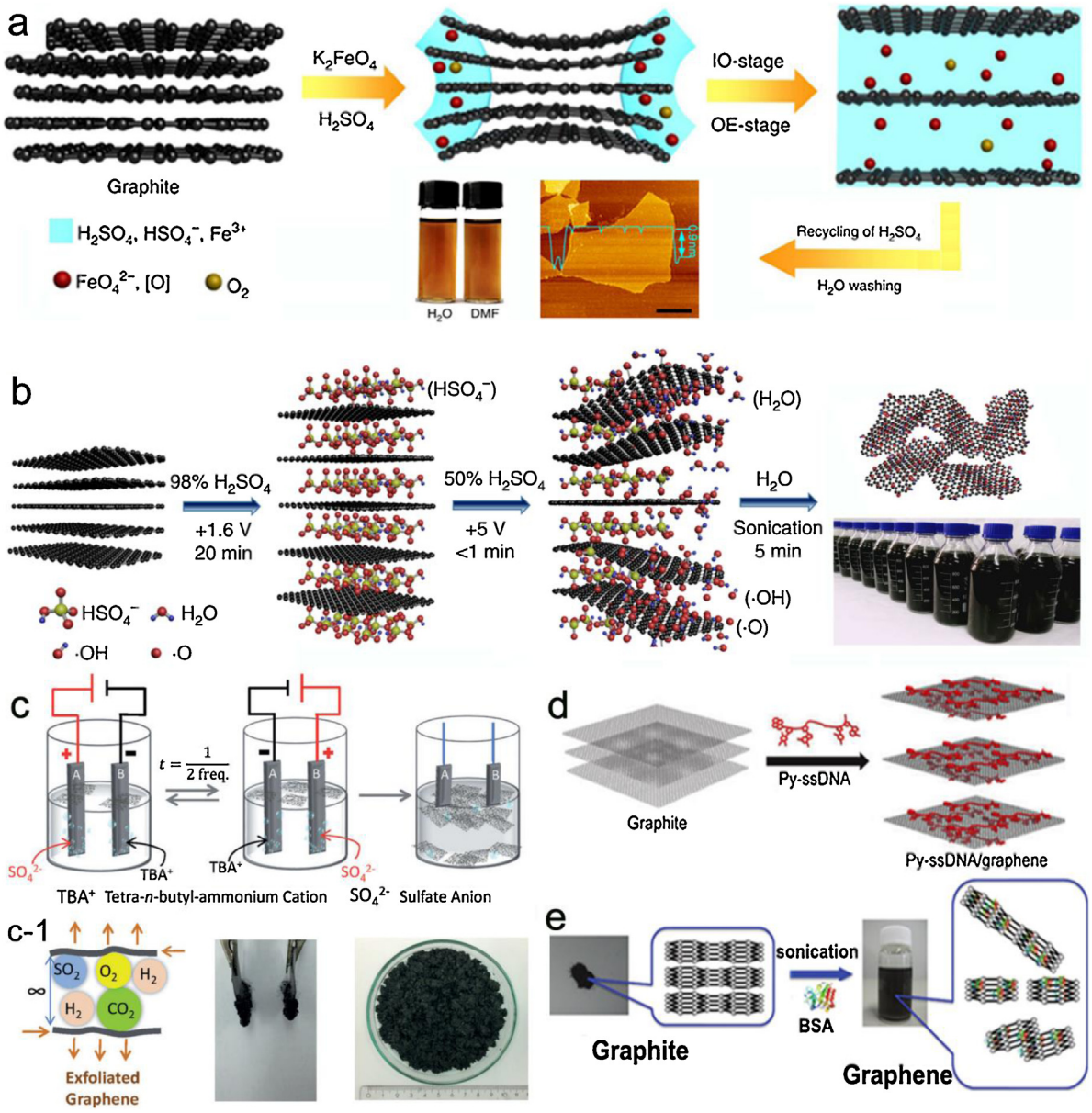

Fig. 1. (a) Synthesis of mono-layered GO by K_2FeO_4. Inserts show the dispersion of the GO in water and *N,N*-dimethylformamide (DMF) and a corresponding atomic force microscopy (AFM) image. Reproduced with permission [62]. Copyright 2015, Nature Publishing Group. (b) Synthesis of GO by water electrolytic oxidation. Reproduced with permission [63]. Copyright 2018, Nature Publishing Group. (c) Applying the alternating currents for exfoliation of graphite to produce graphene. (c-1) Mechanism for graphite exfoliation, the graphite foils after exfoliation and the electrochemically exfoliated graphene in 15 min. Reproduced with permission [73]. Copyright 2017, Wiley-VCH. (d) Schematics of the Py-ssDNA/graphene hybrid and AFM image. Reproduced with permission [74]. Copyright 2010, The Royal Society of Chemistry. (e) Pictures and schematic presentation of the exfoliation of a graphene nanosheet from BSA. Side view of the surface charge density of BSA-decorated graphene, in which white, gray, blue, and red balls represent H, C, N, and O atoms, respectively. Reproduced with permission [75]. Copyright 2015, The Royal Society of Chemistry.

conductive G-BFNs, especially for the fabrication of bioelectronics and biosensors. Generally, an aqueous or organic electrolyte is needed and an electrical current is applied to drive the structural expansion of graphite electrode [72]. Meanwhile, the whole process is typically performed under ambient and eco-friendly conditions. For instance, the butylammonium bisulfate ($TBA{\cdot}HSO_4$) aqueous solution has been proposed to act as conductive media to electrochemically exfoliate graphene with graphite foils as anode and cathode, as illustrated in Fig. 1c [73]. This exfoliation strategy showed high production yield of graphene nanosheets (about 75%, 1–3 layers, production rate exceeding 20 g h^{-1}, Fig. 1c-1), low defect density (the average C/O ratio is 21.2), good electronic conductivity (the hole mobility is 430 $cm^2\ V^{-1}\ s^{-1}$) and high solution-processability.

Besides the electrochemical exfoliation, mechanical exfoliation of graphite with exfoliator has also been developed to produce high quality graphene, GNs and G-BFNs, which utilizes shear force or ultrasonic waves to drive the intercalation and exfoliation of graphene [71]. Inspired by the dispersion of carbon nanotubes by pyrene, water-dispersible graphene sheets by direct exfoliation from graphite flakes using pyrene-labeled single-stranded deoxyribonucleic acid (Py-ssDNA) has been reported, as shown in Fig. 1d. The energy of tightly bound graphene layers was overcome by the strong π-π interaction between the graphene surface and pyrene moieties [74]. Similarly, graphite has also been exfoliated to produce stable aqueous graphene dispersions via sonication in bovine serum albumin (BSA) solution (Fig. 1e) [75].

In summary, compared with the conventional Hummer's method that needs a lot of efforts to remove the residual toxic oxidants, these green approaches significantly reduce or avoid the usage of toxic substances. Meanwhile, many of these green approaches provide G-BFNs with much better conductivity and fine sp^2 graphitic structures than GO produced by Hummer's method. For the disadvantages of these green methods, both the K_2FeO_4 oxidant and electrolytic oxidation of GO require the H_2SO_4, meanwhile, the loss of conductivity is also inevitable. For the mechanical exfoliation of graphite with exfoliator, the low yield ratio, large energy consumption, and unstable quality control limit its large-scale production. Compared with the above green methods, the electrochemical exfoliation of graphite foil/rod by using alternating currents in aqueous or organic electrolyte shows more promising potential to provide high quality graphene and G-BFNs in large scale, but the adaptability for applications in biomedical and biological fields should be carefully evaluated before a conclusion can be made.

Ultra-small G-BFNs from nanographene and graphene quantum dots

It has been widely demonstrated that the GO, RGO and G-BFNs can induce very strong interactions with biological and human systems, thus may cause severe *in vivo* toxicity by damaging cellular membranes and generating reactive oxygen species [31]. Meanwhile, for cancer therapy and diagnostic fields, it always requests the G-BFNs to exhibit with low toxicity towards health cells, high tumor cells uptake, high tumor accumulation and slow clearance [31]. Nanotherapeutics with high tumor cell uptake will show better tumor cell ablation capability than the one with lower uptake efficiency because most of the therapeutic molecules requires the entry of cells to achieve their functions. Meanwhile, the nanomedicines will be cleared by the immune system or accumulated in renal/spleen/liver during the circulation in body, therefore, to increase the treatment efficiency, nanomedicines with high tumor accumulation and slow clearance are considered to be better than the opposite ones [8,31]. For the G-BFNs, it has been revealed that nanosized G-BFNs are less cut-off by the spleen and liver during the circulation and more accumulated into tumor tissues due to the enhance penetration and retention (EPR) effects [76].

As a good example, ultra-small nanographene and NGO with a size smaller than 100 nm have been developed. NGO was initially obtained by isolation from GO solutions via density gradient ultracentrifugation or pH-assisted sedimentation [77,78]. The former method takes advantage of the weight differentiation of large and small GO, while the latter makes use of the ability of NGO to exhibit more negative charges than large GO due to the over-oxidation. However, the isolated yield is not sufficient for large-scale usage, and NGO production by further oxidation of GO and repeated sonication has been reported, as shown in Fig. 2a [79–82]. Additional oxidation can break large GO into small pieces, cause cracks in the GO surface, and then rip the cracked GO via powerful sonication. Scalable production of NGO (10 nm–100 nm) has already been obtained with a quite even size distribution using this method. Recently, "Bottom up" synthesis of nanographene was reported as a straightforward strategy to prepare nanographene with tunable sizes, shapes, and functionalities. In their study, hexabenzocoronene, a polycyclic aromatic hydrocarbon, was used as a precursor, which was then crosslinked to form a planar or warped nanographene sheet [83].

In addition to the decreased toxicity and enhanced cellular uptakes, NGO shows several other advantages over GO. The bare NGO, polyethylene glycol (PEG) anchored reduced NGO (RNGO-PEG), shows lower accumulation in organs, especially in liver and spleen, but higher tumor accumulation than GO, as shown in Fig. 2b-d [76]. This phenomenon is attributed to passive tumor targeting through EPR effects of nanoscaled particles [81,82]. Due to the decreased nanosheet size, the exposed surface area increased, thus showing more binding sites for diverse molecules, including but not limited to genes, peptides, proteins and aromatic drugs. Hence, it has been found that NGO can deliver cargo more efficiently than large GO, making it a more favorable drug delivery carrier [31].

When graphite or graphene were cut into sizes smaller than 20 nm, GQDs could be produced. Due to their ultra-small size, they are also characterized as 0D nanoparticles and exhibit unique quantum confinement and edge effects among the graphene family [84,85]. To date, GQDs are obtained by cutting graphene, GO, carbon black, carbon nanotubes using chemical ablation, electrochemical oxidation, and oxygen plasma treatment [86]. In biomedical areas, GQDs are regarded as emerging bioimaging agents due to their good stability, high quantum yields and low toxicity, as shown in Fig. 2e-g [87]. Since there are already a number of review articles discussing the preparation, properties, functionalization and biological interaction of GQDs [57,82,86,88], we will not focus on discussing the synthesis of biofunctional GQDs; however, some representative GQD-based biomedical nano-platforms will be discussed together with the other G-BFNs.

Chemical approaches to functionalize graphene and GNs

In general, the preparation of G-BFNs from graphene and GNs can be mainly classified as either non-covalent or covalent approaches, as summarized in Table 1. Non-covalent functionalization strategies can avoid complicated reaction processes, most of which can be performed under mild conditions; because no covalent bond is introduced, the functionalized graphene or GNs will maintain a well-ordered 2D structure. However, for biomedical usage, the G-BFNs usually directly contact the biological systems, and in such cases, a gradual leakage of molecules into the physiological fluids will occur for non-covalently prepared G-BFNs [71]. Therefore, covalent approaches are preferred for long-term usages. Furthermore, in biomedical areas, the use of toxic chemical reagents should be controlled, especially when preparing nanomedicine for *in vivo* usage, such as drug delivery vehicles and *in vivo* bio-imaging agents [31]. Even a fraction of residual toxic reagents can cause severe consequences, and hence purification must be carried carefully to ensure the purity of the products. Therefore, some efficient functionalization methods performed in harsh conditions and utilizing toxic molecules would not be suitable for biomedical applications [5].

π-π Stacking and hydrophobic interactions

Graphene is a sp^2 carbon-based π-system and is able to stack other kind of molecules via π-interactions, such as H-π interactions, cation-π interactions, π-π interactions and π_{cation}-π interactions [71]. The effects of the bonding valency of π-π interactions in fullerene/graphene nanocomposites have been studied, a clear multivalent effect of the pyrene units in the tripodal systems can be noticed, as shown in Fig. 3**a** [139]. Furthermore, it has also been found that GQDs can serve as efficient stabilizer for graphene via π-π interactions (Fig. 3b, b-1) with good stability for at least 3 months [140]. Via the strong π-π stacking between the graphene basal plane and other aromatic systems, G-BFNs could be facilely synthesized, including nanocarries, self-standing films, and 3D porous scaffolds, which have been discussed in the following sections in detail [8,71].

Hydrophobic interaction is another popular approach for the non-covalent modification of graphene nanomaterials. Many amphiphilic functional molecules had been designed for the modification of graphene and GNs through hydrophobic interactions

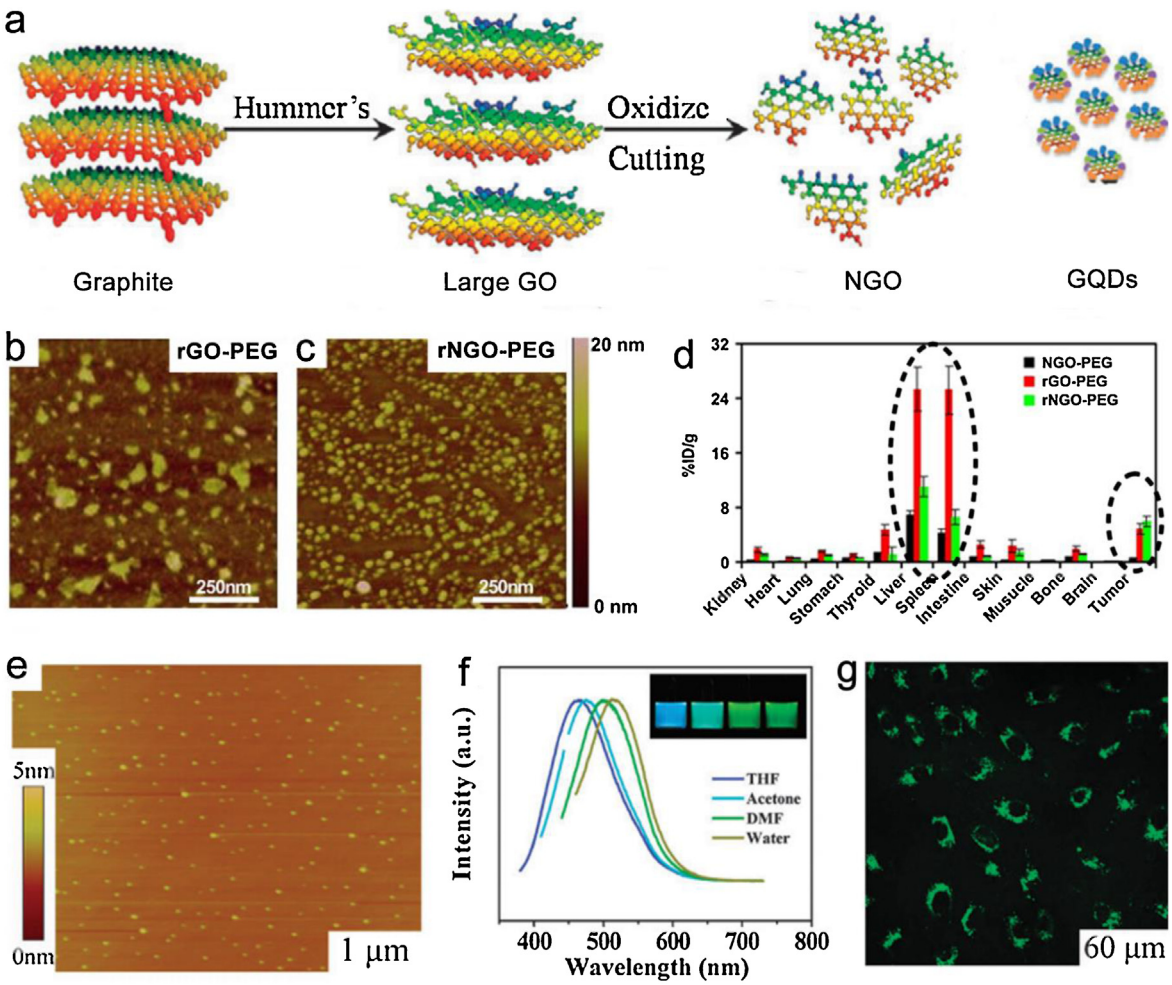

Fig. 2. (a) Synthesis of NGO and GQDs by further oxidation and cutting of large GO. Reproduced with permission. [82] Copyright 2012, The Royal Society of Chemistry. (b, c) AFM images of PEG-anchored RGO (RGO-PEG) and reduced NGO-PEG (RNGO-PEG), respectively. (d) Tissue accumulation of NGO-PEG, RGO-PEG and RNGO-PEG, which indicates that smaller nanosheets have lower accumulation in liver and spleen but higher accumulation in tumors. Reproduced with permission. [76] Copyright 2012, Elsevier Ltd. (e) AFM image of GQDs. (f) Fluorescence of GQDs in tetrahydrofuran (THF), acetone, DMF and water. (g) Imaging of MG-63 cells by GQDs under 405 nm excitation. Reproduced with permission [87]. Copyright 2011, The Royal Society of Chemistry.

[91,141–144]. Poly (propylene oxide) (PPO)-poly (ethylene oxide) (PEO) is a commercially available amphiphilic triblock copolymer and it will form heterogeneous micelles in aqueous solution. In presence of GO, the PPO segment of the block copolymer strongly interacted with the hydrophobic basal plane of GO, thus leading to the attachment of micelles on graphene surface (Fig. 3c, c-1) [145].

Another representative example is surface decoration by biopolymers. Proteins, for instance bovine serum albumin (BSA), could stably adhere on the amphiphilic surface of GO, producing stable graphene dispersions in various biological solutions [65]. Due to the good biocompatibility and abundant sources of the cellulose nanofibers (CNFs), there is an increasing interest to develop CNFs functionalized G-BFNs. Tsukruk's group has reported to utilize the amphiphilicity-driven assembly method to fabricate CNFs decorated unique "hairy" 2D GO nanostructures (Fig. 3d, d-1) [146]. These hairy GO/CNFs nanomaterials constructed membrane composites showed dense interlocked hybrid morphology with excellent mechanical properties and enhanced water transport capability.

Electrostatic interactions and hydrogen bonding

GO is covered with functional hydroxyl, carboxyl and epoxy moieties. These surface groups offer active sites for post-functionalization and the conjugation with molecules through electrostatic interactions has been developed and recognized as an easy and feasible approach for GO modification. Cationic polyelectrolytes, such as protein [65], chitosan [148,149], polyamidoamine [150], and PEI [43], are good candidates to decorate the GO surface and form complexes that are highly stable in physiological solutions, which have also been discussed in the following sections [151]. For hydrogen bonding, there are both donors (oxygenic groups) and acceptors (hydrogen) on the surface of GO. Due to this unique nature, when mixing GO with polymers, an intense hydrogen bond network will form, yielding highly stable GO/polymer composites [152,153]. The gelatin and PVA based dual polymer network has been used to construct the GO reinforced biocomposites and tissue scaffolds, it was proposed that the three components interacted mainly through electrostatic interactions, hydrogen bonding, and ester bonding (Fig. 3e).

It should be noticed that the hydrophobic graphene and amphiphilic GO usually exhibited different interactions [146]. It was found that for the GO nanosheets with different oxygen contents, from 41% to 21%, the amount of decorated CNFs surrounding GO nanosheets decreased along with the increased hydrophilicity (Fig. 4a). The all-atom molecular dynamics (MD) simulations reveal that CNFs generate strong hydrophobic interactions with pristine graphene and GO with low oxidation degree; whereas, CNFs show

Table 1
Representative synthetic methods to fabricate the G-BFNs via different protocols. Due to the similarity on chemical structures, many of the methods presented in the table are universal for the functionalization of both graphene and graphene derivatives.

Substrate	Synthetic Methods	Functional molecules	Notable findings	Ref.
GO	π–π stacking, hydrophobic interactions.	BSA, heparin, gelatin, cellulose etc.	1 Increased solubility in biological solutions. 2 Increased biocompatibility. 3 Increased affinity towards cells and tissues. 4 Possibility of post functionalization.	[89,90,91,92,93]
GO	π–π stacking, hydrophobic interactions.	DNA	1 Increased water solubility and biocompatibility. 2 Formation of 3D network. 3 Recognizing specific DNA sequences. 4 Responsive towards stimuli.	[94,95,96,97,98]
GO, RGO	π–π stacking, hydrophobic interactions.	Enzymes	1 Maintained and even enhanced catalytic activity of enzymes. 2 Loading of multiple enzymes in one graphene nanosheet.	[99,100,101,102,103]
GO	Electrostatic interaction, hydrogen bonding, covalent bonding.	Chitosan	1 Versatile processability to nanosheets, films and hydrogels. 2 Loading and delivery of genes. 3 Promoting cell growth. 4 Inhibiting and killing of bacteria.	[104,105,106,107]
GO, RGO	π–π stacking, hydrophobic interactions, covalent bonding.	PEG	1 Significantly increased stability in biological solutions. 2 Minimized interaction with biological systems. 3 Capability in loading drugs. 4 Established various biomedical applications.	[81,108,109]
Graphene, GNRs	π–π stacking, hydrophobic interactions,	Porphyrin	1 Excellent electrocatalysis 2 Can detect glucose in human serum 3 Detect adenosine triphosphate	[110,111,112]
GO	Covalent bonding	Polyglycerol (PG)	1 Tunable cell interactions for different charges and sizes. 2 Guiding stem cell differentiation. 3 Interaction and inhibition to virus.	[44,113,114,115]
GO	Electrostatic interaction, hydrogen bonding, covalent bonding	Polyethylenimine (PEI), polyamidoamine etc.	1 Increased stability in biological solutions. 2 Delivery of genes. 3 Inhibiting and killing of bacteria.	[116,117,118]
GO	Covalent bonding, *in situ* polymerization & crosslinking	Poly (N-isopropylacrylamide) (PNIPAM), Pluronic etc.	Change of water solubility in response to heat.	[119,120,121,122]
GO, RGO, GQDs	Mussel inspired coating	Dopamine (DA) and DA grafted polymers	1 Green, facile and stable binding to GO. 2 Platform for further bonding with functional molecules and nanoparticles. 3 Versatile processablity to nanoplatelets, films/papers and 3D networks.	[50,92,93,123,124,125,126]
GO, RGO	*In situ* growth	Hydroxyapatite (HAp), $CaCO_3$, strontium etc.	1 Stable binding. 2 Promoting osteoblast proliferation and differentiation. 3 Biopolymers enhanced interaction with osteoblast.	[127,128,129,130,131]
GO	*In situ* growth	Au, Pt, Pd, Fe_3O_4, CdS, Cu etc.	1 Artificial enzymes with higher catalytic activity than peroxidase. 2 Synergistically photothermal and photodynamic activities.	[132,133,134,135]
Graphene, RGO	*In situ* growth	Au, Pt, Pd, Fe_3O_4, etc.	1 Catalytic peroxidase-like activity. 2 Electrochemical biosensing for H_2O_2, glucose and acetylcholine.	[136,137,138]

low interaction with highly oxidized GO surface (Fig. 4 b). Furthermore, they find that when the surface oxidation degree exceeds 20%, Fig. 4c, d, the interfacial non-bonded energy and hydrogen bonds between CNFs and GO surfaces decrease significantly. It is supposed that the decrease of hydrophobic interactions between CNFs and GO with higher oxidation degree will inhibit the formation of strong non-bonded interactions and hydrogen bonds with GO surface [146]. While, compared to the slightly oxidized GO (21.2%), CNFs show lower decoration coverage on the surface of pristine graphene due to the lack of interfacial hydrogen bonds (Fig. 4d). These findings demonstrate that it is possible to control the interfacial hydrophobic–hydrophilic interactions to realize fully or partially decorate graphene or GO surface by carefully tailoring their surface chemistry and amphiphilicity.

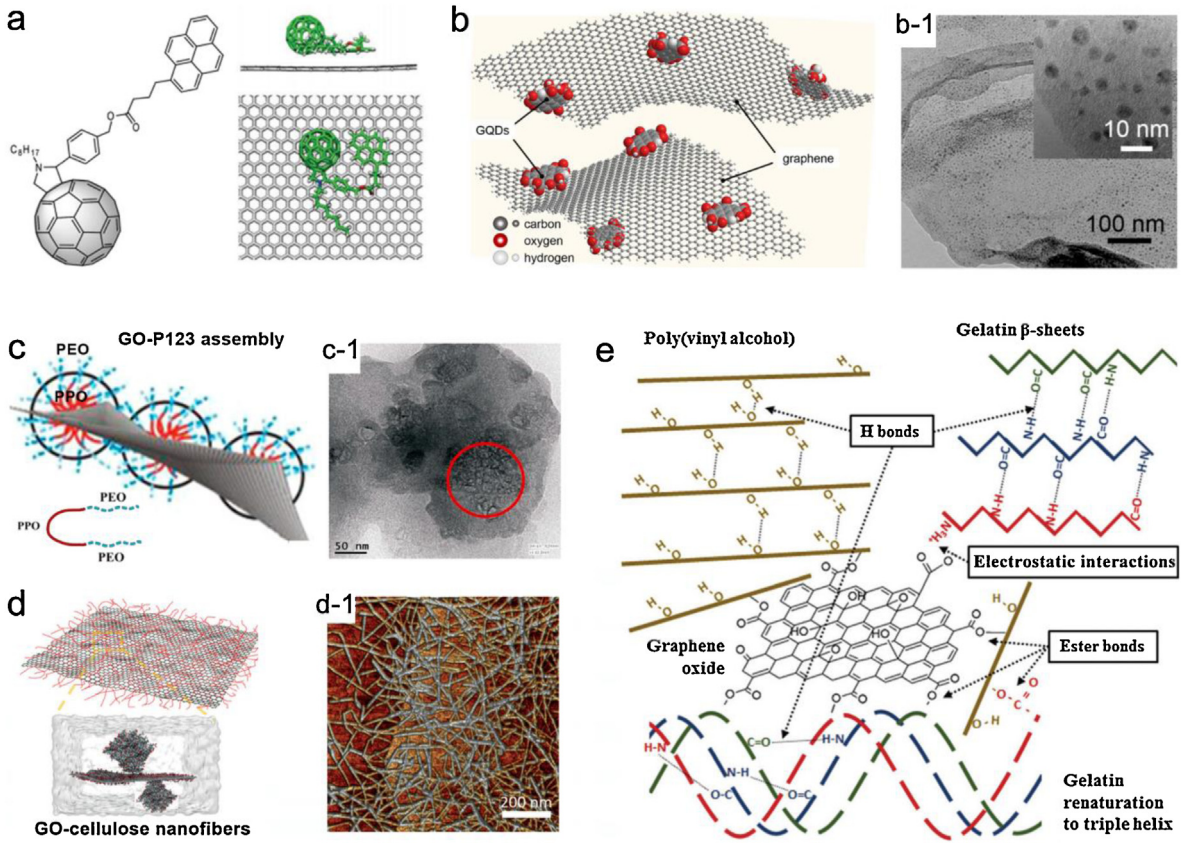

Fig. 3. (a) C_{60} derivatives with mono-pyrene unit and the side and top views of the supramolecular assembly of the graphene interface. Reproduced with permission. [139] Copyright 2017, The Royal Society of Chemistry. (b) GQDs stabilize graphene via π-π interactions in water. (b-1) Transmission electron microscopy (TEM) and the high-resolution TEM images of GQDs dispersed graphene, GQD distribution on wrinkled graphene sheets can be observed. Reproduced with permission [140]. Copyright 2015, American Chemical Society. (c) Structure of formed PPO-PEO micelle (Pluronic P123), on GO surface. (c-1) TEM images of GO-5 wt % PPO-PEO micelle, pointed by the red circle. Reproduced with permission. [145] Copyright 2015, American Chemical Society. (d) Amphiphilic CNFs induced assembly and coating with graphene nanosheets. (d-1) AFM image of the assembled GO/CNFs nanosheets. Reproduced with permission [146]. Copyright 2018, Wiley-VCH. (e) Schematic image of the proposed interactions between gelatin-poly(vinyl alcohol) (PVA) and GO nanosheets. Reproduced with permission [147]. Copyright 2016, The Royal Society of Chemistry.

In situ *grafting, polymerization and crosslinking grafting, polymerization and crosslinking*

The abundant oxygen groups on the GO surface provide versatile active sites for covalent functionalization by amidation and esterification of carboxyl groups with amino or hydroxyl molecules. In the presence of dehydration agents, the reaction can proceed at a high rate and without side products [154]. In this approach, to achieve a high grafting yield, chloroacetic acid or di-anhydrides can be used to turn hydroxyl groups into additional carboxyl groups for functionalization [71]. Until now, various molecules such as PEG [78], PVA [155], PEI [156], polyaminoacid [157], and chitosan [158] have been attached to the GO surface via covalent bonding with oxygen groups. For instance, Ma group have synthesized the PEG, BSA and PEI functionalized GO via *in situ* grafting methods (PEG and PEI) and hydrophobic interaction (BSA) to yield different surface zeta potential and coating thickness for the investigation of cellular behaviors (Fig. 5a-c) [159].

in situ polymerization is an attractive strategy to modify GNs with functional polymer brushes. In the pool of grafting polymerizations, surface-initiated atom transfer radical polymerization (SI-ATRP) has attracted the most attention and represents the majority of the studies reported [160]. The polymerization is initiated by a pre-grafted halogen, preferably bromide, and it is well controlled by the equilibrium between active propagating species and dormant chains [160]. It has been reported that well-defined polymer brushes (styrene, butyl acrylate, methyl methacrylate, and NIPAM) can be introduced onto the graphene surface by SI-ATRP, as shown in Fig. 5d [161].

Free-radical addition and cycloaddition

The addition reaction to the π-system of graphene can occur at the surface and/or the edges [71]. Free-radical addition is a widely studied approach for the fast functionalization of GNs [164,165]. In a universal example of free-radical addition, the polymer brushes (styrene, glycidyl methacrylate, hydroxyethylmethacrylate, and others) have been grafted onto graphene by free-radical polymerization, as shown in Fig. 5e [162]. After the initiation of vinyl monomers, macromolecular radicals were produced immediately by chain propagation and then added to the C=C bonds of GO, producing polymer brushes and simultaneously generating new radicals at the GO surface. AFM images revealed that abundant protuberances of the grafted polymers were distributed evenly over the entire sheet (Fig. 5f).

In addition to vinyl monomer radicals, the grafting of aryl group to the sp^2 carbon network by diazonium salts can also work. Tour and co-workers have successfully functionalized graphene with nitrobenzene, chlorobenzene, bromobenzene and methoxybenzene [166]. Furthermore, the [2+1] cycloaddition can also occur on the π-system of graphene. Nitrene, an analogue of carbene, is used to introduce the aziridine adduct to the carbon network [167]. Recently, a [2+1] nitrene cycloaddition reaction at ambient conditions has been proposed to functionalize RGO with reactive triazine groups, as shown in Fig. 5g, h. The beauty of this study was that the obtained TRGO-Trz could be used for the post-linkage of many other biofunctional molecules very efficiently, such as $_{L}$- and $_{D}$-cysteine, hyperbranched PG polymer (HPG), dyes, and **gold** nanoparticles, making

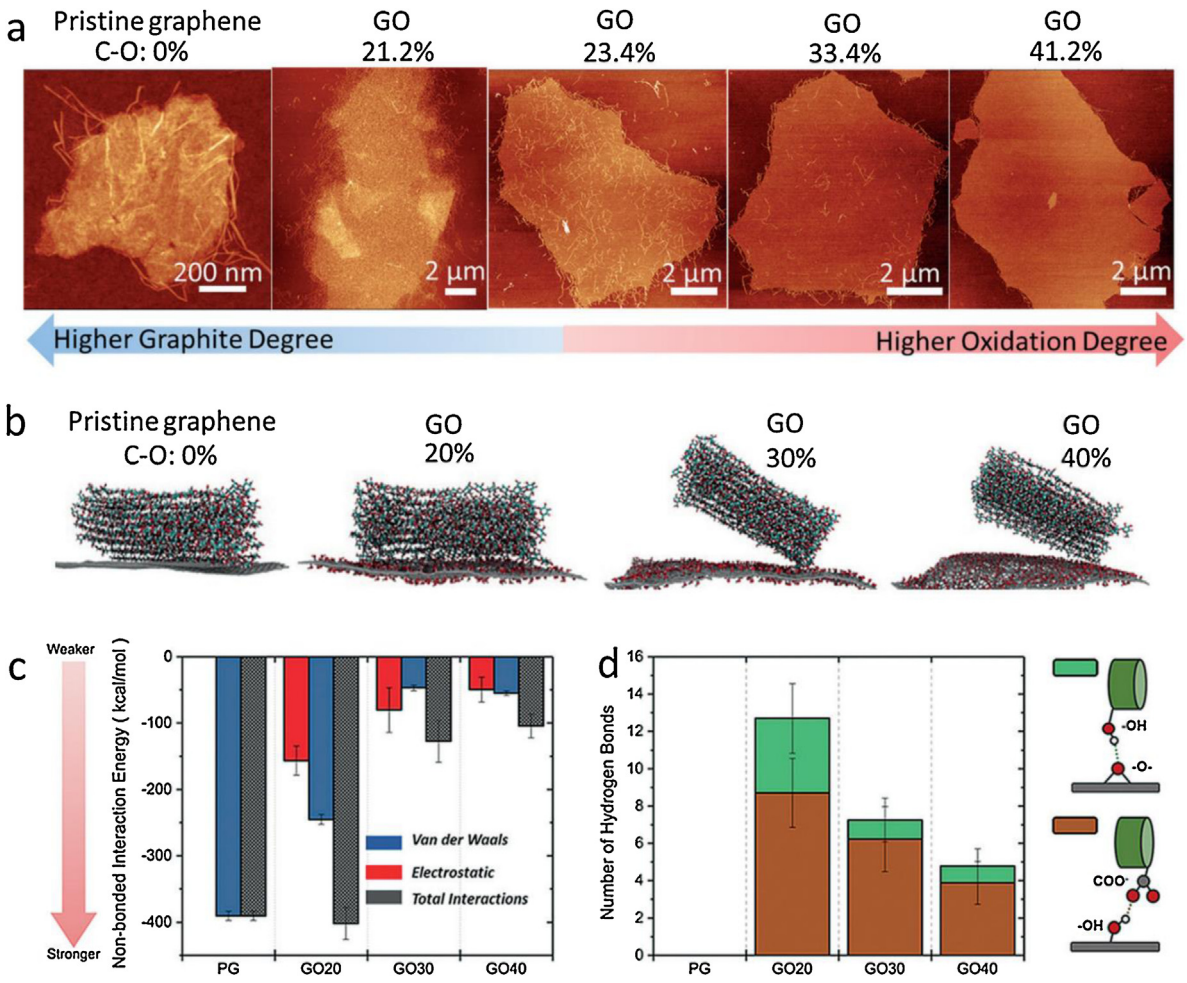

Fig. 4. (a) AFM images of CNFs decorated graphene and GO with different oxidation degrees. (b) All-atom MD simulations for the CNFs decoration processes and interactions with graphene and GO. (c) The non-bonded interactions (van der Waals, electrostatic), and the (d) hydrogen bonds between CNFs and graphene/GO obtained from the MD simulation results (PG = pristine graphene). Reproduced with permission. [146] Copyright 2018, Wiley-VCH.

this protocol highly adaptable to diverse biological applications [163].

Bioinspired coating and in situ *growth for nanointerfacial functionalization growth for nanointerfacial functionalization*

Mussel adheres to virtually all types of materials by using the byssus as an anchor. Inspired by the two most important groups in byssus protein of mussel, catechol and amine, DA has been successfully used as an efficient precursor for universal coating [168–170]. These mussel-inspired coating with GN are carried out in aqueous conditions at room temperature and produce no by-product [93]. Additionally, the anchored PDA layer can be post-functionalized due to the versatile chemical reactivity of the catechol groups, which can react with amino and thiol groups via a Michael addition/Schiff base reaction process, as well as with carboxyl groups via condensation and conjugation to metal particles, as shown in Fig. 6a, b [92,130,171,172].

Benefited from the advantages of PDA coating, functional biopolymers (heparin and BSA) have been successfully anchored onto PDA-coated GO and RGO (Fig. 6a) [92]. Very recently, after integration with hydrophobic moieties (provide with hydrophobic interactions), a hand-shake-based RGO-dispersing agent was developed, as shown in Fig. 6c, c-1. The adhesive linear PG polymer (LPG) could rapidly and evenly attached to the RGO surface (Fig. 6c-2), and the anchored azide group further allowed post functionalization of a broad range of functional molecules [173]. Currently, it has been demonstrated that the DA-decorated GNs have been successfully applied to serve as functional and bioactive G-BFNs for diverse biological applications, such as cancer therapy [125], antibacterial nanoagents [48,174,175], nacre-like film [50], light-triggered self-moving devices [123], stem cell engineering [176], and bioimaging [124].

Graphene/metal nanoparticle composites can be facilely fabricated by *in situ* reduction of metallic ions (Ag^{+}, Au^{3+}, etc.) [8]. The GO and RGO sheets have also been incorporated into the crystals of calcium carbonate and calcium phosphate, as shown in Fig. 6d [127]. By bubbling CO_2 gas into the mixture of GO/Ca^{2+}, spherical $CaCO_3$ microspheres that were wrapped and interconnected by the GO network were prepared (Fig. 6e). After being incubated in simulated body fluid, the hybrid spheres were transformed to graphene-incorporated HAp hybrid crystals (Fig. 6f) [127]. By controlling the density of functional groups on the GO surface, the density and size of the nanoparticles could be tuned [177]. Other graphene/metal oxide (graphene/ZnO, graphene/TiO_2, graphene/Fe_3O_4, and graphene/SnO_2, etc.) and graphene/inorganic quantum dots have also been prepared via similar *in situ* growth approaches [8,14,178].

To achieve a maximum loading ratio of nanoparticles and increase the biocompatibility of the graphene/nanoparticle hybrids, GNs are usually pre-functionalized with additional biomolecules [8]. It was revealed that BSA could be utilized to conjugate metal nanoparticles and form GO/nanoparticle nanohybrids

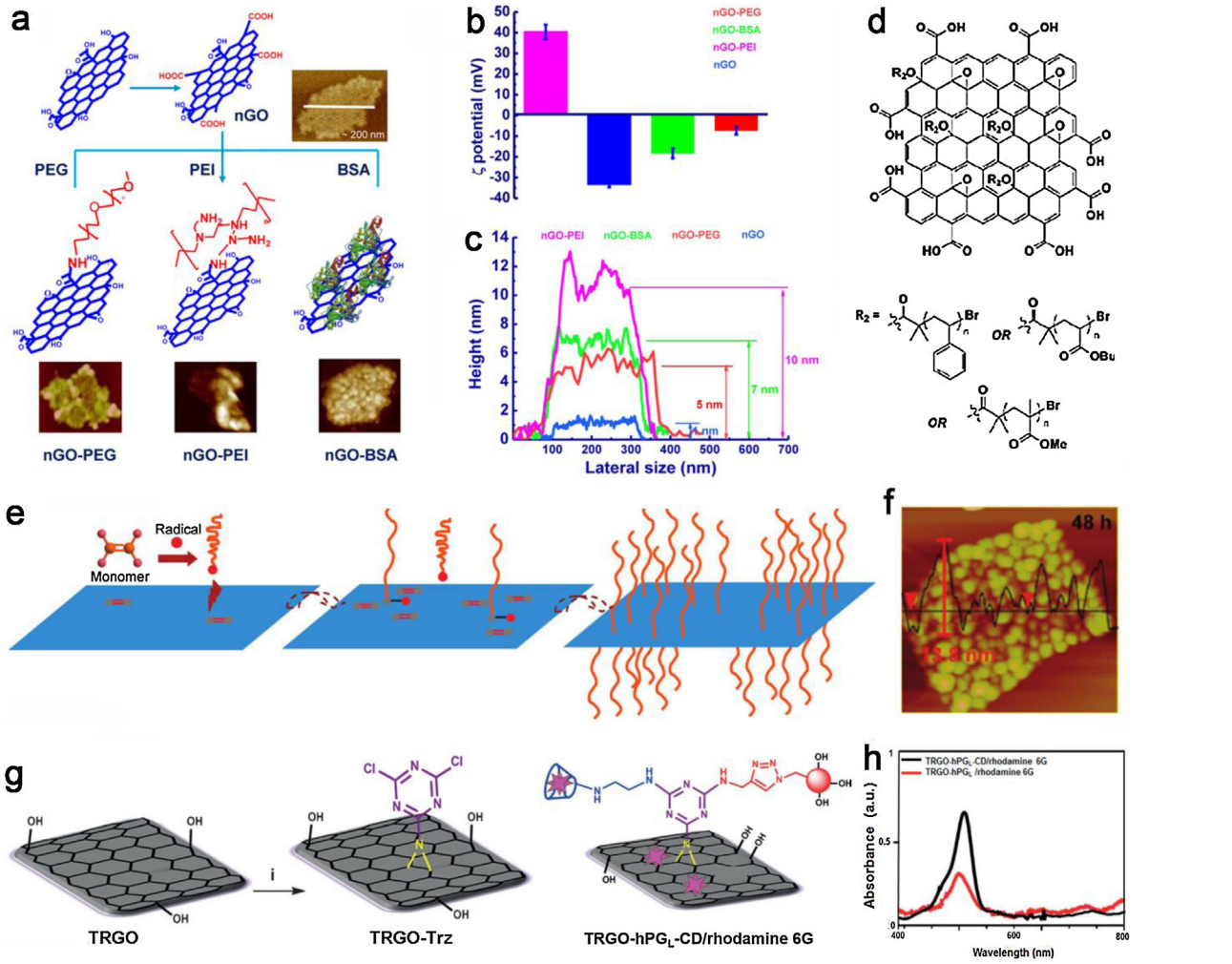

Fig. 5. (a) Schematic image for the grafting and decoration of GO with PEG, PEI and BSA. (b) Zeta potential and (c) surface height profiles for the polymers decorated GO complexes. Reproduced with permission. [159] Copyright 2015, American Chemical Society. (d) Schematic presentation of SI-ATRP on the graphene surface. Reproduced with permission [161]. Copyright 2010, Wiley-VCH. (e) Illustration of free-radical polymer addition to graphene. (f) AFM images of the polymer-grafted GO after 48 h of free-radical reaction. Reproduced with permission [162]. Copyright 2011, American Chemical Society. (g) Nitrene [2 + 1] cycloaddition reaction to functionalize thermal reduced GO (TRGO) and the synthesis of TRGO-hPG$_L$/rhodamine 6 G. (h) UV spectra of TRGO-hPG$_L$/rhodamine 6 G and TRGO-hPG$_L$-CD/rhodamine 6 G. Reproduced with permission. [163] Copyright 2017, Wiley-VCH.

(GO/Au, GO/Ag, GO/Pt, and GO/Pd) [65]. The carrageenan-decorated GO-based biocomposites have been synthesized and used for scaffolds in bone cell-induced HAp mineralization [131]. Furthermore, via mussel-inspired adhesives, biofunctional inorganic nanoparticles can also be loaded on the graphene surface. Owing to the strong interaction with metal ions, the PDA layer resulting from DA polymerization can absorb metal ions and reduce them into metal nanoparticles [93]. The mussel-inspired coating has been utilized to prepare GO-nanoparticles via *in situ* nucleation and growth of noble metals, metal oxides and semiconducting nanoparticles without any hazardous chemicals or additional reduced agents [130].

Current horizons of G-BFNs: structures, chemistries, and functionalities

Physiologically-stable & biocompatible nanoagents

For biomedical usage of nanoagents, the physiologically-stability and biocompatibility with biological systems should be seriously considered. The bare graphene and RGO usually show poor stability and dispersibility in aqueous condition, which makes them difficult to be utilized in biological applications. While, for the water-dispersible oxidized-GNs, such as GO, NGO, and GQD, as a result of the unique amphiphilic sp^2 carbon structures, when exposed to physiological media, various biomolecules will be adsorbed onto their surface, especially proteins and DNA [179], which may cause undesired biointeractions and immunological reactions. Therefore, proper surface decoration with hydrophilic and bioactive polymers is quite necessary for both graphene and diverse GNs. As shown in Fig. 7a, the BSA and heparin functionalized RGO show much increased physiologically-stability, it has also been demonstrated that their biocompatibilities and bioactivities are also significantly improved and tuned after anchoring of biopolymers [92].

Among various kinds of hydrophilic polymers, PEG, a clinically approved polymer for biomedical use, has demonstrated excellent antifouling and long-circulating properties [180]. PEG functionalized NGO (NGO-PEG) is highly dispersible and stable in water and several aquatic biological solutions and shows greatly increased biocompatibility compared with bare GO (Fig. 7b and 7b-1), meanwhile, the functionalized NGO-PEG exhibits uniform and nano-sized morphology (Fig. 7b-2) [154]. By now, PEG decorated GNs have been well established in various biological applications, including drug delivery, photothermal therapy (PTT) and bioimag-

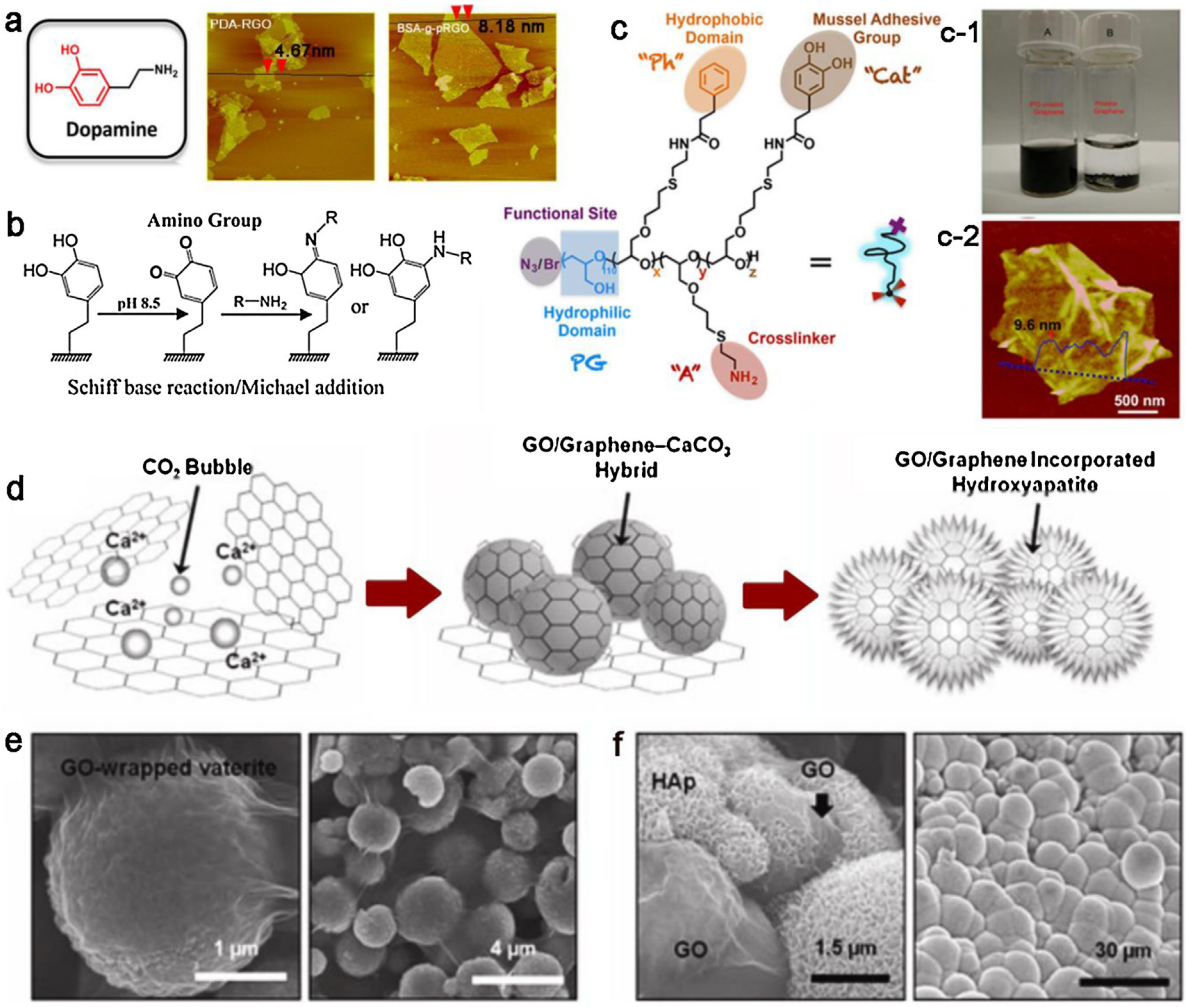

Fig. 6. (a) Structure of DA and AFM images for the products of PDA modified RGO with heparin and BSA biomolecules (Hep-g-pRGO and BSA-g-pRGO). Reproduced with permission. [92] Copyright 2013, The Royal Society of Chemistry. (b) Schematic illustration of the Michael addition/Schiff base reaction process with PDA or DA moieties. Reproduced with permission [172]. Copyright 2010, American Chemical Society. (c) Hand-shaking water-soluble graphene dispersion via the novel DA and benzene grafted LPG. (c-1) The photo image for the dispersed graphene solution and (c-2) the representative AFM image for the LPG decorated graphene nanosheets. Reproduced with permission. [173] Copyright 2017, American Chemical Society. (d) Illustration of GO-$CaCO_3$ and GO-HAp hybrid nanomaterials. The scanning electron microscope (SEM) image for the GO-$CaCO_3$ (e) and GO-HAp (f) nanohybrids. Reproduced with permission. [127] Copyright 2011, Wiley-VCH.

ing [108]. On the other hand, PG analogues, including LPG and HPG, have also been synthesized and recognized as a substitutional hydrophilic and antifouling polymer to PEG for biomedical usage due to their unique multivalent interaction properties [181].

Besides the non-charged hydrophilic molecules, a large number of charged molecules have also been utilized for the functionalization of graphene and GNs, such as the negative charged, zwitterionic, and cationic molecules and polymers [7]. By applying the free-radical polymerization, the sulfonated polymer as a heparin-mimetic brushes have been grafted onto GO surface and the synthetic heparin-mimetic G-BFNs have demonstrated integrated bioactivities, such as anti-coagulant, anti-thrombus and cell-adhesive capabilities [183–186]. The phospholipids is a typical zwitterionic molecule that can adhere to the surface of graphene or GNs easily via the hydrophobic interaction, which thus increases their bio-stealthiness in biological system [187]. Synthetic zwitterionic polymers, such as carboxybetaine and sulfobetaine-bearing polymers, have been realized to prepare the zwitterionic GO nanoagents with no visible cytotoxicity even at 0.5 mg/mL [188]. Although cationic polymers cannot enhance the antifouling capability of GNs, they are recognized as hydrophilic non-viral gene carriers and antibacterial agents, such as chitosan, PEI, branched PEI, polyamidoamine, and quaternary ammonium salts (QAS) grafted polymers [118,151].

Polysaccharides play important role to promote cell proliferation, tissue building, and immune modulation [106,189]. These unique biological activities of polysaccharides inspires the design of advanced G-BFNs for nanomedicine and tissue scaffolds. For example, DA-conjugated heparin has been synthesized for surface functionalization and reduction of GO through the mussel-inspired adhesives and reduction capability of catechol groups [182]. Compared with bare GO, the heparin decorated GO nanoagents showed a greatly suppressed interaction with lipid bilayers of cell membrane (Fig. 7c), thus resulting in extremely low hemolysis ratio and cellular toxicity (Fig. 7d, e) [182]. Furthermore, due to the strong hydrophobic interactions and hydrogen bond, the proteins and nucleic acid can also be applied to functionalize GNs. Proteins could be easily introduced onto GNs via hydrophobic interaction or edge group grafting [190,191]. It is found that the functionalization by proteins is extremely useful to regulate the biological interactions of GN and makes them more adaptable for biological applications [91,192]. Enzyme and nucleic acid have also been regarded as new bioactive decoration reagents for functionalization of GNs [94,103], and can also be used to construct the water-

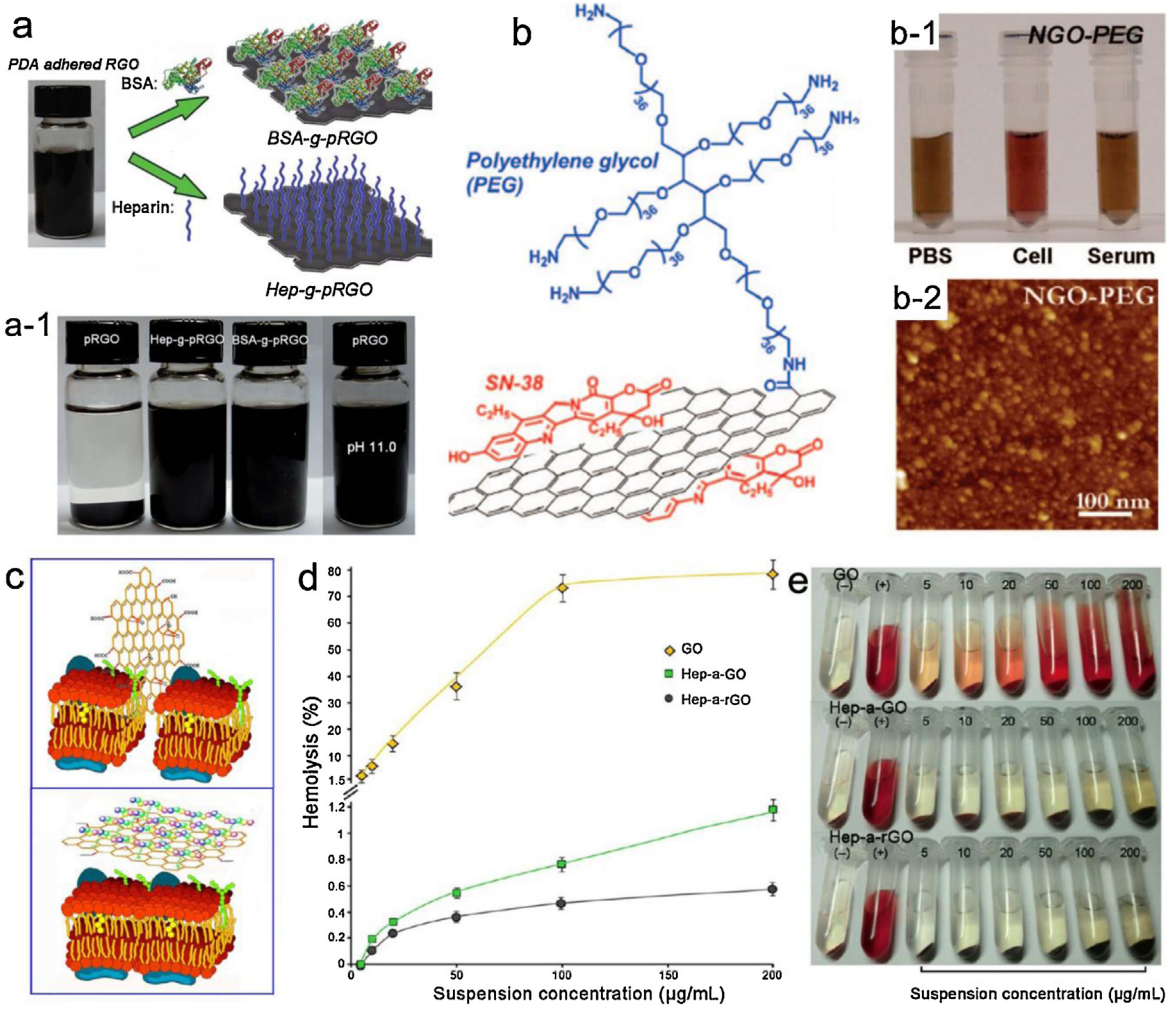

Fig. 7. (a) Schematic for the grafting of BSA and heparin on RGO (named as BSA-g-pRGO and Hep-g-pRGO) to enhance their aqueous stability. (a-1) Photographs of these aqueous dispersions after 2 weeks, the RGO can only be stable in basic solution. Reproduced with permission. [92] Copyright 2013, The Royal Society of Chemistry. (b) Structure of SN-38-loaded NGO-PEG. (b-1) Dispersion of NGO-PEG in different solutions. (b-2) AFM images of NGO-PEG. Reproduced with permission [154]. Copyright 2008, American Chemical Society. (c) The schematic image for GO resulted disruption for the lamellar structure of cellular lipid bilayer, while the heparin decorated GO showed low interaction with lipid bilayer due to the surface well-distributed negative charges. (d) Hemolysis ratios of the human red blood cells for the GO and heparin decorated GO. (e) Photographs of human red blood cells after incubation with samples for 3 h. Reproduced with permission. [182] Copyright 2012, American Chemical Society.

dispersible nanomedicines and biocompatible 3D hydrogels for diverse applications [95,96,142,193].

Stimuli-responsive nano-bio-system

Stimuli-responsive nano-bio-systems have capabilities of adapting to changes in local environments through altering their properties, thus offering with on-demand control of biofunctionalities [194,195]. Thermal-responsiveness, especially the PNIPAM, is a widely studied strategy to combine with graphene for designing to design remote light control smart nano-bio-system, as shown in Fig. 8a [120]. Upon near-infrared (NIR) light, the GO-PNIPAM hydrogel shrank due to the transfer of PNIPAM into the hydrophobic form. Recently, Jandt's group has discovered that the interfacial coating of GO layers on the PNIPAM based microspheres can control the diffusion-driven drug release (Fig. 8b, b-1) [196]. As shown in Fig. 8b-2, the GO coating layer reduces the permeability to an extent that suppresses the initial burst release and prolongs the drug release period. Besides the thermal responsive polymers, the GNs can also respond to the thermal stimuli, for instance the GO-wrapped mesoporous silica nanoparticles (MSN) have been fabricated for light-mediated drug delivery with an aptamer-targeted cancer treatment (Fig. 8c) [197]. Doxorubicin (DOX) was loaded into the MSN by charge adsorption, and then the DOX-MSN was wrapped with GO. Under NIR irradiation, GO generates abundant photothermal heating to kill cancer cells, which simultaneously leads to the "on-demand" release of DOX (Fig. 8c-1, c-2, c-3).

The pH responsive nano-bio-system provides another opportunity for design advanced G-BFNs. In general, two strategies have been proposed: 1) polyelectrolytes that ionize or swell at different pH values and 2) cleavable bonds that are sensitive to environmental pH [198]. For the pH-sensitive polyelectrolytes, poly (acrylic acid), poly (2-vinylpyridine), chitosan and hyaluronic acid have been used [5,71,199]. The cleavable bonds strategy is based on an equilibrium between bond formation and cleavage over protons for dynamic bonds. For example, a pH-responsive GN-based delivery platform had been designed, in which, the 2,3-dimethylmaleic anhydride coupled to the graphene-NH_2 and resulted in a stable negatively charged nanoagent [200]. In the tumor environment (pH$\tilde{6}$.5), 2,3-dimethylmaleic anhydride was removed, thus resulting in a positively charged tumor-adaptive nanoagent for tumor cell taken up efficiently, thus leading to high tumor inhibition.

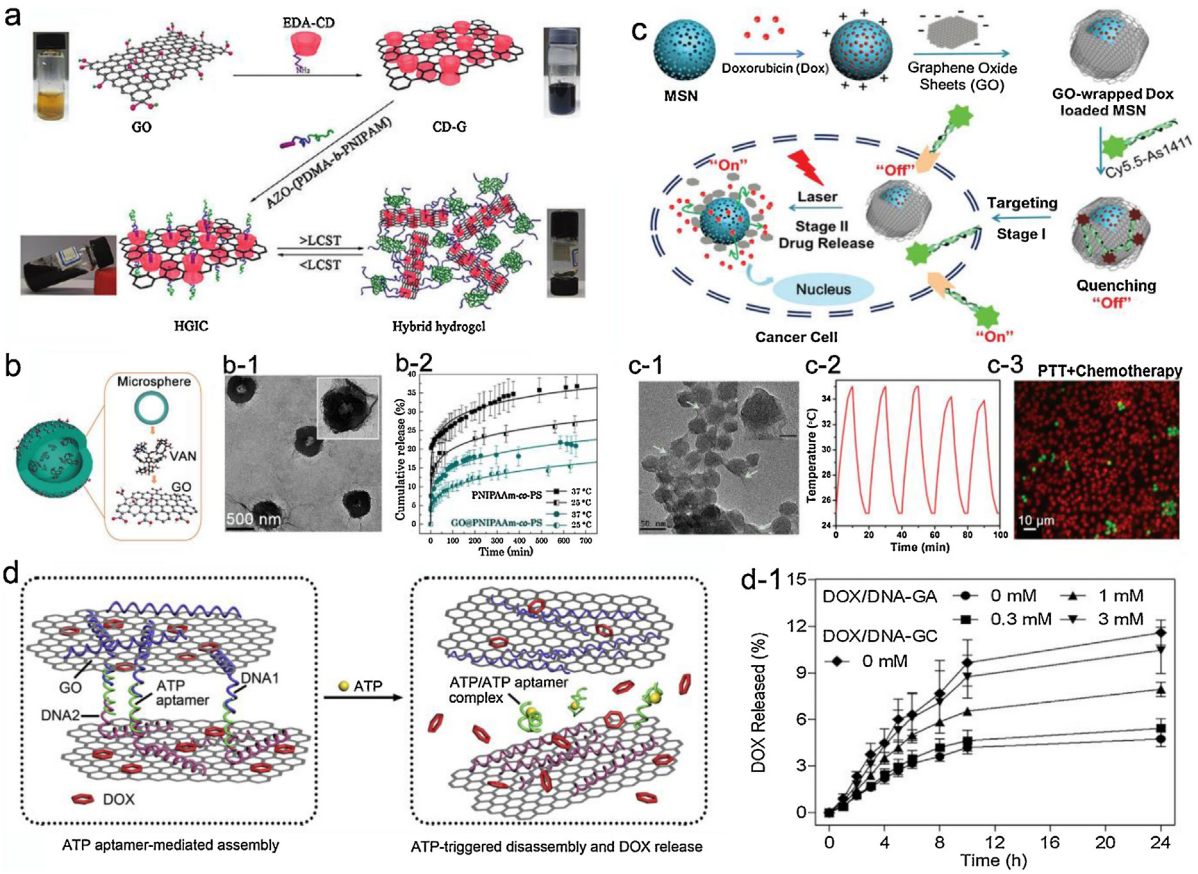

Fig. 8. (a) Formation of GO hydrogel via host-guest interactions. EDA-CD: ethylenediamino-β-cyclodextrin. CD-G: cyclodextrin-graphene. HGIC: hybrid graphene inclusion complex. Reproduced with permission. [201] Copyright 2011, American Chemical Society. (b) Illustration of the synthesized PNIPAM based hollow microsphere loaded with vancomycin (VAN) and coating with GO nanosheets (b-1). TEM image for the GO coated microsphere. (b-2) In vitro VAN release profile of the bare and GO coated hollow microspheres. Reproduced with permission [196]. Copyright 2017, The Royal Society of Chemistry. (c) Schematic image of GO-wrapped DOX-loaded MSN and the corresponding NIR-controlled intracellular drug release. (c-1) TEM images of GO-wrapped DOX-loaded MSN. (c-2) Temperature curves of MSN-DOX@GO solution irradiated by NIR. (c-3) Live/dead cell images of MCF-7 after treatment with MSN-DOX@GO. Reproduced with permission. [197] Copyright 2015, The Royal Society of Chemistry. (d) An ATP-responsive DNA conjugated GO for controlled drug delivery. (d-1) DOX release form GO at different ATP concentrations. GA: GO nanoaggregates. GC: GO complex. Reproduced with permission [98]. Copyright 2015, Elsevier Ltd.

Beyond thermal and pH-responsive nano-bio-systems, smart G-BFNs carriers that respond to adenosine-5′-triphosphate (ATP) have also been established [98]. It was found that the interaction between ATP and ATP aptamer would lead to the dissociation of GO-DNA nano-aggregates, thus enhancing the drug release from GO, as shown in Fig. 8d, d-1, which provided a new possibility to develop ATP-responsive nano-system for targeted on-demand delivery of anticancer drugs inside specific cells.

GNs-inorganic nanohybrids for multifunctional biocomposites

Recent reports have demonstrated that GNs-inorganic nanohybrids offer a number of integrated properties and novel biofunctions that are markedly advantageous for constructing bioactive or biomimetic biomaterials. The GNs-inorganic nanohybrids not only display the individual characteristics of the nanoparticles and GNs but also exhibit additional synergistic properties that greatly augment their application fields. By combining GNs with metal oxide (TiO_2, MnO_2, Fe_3O_4, etc.), nanoparticles including metal (Ag, Au, Pt, etc.), or other inorganic nanoparticles, it is possible to enable complementary multi-functionalities for diverse biomedical applications, such as tissue regeneration, bioimaging, and hyperthermia treatment of cancer cells [8].

Bioactive composites and cellular scaffolds

In tissue regeneration, GNs-calcium hybrid scaffolds have come to serve as promising candidates for bone repair due to their superior mechanical stiffness and biocompatibility. The biomineralization of $CaCO_3$ in the presence of GO nanosheets with CO_2 was studied, after chemical reduction of GO, the fabricated RGO-$CaCO_3$ composites showed enhanced formation of HAp in simulated body fluid and superior growth of osteoblast cells [127]. This GO/HAp composite can also be coated onto titanium substrate, which exhibits comparable differentiation rate for fibroblast cells when comparing to the cells cultured with bone morphogenetic protein-2 growth factor, suggesting that GO/Hap composite provides opportunities to improve orthopedic implant applications [129]. In addition to calcium minerals, strontium can also promote the formation of bones. RGO-strontium hybrid nanoparticles have also been incorporated into poly (epsilon-caprolactone) matrix as scaffolds to promote osteoblast proliferation and differentiation [128].

Therapeutic and diagnostic nanohybrids

GNs-metal nanoparticle has also been realized as a multifunctional nano-platform. GO has a negatively charged surface, which can bind metal ions; after reduction at proper conditions, GO-metal

nanoparticles are obtained with integrated functionalities from both sides, which not only satisfies their usage for electronics but also facilitates the development of new platform for diagnostics and therapeutics. For example, AuNPs have shown versatile physical, chemical, and biological functionalities, such as the conversion of NIR into heat and photoacoustic signals, and they have been combined with GNs for photothermal treatment and bioimaging of cancer [202]. AuNPs have been deposited onto GNs surface for the surface-enhanced Raman spectroscopy, surface plasmon resonance, fluorescence resonance energy transfer and many other kinds of biosensing applications [8]. AuNPs can also be easily functionalized with biomolecules for detection purposes, while GNs enhance signaling properties by means of multivalent interaction. Such a platform of GO-AuNPs is able to detect 4.03×10^{-14} mol/L DNA, which is much lower than any other kind of sensing platform [203].

Enzyme-mimetic nano-catalysts

Recently, it was reported that Cu^{2+} ions decorated GO (GO/Cu^{2+}) can serve as nanoenzyme to catalyze the multiple oxidation reactions with H_2O_2, e.g. dopamine to aminochrome and luminol to aminophthalate, such as HRP and NADH peroxidase [51]. Interestingly, they only observed catalytic activity on GO/Cu^{2+}, and other kinds of bare metal ions (Ni^{2+}, Co^{2+}, Pd^{2+}, Cd^{2+}) showed no catalytic activities. In addition to Cu^{2+} ions, Au, Pt, and Au-Pd nanoparticles also show horseradish peroxidase (HRP)-like enzymatic catalytic activity [132–134,204]. The GO-AuNPs can convert H_2O_2 to H_2O and transfer 3,3′,5,5′-tetramethylbenzidine (TMB) to its oxidative form, oxTMB, as shown in Fig. 9a, b [205]. Further functionalization of folic acid facilitates targeting towards cancer cells and allows rapid and colorimetric detection.

Similar catalytic activities have also been reported on GO/Fe_3O_4 [206], GO/CuS [135] and others, which have been used for colorimetric detection like the GO/enzyme nanosystems. As shown in Fig. 9c, d, the GO-Fe_3O_4/Pt composites have been designed as a highly efficient colorimetric detection platform [134]. Via functionalization of the targeting antibody, the platform can selectively detect human breast adenocarcinoma cells over human melanoma cells with better detection resolution than HRP.

In addition to detections, these nanoenzymes have also been used for cancer treatment. The TiO_2/AuNPs decorated GO has been used for sunlight-mediated photodynamic therapy (PDT) for melanoma skin cancer (Fig. 9e-g) [207]. Under sunlight radiation, the electrons of AuNPs can be excited and transferred to TiO_2, and further to GNs, due to staggered energy levels that leave holes in the highest occupied molecular orbital. Then, free electrons in GNs and free holes in AuNPs can react with O_2 and H_2O to form $O_2\bullet^-$ and HO•, respectively, producing significantly enhanced PDT effects.

G-BFNs based functional nano-inks for bioelectronics

Due to the excellent chemical, rheological, electrical, electrochemical, and biological properties, developing conductive GNs for lightweight, portable, flexible and printable bio-electronics in various bionic and biomedical applications have attracted great attention in recent years, such as blood glucose biosensors, neuron-to-machine devices, implantable stimulators, tissue monitors, and artificial skins [4]. Recent studies reveal that the liquid GNs dispersion based nano-inks have shown promising potential for applications in diverse flexible bio-electronics, such as patterned thin films, textiles and elastomers [208,209]. For instance, the graphene/ethyl cellulose has been successfully dispersed in cyclohexanone/terpineol solvent to prepare nano-ink, then the coupling inkjet printing with intense pulsed light annealing method is utilized to construct electronic patterns on myriad substrates, which shows a conductivity of about 25 000 S m^{-1} [210]. Besides mixed solvent, mild heating induced gelation of graphene/polymer dispersions has also been used to prepare nano-inks with high viscosity (Fig. 10a-c) [211]. This gel-like nano-ink can be utilized for screen printing one plastic and paper substrates with roll-to-roll characteristics for printing flexible electronics (Fig. 10d).

Currently, most of the graphene based nano-inks are established via organic solvents, bioactive graphene nano-inks integrated with high water-processability, conductivity, and electrochemical activity are also highly needed. To overcome this challenge, very recently, a water-processable and bioactive multivalent conductive nano-ink has been developed by utilizing highly reduced graphene (HRG) and sulfated HPG (HPGS), as shown in Fig. 10e [114]. The obtained HRG-HPGS showed uniform 2D morphology, excellent solubility and water-processing ability (Fig. 10f, g), and it could work as a conductive and bioactive nano-ink for brush-printing electrical patterns, nanofibers and thin films with robust flexibility and conductivity (Fig. 10h-j) [114]. Furthermore, the biofunctional molecule-decorated GNs dispersions in suitable solvents can also be applied for 3D printing of porous microlattices with sophisticated shapes as tissue scaffolds, which will be separately discussed in section 3.7.

Nacre-like layered G-BFNs composites

Owning to the layered deposition of platelet-shaped $CaCO_3$ particles and protein linker, nacre reveals a “bricks/mortar” structure with high toughness, which has inspired numerous efforts to mimic its excellent mechanical properties by designing the nacre-like layered structures [212]. It has been widely established that the bare GO suspension can be applied to construct mechanically robust and conductive layered films via a casting-drying and reduction process [213,214]. Besides the bare graphene film, currently, the fabrication of nacre-like layered G-BFNs composites have also attracted great attention for the construction of ultra-strong materials with light weight, high conductivity, good biocompatibility, and versatile biofunctionalities [107,212,215–217].

One of the key challenges that need to be overcome for construction of high-performance GNs based film is the interaction and adhesion between hard (GNs) and soft (molecules or polymers) phases as well as maintain sufficient volume fraction of GNs in the structure. As a representative fabrication process, the gel-film transition method to prepare strong, conductive and foldable GNs based nacre-like film has been established by Li and Shi et al. as shown in Fig. 11a [218]. In this study, poly(acrylic acid-co-(4-acrylamidophenyl)boronic acid) ($PAPB_x$) was used as the soft phase to form the GO-$PAPB_x$ hydrogel due to the strong hydrophobic interactions and π–π stacking, which allowed the construction of composite film via a casting-drying process. After the reduction of the GO, a RGO film that integrates high conductivity (337 ± 12 S cm^{-1}) and high tensile strength (382 ± 12 MPa) can be obtained (Fig. 11b, c).

Besides the gel-film transition method, vacuum filtration assisted fabrication protocols have also been applied for constructing nacre-like layered G-BFNs composites [219,220]. Tsukruk group has used the vacuum-assisted filtration to fabricate the layered film via a homogeneous mixture of GO and silk fibroin [220]. By applying a specific reduction process, the conductive micropatterns with resolution comparable to traditional photolithography could be obtained, and the RGO area showed a high conductivity of 1350 S m^{-1}. The facile process enables this approach great potential for advanced bioelectronics, such as sensory skin and flexible papers with written-in patterns. In another report, Cheng et al. designed a polymer crosslinked RGO-tungsten disulfide (WS_2) nacre-like layered composite film (Fig. 11d, e) [221]. The fatigue life of resultant

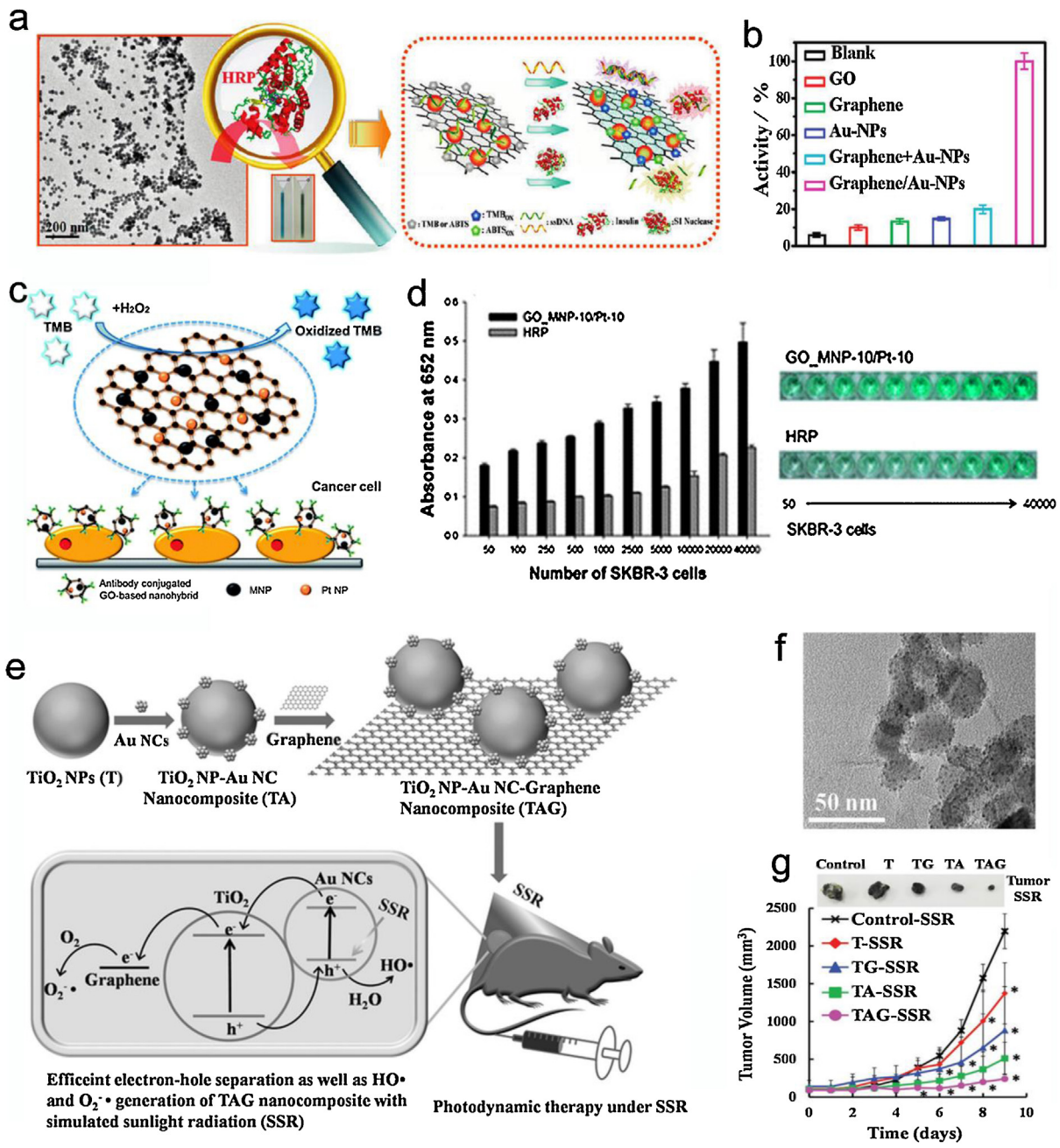

Fig. 9. (a) Hybridization of AuNPs with graphene, yielding peroxidase-mimetic activity. (b) Comparison of the catalytic activities of the samples under the same conditions. Reproduced with permission. [205] Copyright 2012, American Chemical Society. (c) Colorimetric detection of cancer cells using the GO-magnetic nanoparticles (MNPs)/Pt. (d) Human breast adenocarcinoma cell number-absorption intensity curves for GO-MNP/Pt and HRP control. Reproduced with permission [134]. Copyright 2014, The Royal Society of Chemistry. (e) Preparation of the nanocomposites and their usage for PDT with radiation of simulated sunlight. (f) TEM images of TiO_2-Au-graphene nanomaterials. (g) Tumor growth curves of mice intratumorally injected with different nanomaterials with simulated sunlight radiation treatment. SSR: simulated sunlight radiation. T-SSR: simulated sunlight radiation with TiO_2. TG: TiO_2-NP-graphene nanocomposites. TA: TiO_2-NP-Au-NCs nanocomposites. TAG: TiO_2-NP-Au-NC-graphene. Reproduced with permission. [207] Copyright 2017, Wiley-VCH.

nacre-like film can reach to more than one million times at the stress level of 270 MPa with a high retention of conductivity of 197.1 S/cm.

In addition to these conventional polymers, the mussel-inspired molecule, dopamine, induced crosslinking has also been proposed to achieve polymer covalently interlinked layered thin film, as a result, the RGO/PDA films show much higher tensile strength and toughness compared with other kinds of GNs-based films [50]. Meanwhile, it has also been found that the RGO/PDA composite can serve as an excellent building block for origami-inspired programmable devices, which can work as the robotics upon stimuli from NIR light [123]. The action of GNs based films can be programmed by the GO/PDA gradients, which has been achieved by adopting a predesigned shape, walking, turning a corner and transporting a cargo. Beyond the nacre-like 2D thin film, very recently, inspired by the nacre-like multilevel structural design, the RGO/PDA-based 1D microfiber can be achieved via an interface-reinforced method (Fig. 11g-i). The PDA acted as a resistance enhancer, binding molecule, and conductive connection "bridges" [222]. Remarkably, the tensile strength increased to 724 MPa, and the electrical conductivity of the fiber reached as high as 6.6×10^4 S m^{-1}, guaranteeing its promising application potential in diverse G-

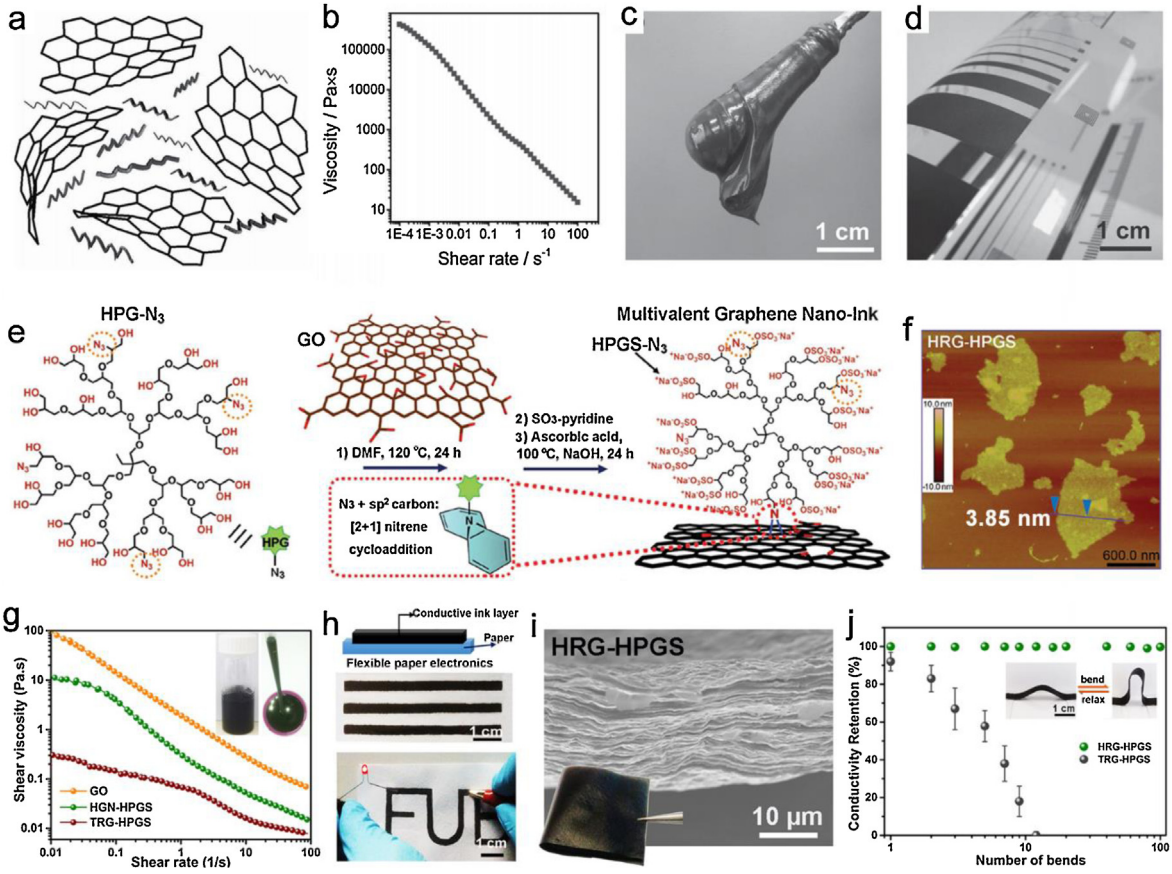

Fig. 10. (a) Scheme image for the graphene/polymer dispersion. (b) Shear viscosity of graphene paste with a high concentration of 52 mg mL^{-1}. (c) Photo image for the graphene/polymer paste. (d) The graphene/polymer paste for screen printing on PET foil. Reproduced with permission. [211] Copyright 2016, Wiley-VCH. (e) Synthesis process of the water-processable graphene-based nano-ink. (f) A representative AFM image of HRG-HPGS nano-ink. (g) The shear viscosity of the nano-inks. (h) Designing brush-painted paper electronics and (i) free-standing thin film. (j) Conductivity retention ratio for the HRG-HPGS based thin films. Reproduced with permission [114]. Copyright 2018, Wiley-VCH.

BFNs-based flexible microdevices, such as sensors, actuators, and implantable neural probes [222,223].

G-BFNs assembled superstructures and macroporous composites

For the preparation of G-BFNs-based 3D superstructures, hydrothermal treatment is a favorable approach. The π-π interactions between graphene nanosheets and water encapsulation by residual oxygen functional groups can lead to the successful assembly of 3D architectures, for instance the bulk RGO hydrogel prepared by subjecting the GO dispersion in a Teflon tube for hydrothermal treatment [126]. The fabricated 3D structures exhibited an interconnected porous morphology with excellent mechanical properties and good electrical conductivity (10^{-3} S/cm). Additionally, hydrothermal protocols have also been applied for the fabrication of porous RGO-inorganic composite aerogel using different organic or inorganic chemical reagents for crosslinking or reduction. Furthermore, divalent ions (Ca^{2+}, Ni^{2+}, Co^{2+} or Fe^{2+}) have been used to form GN-metal oxide hybrid aerogels via hydrothermal treatments [224]. The combination of hydrothermal treatment and self-polymerization of PDA also facilitated the formation of G-BFNs-based 3D superstructures [225]. PDA has abundant groups for conjugation to other molecules, and graphene functions as a substrate to interlink the PDA layer and create a porous structure. Therefore, these composites can be used as good candidate as absorbents, membranes and catalysts [93,225].

However, in many system, the hydrothermal based assembly strategies may be not adaptable, for instance the preparation of MXene–RGO composite aerogel, the high temperature can destroy the structure of MXene due to its poor antioxidant activity [226]. The freeze-drying method has been proposed to fabricate the MXene–RGO composite aerogel (Fig. 12a, b) [226]. Furthermore, it was found that further wrapping the superstructures with a self-healing carboxylated polyurethane shell, the whole composites became a self-healable aerogel with good retention of mechanical properties and electrochemical capacitance, which provided a new method for fabricating next-generation long-life bio-electronic devices.

Another representative protocol to fabricate the G-BFNs-based macroporous composites is using the chemical vapor deposition method to directly synthesize 3D graphene foam (GF) on nickel foam substrates [227]. However, this method is only suitable for fabrication of pure GF, it is hard to integrate other bioactive molecules. Currently, the interfacial coating on 3D porous template provide a more adaptable protocol for construction of G-BFNs-based GF. For example, the 3D GF has been successfully fabricated via using the GO coating on a polyurethane foam (PUF), meanwhile, the PUF template can be removed subsequently via the ethanol flame for less than 60 s [228]. Furthermore, the GO interfacial coated PUF can also be applied for pyrolysis process to generate highly porous 3D GF, which can adsorb 2D peptide nanosheets (PNSs) to generate a novel macroporous scaffold for the controllable growth of HAp, as shown in Fig. 12c-e [229]. The fabricated biomimetic 3D GF-PNSs-HAp minerals show adjustable shape, light weight (0.017 g cm^{-3}), large porosity (5.17 m^2 g^{-1}), and good cell compatibility, thus proving new

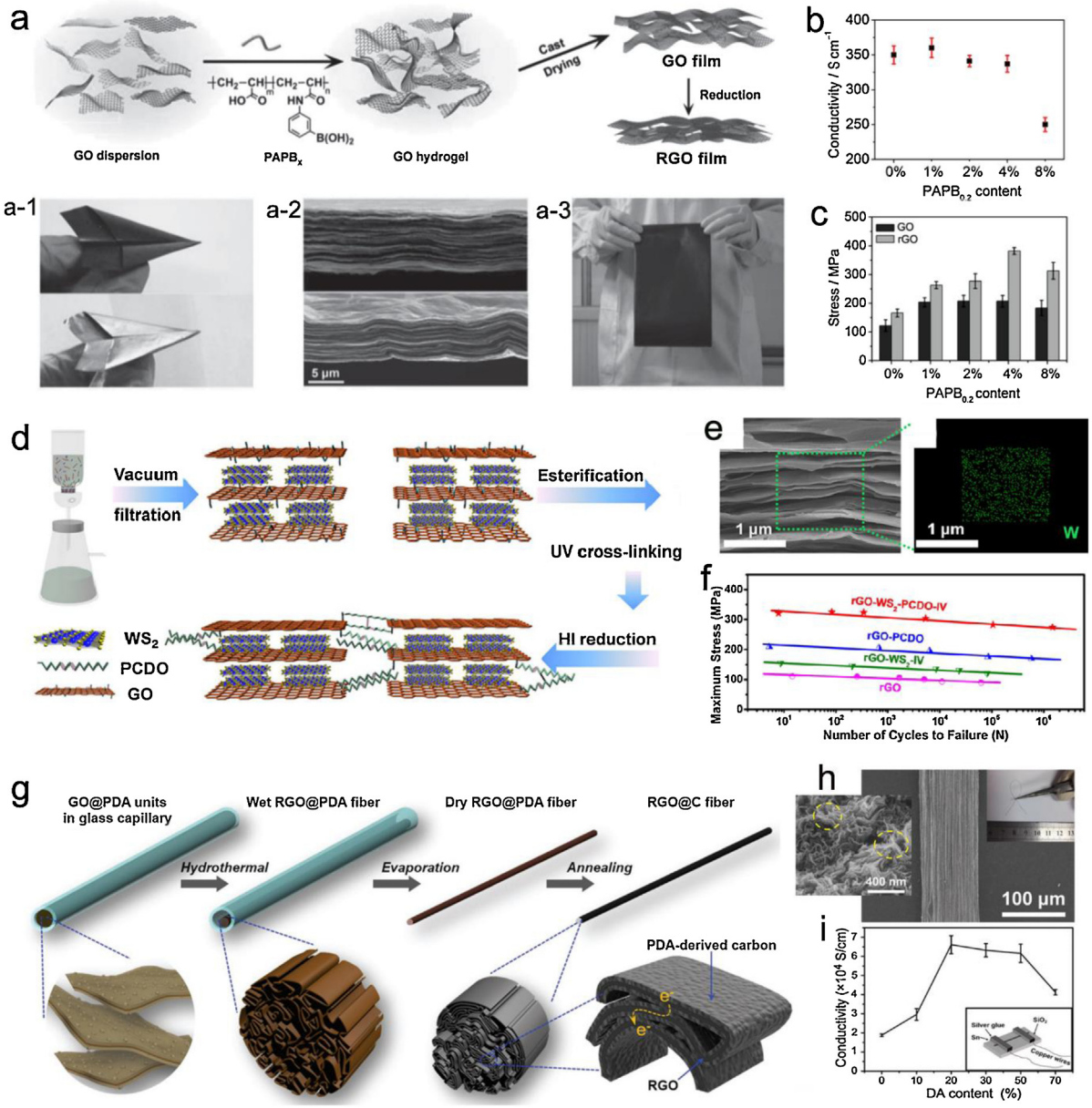

Fig. 11. (a) Schematic image for the preparation of nacre-like films. (a-1) Photographs of GO (top) and RGO (bottom) films to depict their flexibility. (a-2) Cross-section SEM images of the fractured GO (top) and RGO (bottom) films. (a-3) Picture for a large GO film. (b) Conductivities of the RGO film with different contents of polymers. (c) Stress of GO and RGO films with different ratios of polymers. Reproduced with permission. [218] Copyright 2014, Wiley-VCH. (d) Illustration image for preparation of the 10, 12-Pentacosadiyn-1-ol (PCDO) polymer crosslinked RGO-WS_2 nacre-like film. (e) SEM and element mapping of the nanocomposites. (f) Tensile fatigue testing of the composite films and control samples. Reproduced with permission. [221] Copyright 2017, American Chemical Society. (g) Illustrative image of the production process of RGO@C fibers. (h) Surface and cross-section morphologies of RGO@PDA fibers. (i) Electrical conductivity of RGO@C fibers after 1200 °C annealing with different DA contents. Reproduced with permission [222]. Copyright 2018, Wiley-VCH.

possibilities in bone regeneration and other biomedical applications.

D printing of G-BFNs-Based porous microlattices

As discussed in above sections, although G-BFNs-based 3D macroporous composites can be facilely fabricated via diverse conventional approaches, they methods are limited for the generation of stochastic and random porous structures, for which the functionalities and applications are rather hindered due to the lack of adaptiveness to the biological and human system; especially for the development of implantable devices, a shape matching the desired area is highly required [230]. To overcome this challenge, the 3D printing technique has been applied for construction of periodic GNs-based microlattices. First, the GO dispersion should be developed into a printable GNs-based nano-ink, for instance by using the resorcinol-formaldehyde based organic sol-gel chemistry [231]. To reduce the usage of high content of additives or complex processes, the ion-induced gelation method has also been introduced to directly print GN-based scaffold from GO-based nano-ink via using of trace addition of Ca^{2+} ions as gelators (Fig. 13a) [232]. As shown in Fig. 13 b–d, a programed 3D microlattice can be directly printed, the structure is highly porous with abundant macropores, which can provide new kind of GNs-based scaffolds for tissue engineering and other biomedical fields, but the long-term stability of this ions crosslinked structures in physiological conditions should be carefully tested [232].

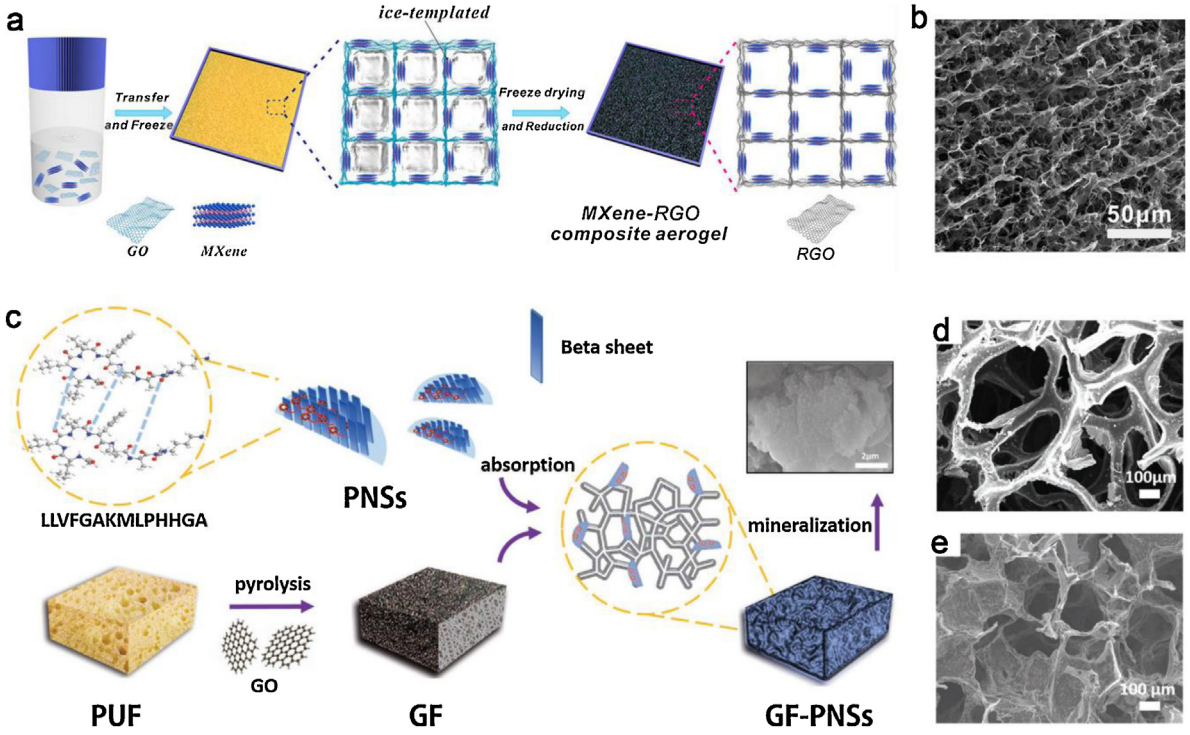

Fig. 12. (a) Illustration image for the fabrication of MXene–RGO composite aerogels. (b) SEM image for the MXene – RGO composite aerogel. Reproduced with permission. [226] Copyright 2017, American Chemical Society. (c) Schematic image for the preparation of 3D GF-PNSs-HAp minerals. SEM images for PUF coated with GO (d) and the fabricated 3D GF (e), Reproduced with permission. [229] Copyright 2018, Wiley-VCH.

In a recent study, the 3D printing technique has been applied to construct functional polymers and nanomaterials mixed 3D microlattices. By using additional components, the GNs-based nano-ink with very high viscosity can be obtained for achieving a self-supporting 3D structure. For instance, a series of arbitrarily scaffolds via using graphene/polylactide-co-glycolide (PLG) nano-inks have been developed with controlled porous morphology, high flexibility, good compatibility for stem cell growth and neurogenic activity [233]. To overcome the limitations of multi-components inhomogeneous incorporation and complicate post-treatments for the removal of additives, designing the hybrid inks and universal printing schemes was proposed to enable mix-dimensional hybrids printability, as shown in Fig. 13e [234]. This fabrication process was achieved by using the progressively crosslinking of GO nanosheets in a mild and uniform manner. Notably, beyond arbitrary predesigned structures and composites, micro-patterns on curved surfaces could also be accomplished (Fig. 13f-h). Due to significant benefits in mechanical, electrical, cell adhesion, and facile fabrication, the 3D printed G-BFNs-based scaffolds will provide new pathways for the designing of medical devices and scaffolds for a range of clinical treatments [234].

G-BFNs based injectable 3D hydrogels

Besides the above G-BFNs-based aerogels or macroporous scaffolds, another important 3D G-BFNs-based structure is the injectable hydrogels. Due to the multiple similarities to human soft tissue systems, the hydrogel can be recognized as a biomimetic extra-cellular-matrix (ECM) with versatile *in vitro* and *in vivo* bio-functionalities. However, the weak mechanical properties and poor interaction with cells for most traditional polymeric hydrogels have hindered their wide application. Due to the excellent mechanical and versatile physiochemical properties, it was found that incorporation of GNs not only significantly increased the mechanical performance of the composite hydrogel but also improved cell adhesion by creating porous structures for cell loading [235]. As a representative system, the water-soluble 2,2′-(ethylenedioxy)-diethanethiol was used to crosslink the GO skeleton, which was then incorporated *in situ* with PVA to form composite hydrogels [236]. The GO-PVA hydrogels were found to be supportive for chondrocyte adhesion and growth, becoming a potential candidate for the construction of load-bearing artificial tissue.

In addition, multifunctional hydrogels with diverse physical, chemical and biological characteristics, such as tunable swelling properties, good cell adhesiveness, and excellent cell proliferation, have been fabricated using the GN-protein hybrid hydrogels [237]. The GO-polymer-based heparin-mimetic hydrogels with high blood and cellular compatibility have been synthesized [238,239]. These hydrogels are prepared via *in situ* polymerization of sulfonated sodium styrene, and its mechanical properties can be easily tuned to match different kinds of tissues. These heparin-mimetic GO hydrogels show low hemolysis ratio, good platelet adhesion resistance, and superior anti-clotting capability, thus exhibiting great potential to serve as therapeutic and injectable synthetic hydrogel for diverse biomedical applications, especially in antibacterial coating and wound healing.

GN-embedded biomacromolecule-based hydrogels, e.g., collagen, DNA, chitosan, and heparin, have also been intensively explored for therapeutic and injectable applications due to their good biocompatibility and bio-degradability [240]. The GO-gelatin based injectable hydrogel has been designed for gene delivery and cardiac repair through UV-induced coupling, as shown in Fig. 14a [43]. GO was first coated with PEI for loading of VEGF (fGO_{VEGF}) and then mixed with GelMA. Under mild exposure to UV light in the presence of a photoinitiator, gelation rapidly formed by the coupling of vinyl moieties. Due to its low modulus, the fGO_{VEGF}/GelMA hydrogels could transfect myocardial tissues very efficiently and induced excellent therapeutic results without cytotoxicity, as revealed by a rat model with acute myocardial infarction (Fig. 14b). The synthesized fGO_{VEGF}/GelMA hydrogels

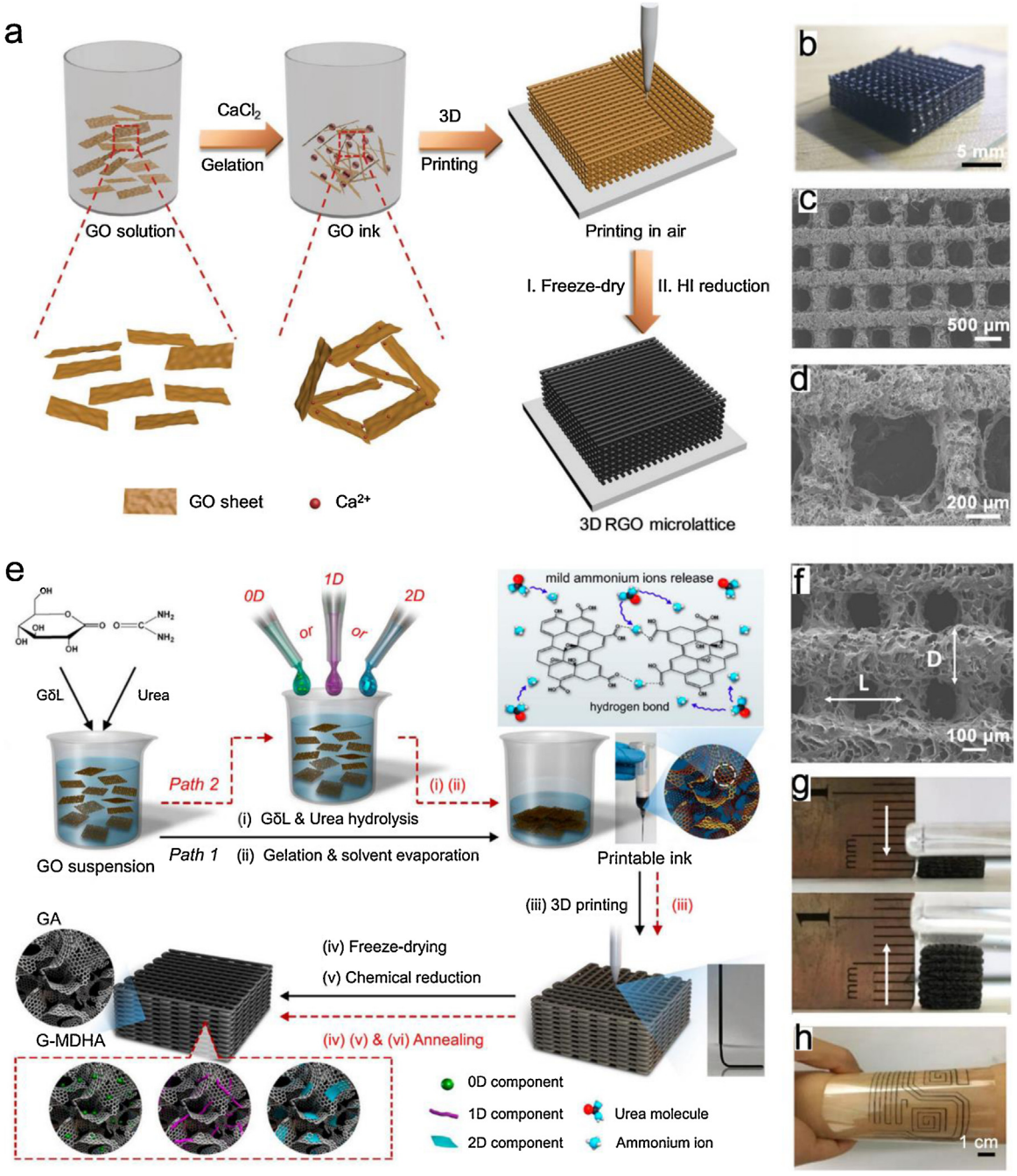

Fig. 13. (a) Schematic illustration of ions crosslinked 3D printing process for microlattices. (b) Photo images of the printed microlattice structure from a top view. (c, d) SEM images of the 3D microlattice with macroporous structure. Reproduced with permission. [232] Copyright 2018, Wiley-VCH. (e) Schematic image for the 3D printing of graphene aerogels (GA) and graphene-based mixed-dimensional hybrid aerogels (G-MDHA). Urea and gluconic-δ-lactone (GδL) were used to crosslink GO suspension and enhance its viscosity. (f) SEM of the 3D printed porous structures. (g) Photo pictures for the 3D printed GA: fully compressed state (upper) and stress release state (lower). (h) Printed circuits on a flexible substrate. Reproduced with permission [234]. Copyright 2018, American Chemical Society.

showed a significant increase in myocardial capillary density at the injected region, as well as a reduction in the scar area (Fig. 14c, d). Furthermore, the fGO_{VEGF}/GelMA group showed significantly higher cardiac performance in echocardiography compared with the other groups after 14 days of injection (Fig. 14e). In another injectable hydrogel system, the *in situ* formation of a therapeutic GO/peptide hydrogel was reported, for which the peptide was deigned to be photocrosslinkable [240]. The hydrogel contained permanent crosslinks that warranted the mechanical stability and the integrated weak interactions could be temporarily broken upon external triggering. Such a design makes the composite hydrogel could be directly injected into the tumor lesion for cancer therapy by NIR or DOX release.

Toxicity and interfacial biointeractions of graphene, GNs and G-BFNs

Toxicity of graphene, GNs and G-BFNs

Although graphene and GNs have been widely used as potential nanomedicines and biomedical materials, their toxicities at molecular, cellular and tissue levels have been gradually revealed and

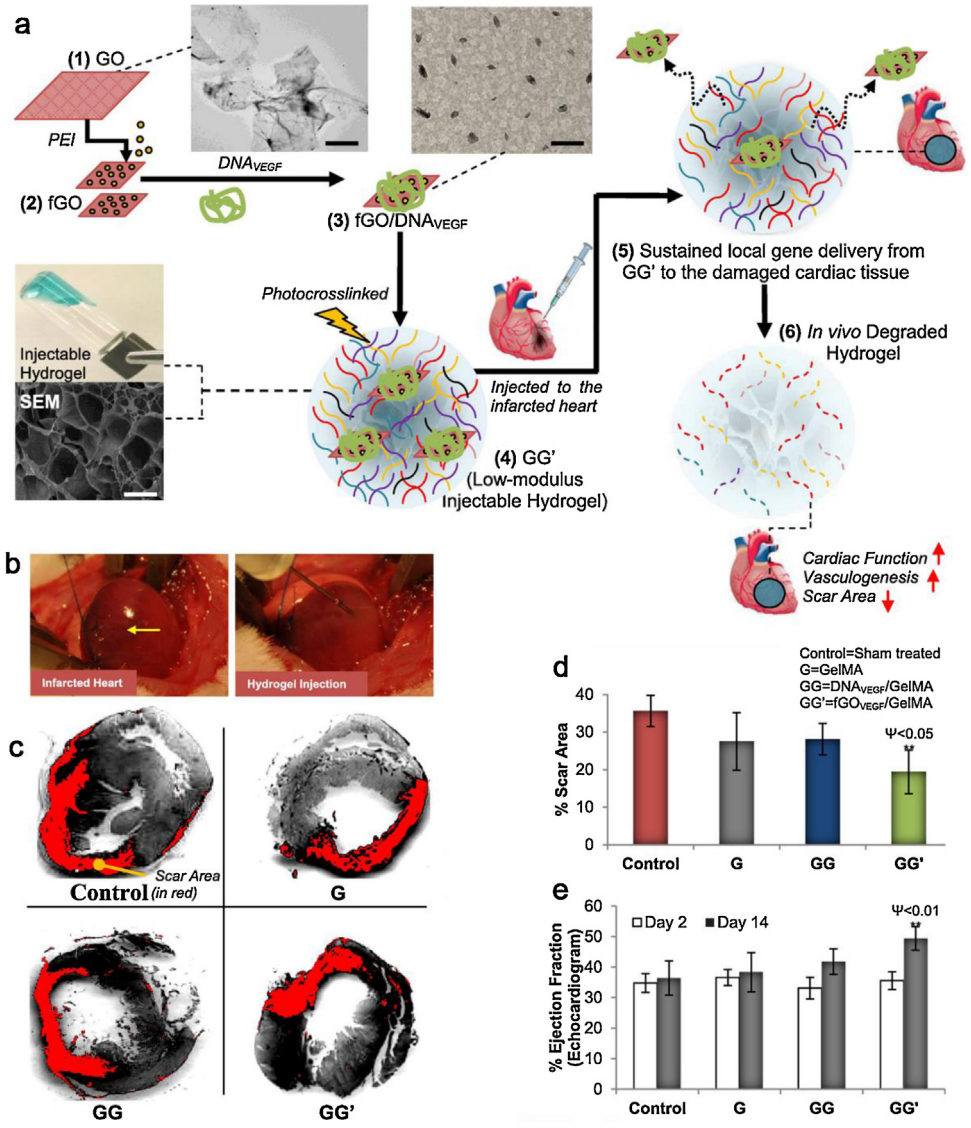

Fig. 14. (a) Schematic illustration of the preparation of the fGO/DNA$_{VEGF}$/GelMA hydrogel and injection in the infarcted rat heart. (b) Schematic of rat heart with acute myocardial infarction. (c) Scar area tested by morphometric analysis via different samples. The left ventricle myocardial sections stained with Sirius red (marked with red). (d) Scar area of the left ventricle in different groups. (e) Echocardiographic assessment of cardiac function. Reproduced with permission. [43] Copyright 2014, American Chemical Society.

aroused as a major concern for researchers worldwide. In general, the toxicity of graphene and GNs should not be ignored when designing materials for biological and biomedical fields, especially for *in vivo* applications [61]. Even being studied for many years, the detailed mechanisms behind the toxicity of graphene and GNs still haven't been fully discovered. Since this review aims to discuss the current advancements on fabrication of graphene and GNs based bio-functional biomaterials for biological applications, thus the toxicity discuss is not the main focus of this review. Meanwhile, we have noticed that there are already some good review articles that have illustrated the possible mechanisms and pathways for toxicities induced by graphene and GNs based nanomaterials [4,5,241,242]. Therefore, in this section, we will only make a brief introduction and discussion for the recent discovery and advancements on the graphene and GNs induced toxicity.

One of the most well-known reasons for the graphene and GNs induced toxicity is their strong interaction with biomolecules, including proteins, phospholipids (cellular membrane), RNA, DNA and others [5,243]. The non-specific adsorption of biomolecules on graphene or GNs surfaces always cause damage to their 3D conformations and structures, associating with denaturing and degradation [91,198,244]. These side effects have been observed in red blood cells, platelets, macrophages, endothelial cells and nearly every type of cells [245]. For example, most of *in vivo* applications demand intravenous injection of GNs and G-BFNs, however, their amphiphilic structures may cause hemolysis and platelet aggregation and activation, which will then trigger thrombus formation in blood [244,246]. Furthermore, the immune cells, like macrophage, can be strongly activated by GNs and G-BFNs, which will release Th1/Th2 cytokines and chemokines and then cause inflammation [247]. Additionally, because of the strong interaction with tissues, the clearances of GNs and G-BFNs are quite slow, which may also cause pulmonary edema, granulomatous lesions, inflammation, and fibrosis [242].

In addition to the cellular and tissue toxicities, due to the non-degradable nature of graphene and GNs, the bio-distribution should also be taken into consideration and carefully studied before clinical usage. It has been noticed that most of GNs end up in liver and spleen after travelling around in different organs, which may cause liver and spleen damage [248,249]. Furthermore, though it

had been reported that the EPR effects could enhance the accumulation of GNs-based nanomedicine in tumor sites, the potential non-targeted accumulation of the GNs in the other tissues or organs should also be seriously concerned. To overcome this problem, highly efficient targeting ligands are always necessary to minimize this potential non-targeted accumulation side effects, especially for gold and other non-degradable inorganic compounds integrated GNs.

To decrease the toxicity of GNs, one representative approach is the functionalization of GNs with diverse functional and bioactive biopolymers, as discussed in the previous sections. For example, serious hemolysis was observed when incubating GO with blood cells; however, surface coating of chitosan or heparin could significantly eliminate the hemolysis [182,250]. In another example, the PEG and BSA conjugated GO are found to show remarkably decreased cytotoxicity compared to bare GO [251]. Besides the surface decoration with biopolymers, cutting GNs into smaller nano-sized species is another highly effective protocol to decrease the toxicity [31,79]. It was noticed that large GO showed greater adsorption than smaller GO on cellular membranes because of the stronger binding to Toll-like receptors (TLRs), the activation of NF-κB pathways was also more intense than small GO [252]. Furthermore, large GO would induce more macrophage polarization than small GO and promote inflammatory cytokine secretion and immune cell recruitment [243,252].

Overall, the current studies into the graphene and GNs induced toxicity are still at an early stage and comprehensive evaluations about the biological behaviors of graphene, GNs and G-BFNs in diverse animal models are quite needed, which should cover the stability, distribution, excretion and chronic effects. In many studies, the graphene and GNs are found to induce toxicity to bacteria while they show minor toxicity to mammalian cells, much more efforts are need to fully disclose the detailed mechanisms [253,254]. Meanwhile, since the toxicity of graphene and GNs can also be considered as a consequence of multiple biological interactions, thus, we believe that it is necessary to discuss these detailed biointeractions of graphene, GNs and G-BFNs with cells, bacterial, and even virus. Meanwhile, these biointeractions are important for guiding the future design of biofunctional GNs as well, therefore, we will carefully discuss these biointeractions in the following sections.

Interfacial biointeractions of graphene, GNs and G-BFNs with pathogen and mammalian cells

Pathogen interactions

To achieve high adaptability towards pathogen systems, an optimal nano-bio interfacial interaction is desired, not only for pathogen killing but also for pathogen detection devices. The interactions between bare GNs and microbes include adhesion, membrane penetration, phospholipid extraction and reactive oxygen species (ROS) generation [56]. For GO interaction with the bacterial membrane, a three-stage process has been proposed based on TEM observations. During initial contact, *E. coli* can tolerate GO; subsequently, the membranes are partially damaged with lower phospholipid density; finally, the bacteria lose their cellular integrity with membranes showing severe damage and part of the cytoplasm missing [255]. It was noticed that the size of GO could significantly influence the interaction with bacteria, as shown in Fig. 15a [256]. When coated onto a surface, GO with a smaller size showed higher antibacterial activity since more defect densities were introduced, which would benefit the generation of high oxidative stress. For suspensions, GO could affect the development of bacteria via the mechanism of cell entrapment, and the interactions enhanced when the sizes of GO increased (Fig. 15a-1, a-2, a-3).

To achieve a maximum interaction for a bacterial-adaptable interface, diverse adhesive ligands have been introduced to decorate the graphene surface, where face-to-face contacts could in turn enhance the interaction via multivalent effects. It was found that GNs functionalized with magnetic nanoparticles and glutaraldehyde could crosslink with bacterial surface proteins and effectively capture bacteria via a magnetic field [257]. The multivalent mannose-functionalized GNs can serve as a capture nano-platform for *E. coli,* as shown in Fig. 15b, b-1, b-2 [258]. Mannose recognizes the C-type lectin on the *E. coli* surface, but the individual binding is too weak for bacteria to capture. Thus, multiple mannoses were introduced on the GN surface by “host-guest” inclusion, and the yielded GN-mannose could selectively wrap and agglutinate *E. coli*. With further NIR irradiation, heat was generated, and the bacteria were inactivated. The multivalent GNs offer a new approach to prevent bacterial infection and to design targeted bacterial adhesion interfaces for pathogenic blocking or detecting [259–261].

The interfacial interaction between GNs and viruses has also been extensively studied. Since GNs can change the protein conformation and possibly denatures the protein, it has been used as a promising electrode to detect viruses by making use of the excellent conductivity of graphene. An Au-GNs-based nano-platform for electrochemical gene detection of the human immunodeficiency virus has been developed recently [262]. Combined with the fluorescence spectra, GNs can also been used for the gene detection of Ebola virus with a concentration limit of 1.4 pM [263].

In addition to the detection of virus, graphene can also be used for virus inhibition [264]. For example, it was reported that a heparin-mimic graphene nanoagent, rGO-SO_3, could inhibit the attachment of Herpes Simplex Virus Type-1 to Vero cells via competitive binding with cell membrane glycan, hence preventing the subsequent viral infection [265]. By taking advantage of the flexible RGO and the multivalent dendritic polyglycerol sulfate (dPGS), a RGO-dPGS based multivalent virus inhibitor has been synthesized for blocking orthopoxvirus, as shown in Fig. 15c, c-1, c-2 [44]. The inhibition rate for Vaccinia Virus (VACV) is up to 80% and for Cowpox Virus Brighton Red (CPXV) is up to 50%. The superior virus inhibition capability should be attributed to the large contact area of the GNs and the strong binding activity of dPGS. Considering that dPGS itself showed no virus inhibition, it was believed that 2D GNs inhibitors were more effective for the prevention of pathogen adhesion and infection [259].

Mammalian cell and stem cell interactions

The mammalian cell interactions with the interfaces of graphene and GNs show some similarities to that of bacterial interactions, but there are more sophisticated phenomena. Like microbes, when contacting a mammalian cell, graphene will first interact with the phospholipid bilayers with cellular membranes. The sharp graphene nanosheet can cut into the lipids and penetrate cell membranes due to the strong hydrophobic interactions, which may result in physical membrane cutting (Fig. 16a) [266]. By simulation-assisted analysis, it has been demonstrated that there are four typical states in graphene-lipid bilayer interactions, including sandwiching into the lipid superstructure, adhering to and lying across the membrane, and finally forming hemisphere vesicles. It was found that this process was dependent on the size and oxidization of graphene [267]. Moreover, it was also reported that direct contact and uptake of graphene will increase cellular ROS levels [245]. To elucidate the induction of ROS by GO, three different kinds of redox-activated GO were investigated, such as the Mn^{2+} ions, C-centered radicals, and endoperoxides, using a human cervical cancer cell line as a model system [268]. For the first time, they revealed that endoperoxide of GO was responsible for the induction of ROS [268].

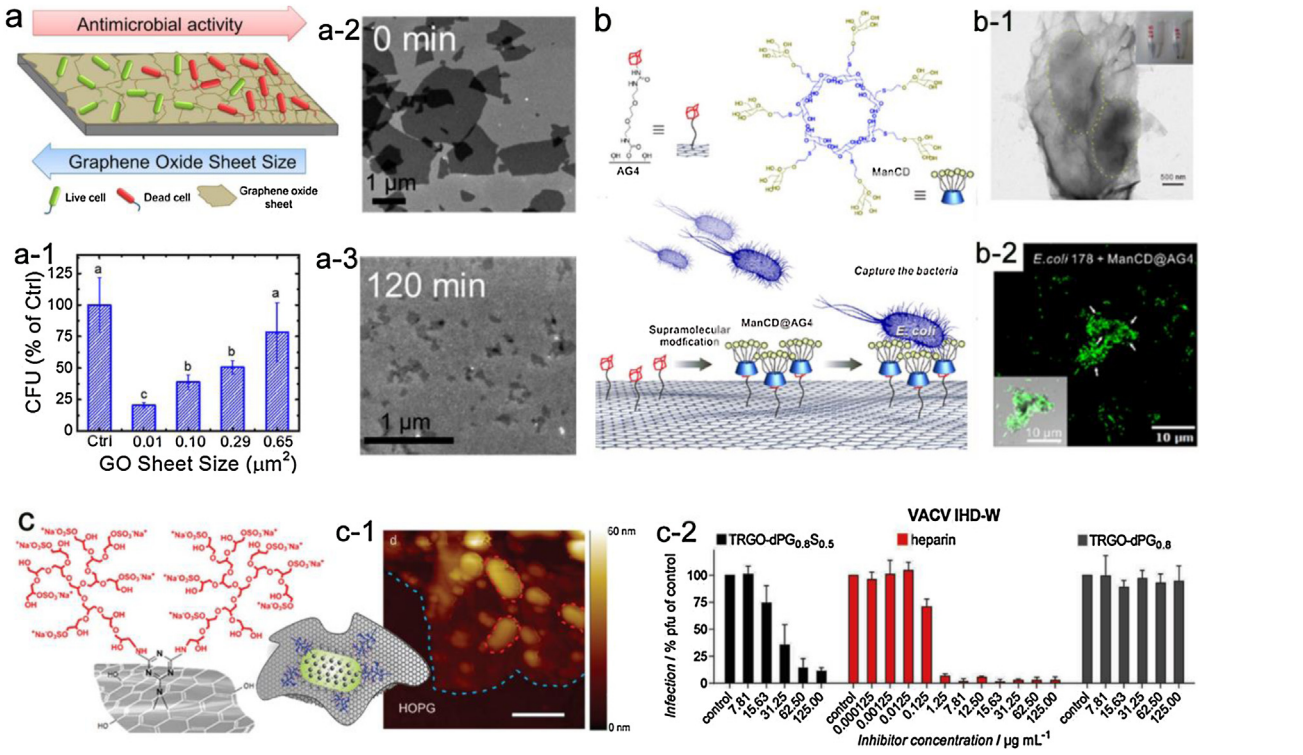

Fig. 15. (a) Size effects of the antibacterial activity of graphene. (a-1) The colony-forming units (CFUs) for bacteria cultured on the GO surface. (a-2, a-3) TEM images of the GO after sonication for different times with different sizes. Reproduced with permission. [256] Copyright 2015, American Chemical Society. (b) Schematic presentation of the binding of *E. coli* to a graphene complex in a multivalent interaction manner. (b-1) TEM and (b-2) confocal laser scanning microscopy (CLSM) of the graphene/*E. coli* binding, respectively. Reproduced with permission. [258] Copyright 2015, American Chemical Society. (c) Interaction between orthopoxvirus particles and RGO-dPGS. (c-1) AFM image of the RGO-dPGS/virus interaction. Scale bar: 200 nm. Reproduced with permission [115]. Copyright 2017, Wiley-VCH. (c-2) Inhibition of viral infection (VACV) in Vero E6 cells by RGO-dPGS. Reproduced with permission [44]. Copyright 2016, Wiley-VCH.

The interfacial interactions between G-BFNs and mammalian cells are considered to be size-, thickness- and surface chemistry-dependent. The cellular uptakes of protein-coated GO (PCGO) with different lateral sizes have been investigated as a model system [269]. It was noted that small PCGO entered cells mostly through clathrin-mediated endocytosis (CME), while large PCGO was taken up through both CME and phagocytosis. Recently, the effects of charge and lateral size on the uptake of HPG functionalized TRGO (TRGO-HPG) by mammalian cells were studied [113]. It was found that neutral TRGO-HPG tended to wander extracellularly regardless of size, while the introduction of either positive charges or negative charges could enhance cellular uptake but with different size effects, as shown in Fig. 16b. The uptake of GN sheets with positive charges occurred both through phagocytosis and CME pathways, regardless of size. In contrast, cellular uptake of negatively charged GN sheets was highly dependent on GN size.

For stem cells, the unique chemical and physical properties of graphene, GNs, and G-BFNs, such as high surface area, ROS scavenger, and high stiffness and conductivity, showed strong influences on stem cell adhesion, growth and differentiation. GNs has been found to be able to protect cells from hazardous molecules, such as hydrophobic molecules, siRNA, plasmid DNA and ROS [270,271]. Compared with bare MSC, it was noticed that MSCs protected by GO showed much higher survival after being subsequently exposed to ROS *in vitro* or implanted into ischemia damaged and reperfused myocardium, because GO prevented adverse cell signaling cascades during MSC responses to ROS [271]. The modified GNs with positive charges provide a very beneficial microenvironment for neurite outgrowth and branching of NSC compared with negatively charged or neutral nanosheets [272]. Notably, the GNs have obvious effects on stem cell adhesion, growth and differentiation via different pathways, for instance, GNs can adsorb ECM proteins and growth factors, thus controlling the cell adhesion and differentiation [273–275].

Additionally, GNs-based scaffolds are able to affect the cellular shape of stem cells because of the controlled formation of focal adhesion, which can lead to more obvious filopodial extensions and cellular protrusions [276]. Recent studies have revealed ECM-like GNs-based patterned structures can serve as a potential substrate to direct stem cell differentiation. For instance, the GO microstructures with combinatorial patterns (line or grid) to regulate the specific differentiation of human adipose-derived mesenchymal stem cells (hADMSCs) into osteoblasts or ectodermal neuronal cells, as shown in Fig. 16c-e [42]. On grid patterns, due to the mimicry to interconnected/elongated neuronal networks, the conversion to ectodermal neuronal cells of mesodermal stem cells reached 30%. In general, the high stiffness of GNs-embedded substrates can accelerate osteogenic differentiation, while the electrical conductivity stimulates signaling pathways to promote neural stem cell (NSC) differentiation [277]. Recently, the corresponding external electrical stimulation by using graphene based electroactive scaffolds for neurogenesis and myogenesis has been carefully discussed by Dong et al. [278].

Besides the external electrical stimulation, the photo stimulation are also important for affecting the cellular behaviors and functions for stem cells. By using light, the behaviors of the cells that adhere onto the G-BFNs can be affected and stimulated. Akhavan et al. have studied the effects of flash photo on the behavior of hNSCs on a RGO/TiO_2 heterojunction film [279]. With the light stimuli, more proliferated hNSCs were observed than the bare TiO_2, as well as more differentiation into neuron instead of glia. It was suggested that the accelerated neuron differentiation was caused by electron injection into cells through the RGO via the photocatalyst [280]. Later, the same group noticed that the pulsed laser could

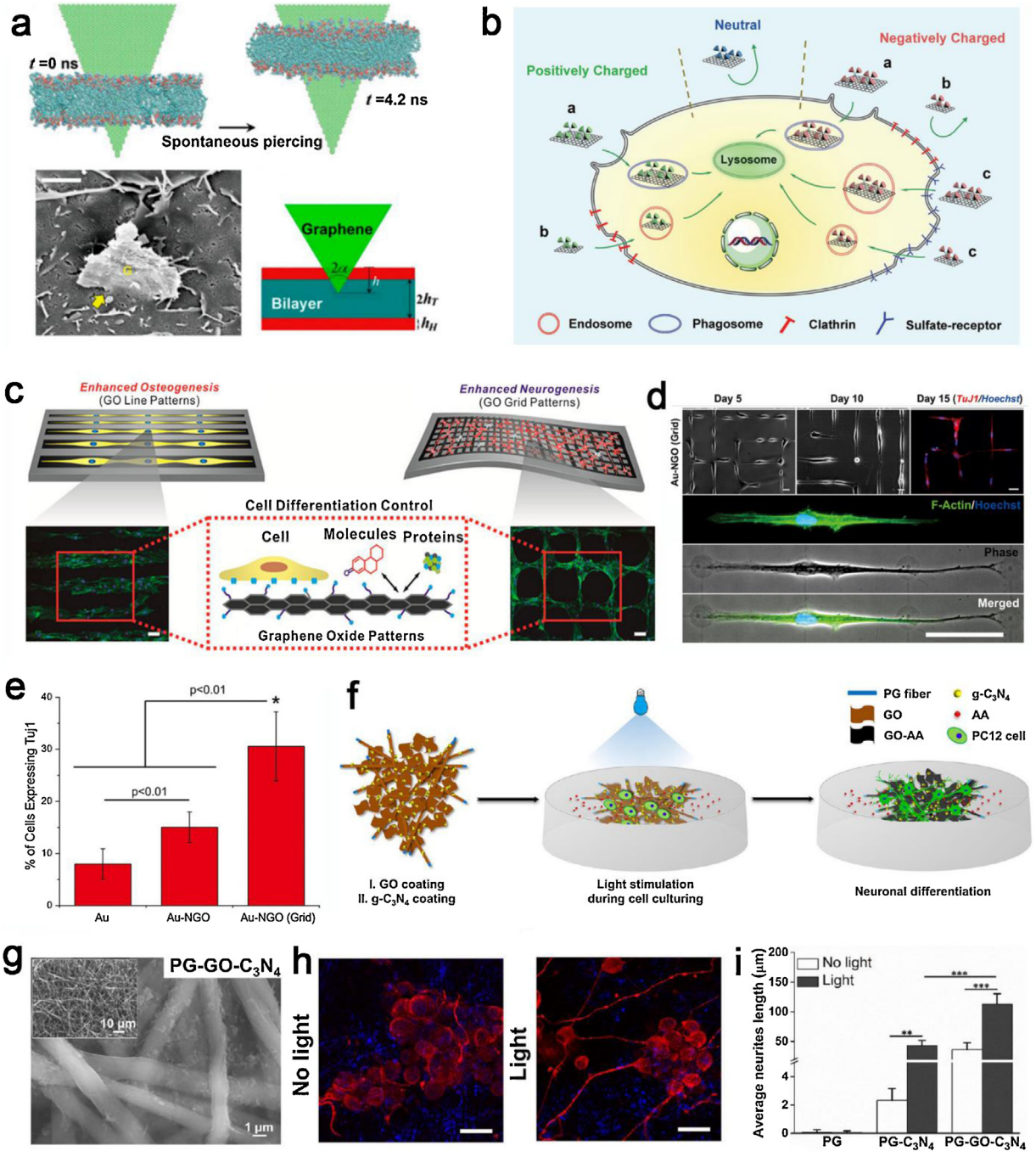

Fig. 16. (a) Simulations showing the piercing of graphene nanosheets into cell membrane and a corresponding SEM image. Reproduced with permission. [266] Copyright 2013, National Academy of Sciences. (b) Schematic illustration of cell uptake of different GO-HPG complexes. Reproduced with permission [113]. Copyright 2017, Wiley-VCH. (c) Schematic diagram illustrating control over the differentiation of hADMSCs using combinatorial graphene hybrid-pattern arrays. (d) Neuronal differentiation of hADMSCs on an NGO-coated Au grid. Scale bar: 20 μm (top) and 50 μm (bottom). (e) Quantitative comparison of the percentage of cells expressing the neuronal marker (TuJ1) on substrates. Reproduced with permission [42]. Copyright 2015, American Chemical Society. (f) Scheme image for the neural stimulation on the photocatalytic fibers, (g) SEM image for the photocatalytic fibers (PG-GO-C_3N_4), PG: GO-coated electrospun polycaprolactone (PCL)/gelatin. (h) Immunofluorescence picture for neural cells after 11 days on PG-GO-C_3N_4 with/without stimulation by visible-light. Scale bars: 20 μm. Red: anti-β III tubulin, blue: DAPI. (i) The average neurite length for the neural cells on different substrates. Reproduced with permission. [282] Copyright 2017, American Chemical Society.

also promote the hNSCs' differentiation into neurons instead of glia on the surface of RGO sheets, which was believed to be resulted from the radial stress originated from the pulsed laser [281]. Very recently, Zhang et al. have reported that the visible-light can also be used for neural stimulation on the photocatalytic fibers made by graphitic-carbon nitride/graphene (Fig. 16f-i) [282]. It is interesting to find that the g-C_3N_4 can serve as a biocompatible photocatalyst to generate electrons. Meanwhile, the graphene based photocatalytic fibers demonstrate promising potential to serve as a visible-light neural stimulator on improving the proliferation of neural cells in a spatiotemporal-specific manner [282].

Bio-adhesive molecules enhanced interfacial biointeractions and functionalities

To enhance the cellular compatibilities and interfacial activities of graphene/GNs doped biomedical materials and devices, the interfacial anchoring of universal or specific cell-adhesive-molecules are quite favored to enhance the cellular interactions

and functionalities, especially for the tissue engineering scaffold, to which the adhesion of cells at the interface is quite important for cell proliferation and tissue regeneration [191]. To achieve a cellular adhesive surface, graphene has been integrated with many kinds of molecules, such as peptides (e.g., RGD), proteins (e.g., fibronectin, biotin, collagen, gelatin), polysaccharides (e.g., heparin, chitosan, HA) [4].

The RGD molecule is one of the most commonly used peptide motifs to enhance interfacial cell-adhesive capability, which binds to integrins on cell surface, including fibronectin, fibrinogen, vitronectin and osteopontin [283,284]. RGD anchored GO-PNIPAM hybridized scaffold has been fabricated for the efficient capture and on-demand release of targeted cells via a NIR stimulus [119]. In the study, RGD promoted the adhesion of cells onto the hydrogel, while GO served as a NIR light-responsive nano-platform to induce the "on-off" switch for on-demand control of targeted cell capture and release. It was found that the incorporation of RGD could significantly increase the affinity of the GO/PPO-PEO hydrogel towards osteoblastic cell line MC3T3-E1, which could be potentially used as tissue scaffolds or injectable drug release systems [285]. Besides RGD, the fibronectin (FN) functionalized RGO had also been investigate for the interactions with MSCs, it was found that the cell-ECM interactions in the MSC spheroids could be enhanced by introducing FN-RGO nanoagents, as shown in Fig. 17a. The immune staining tests show that the FNs are homogenously distributed in the hybrid MSC spheroids, which can provide strong cell-ECM interactions (Fig. 17b). The western blot analysis revealed that the expression of integrin β1, an FN-interacting integrin, was enhanced obviously in the FN-RGO hybrid MSC spheroids due to the enhanced paracrine factor expression and electrical conductivity of RGO (Fig. 17c). [273]

However, RGD and FN are too expensive for large-scale use, such as therapeutic hydrogels. Collagen and gelatin moieties have been proposed to exhibit a similar bioadhesiveness to RGD. Khademhosseini's group presented an approach to prepare cell-adhesive hydrogels using GO and gelatin methacrylate (GelMA) [286]. First, the methacrylate GO (MeGO) was synthesized and then conjugated to GelMA to form a 3D hydrogel network by UV irradiation with encapsulation of living cells. Interestingly, they found that the fibroblasts encapsulated in GO-GelMA and MeGO-GelMA hydrogels exhibited higher viability than those encapsulated in bare GelMA hydrogels, which suggested that the presence of GO protected the cells from the harmful environment during the crosslinking reaction. The developed GO-GelMA hydrogel could be used for various kinds of tissue regeneration studies, such as the layer-by-layer assembly of cells for the fabrication of 3D tissue constructs (Fig. 17d-f) [287]. and also be used to fabricate the cell-laden hydrogels into micro-fabricated blocks, microspheres, and hexagonal and microchannel patterns (Fig. 17g-i). It was noticed that the GO-GelMA hydrogels could effectively support cellular adhesion, spreading and alignment with enhanced viability and proliferation in the layered composites and also 3D hydrogel microenvironment [287,288].

Representative applications of G-BFNs-based bio-platforms

In the above sections, we have discussed the general paradigms, synthesis, and biointeractions of functional GNs with a focus on the design of G-BFNs-based favorable bio-platforms with good bioactivities, functionalities and bio-adaptability. Due to diverse formulation and versatile functionalization protocols of graphene and GNs, these G-BFNs-based nano-/super-structures, including nanomedicine, surface coating, 3D hydrogels, and composite scaffolds, have established promising potential in diverse kinds of biological and biomedical applications, such as drug and gene delivery, PTT and PDT treatment, bioimaging and cancer theranostic, bacteria and virus inhibition, tissue regenerative scaffolds, and monitoring biosensors, as discussed in the following sections and listed in Table 2.

Smart carriers for nanomedicines

With carbon atoms evenly distributed on the surface, graphene and GNs show abundant binding sites for molecule uptake, including but not limited to genes, proteins and aromatic drugs. Inspired by the success of carbon nanotube as drug delivery vehicles, graphene had been exploited as carriers to load anti-cancer drugs including DOX, camptothecin, SN38, ellagic acid, β-lapachone and curcumin [31]. Typically, in 2008, Dai's group found that PEGylated GO showed physiological stability and solubility and was used to deliver water-insoluble aromatic anticancer medicine via π-π stacking [154]. Via the EPR effect, drug-loaded GO was able to overcome biological barriers and resulted in superior therapeutic efficacy compared with bare drugs. In addition to chemotherapy drugs, gene therapy has emerged as a promising treatment for many fatal diseases. Later, the GO-PEI nanocomplexes via simple electrostatic interactions have been synthesized for gene transfection with limited cell cytotoxicity compared to bare PEI [151].

To effectively deliver drug/gene to the desired area, active targeting and controlled release adapted to tumor conditions are highly required, which have been achieved by combining graphene or GO with smart polymers/nanomaterials. The biological environment in the cancerous area is different from normal tissues, exhibiting a higher temperature, lower pH and more redox effects. Therefore, GNs based carriers with high adaptabilities to tumor environments have been developed for the passive targeted release of therapeutics, for instance, a redox-responsive G-BFNs-based nano-carrier is synthesized by disulfide bonding of PEG [302]. In cancer cells, glutathione breaks the disulfide linkage and triggers the detachment of PEG, as well as the release of DOX from GNs. However, applying an additional stimulus to actively guide drug release has also been developed with light, magnet, electrical field and ultrasound. For example, with the guidance of a magnet, GO/Fe_3O_4 could selectively accumulate in tumors, thus avoiding the nonspecific release of drug, as shown in Fig. 18a-f [296]. Such nanocomposites integrate the functionalities of MRI, PTT and drug delivery, which not only allows the tracking of the distribution of GO/Fe_3O_4 and drug release in biological systems but also boosts tumor ablation in terms of synergistic effects. For the electrical stimulation, the GO and polypyrrole (PPy) nanocomposite was designed for electrically controlled drug release system [303]. By applying an electric field, the nanocomposite based film was electrochemically reduced, and the anionic dexamethasone previously associated with PPy was released as the charges of PPy were neutralized.

Photothermal and photodynamic for cancer therapeutics

PTT is a recently developed anticancer strategy that employs a light-active agent to create heat with light irradiation, preferably NIR irradiation, with superior tissue-penetrating efficiency, resulting in ablation of the targeted cells [53]. In pre-clinical research and clinical practices, PTT has attracted numerous interest because it can be fixed to the area of interest. In terms of light-absorbing agents, compared with other PTT nanoagents (Table 3), graphene and GNs with atomic thickness exhibited high photo-to-thermal conversion efficiency within a therapeutic window (700–900 nm) [304]. *In vivo* graphene-based PTT nanoagents have also been discovered in recent years and achieved excellent tumor inhibiting efficiencies. After intravenous injection, the GNs-based nanoagents can accumulate in highly passive tumors due to the EPR effect of cancerous tumors; after laser irradiation, GNs-based nanoagents

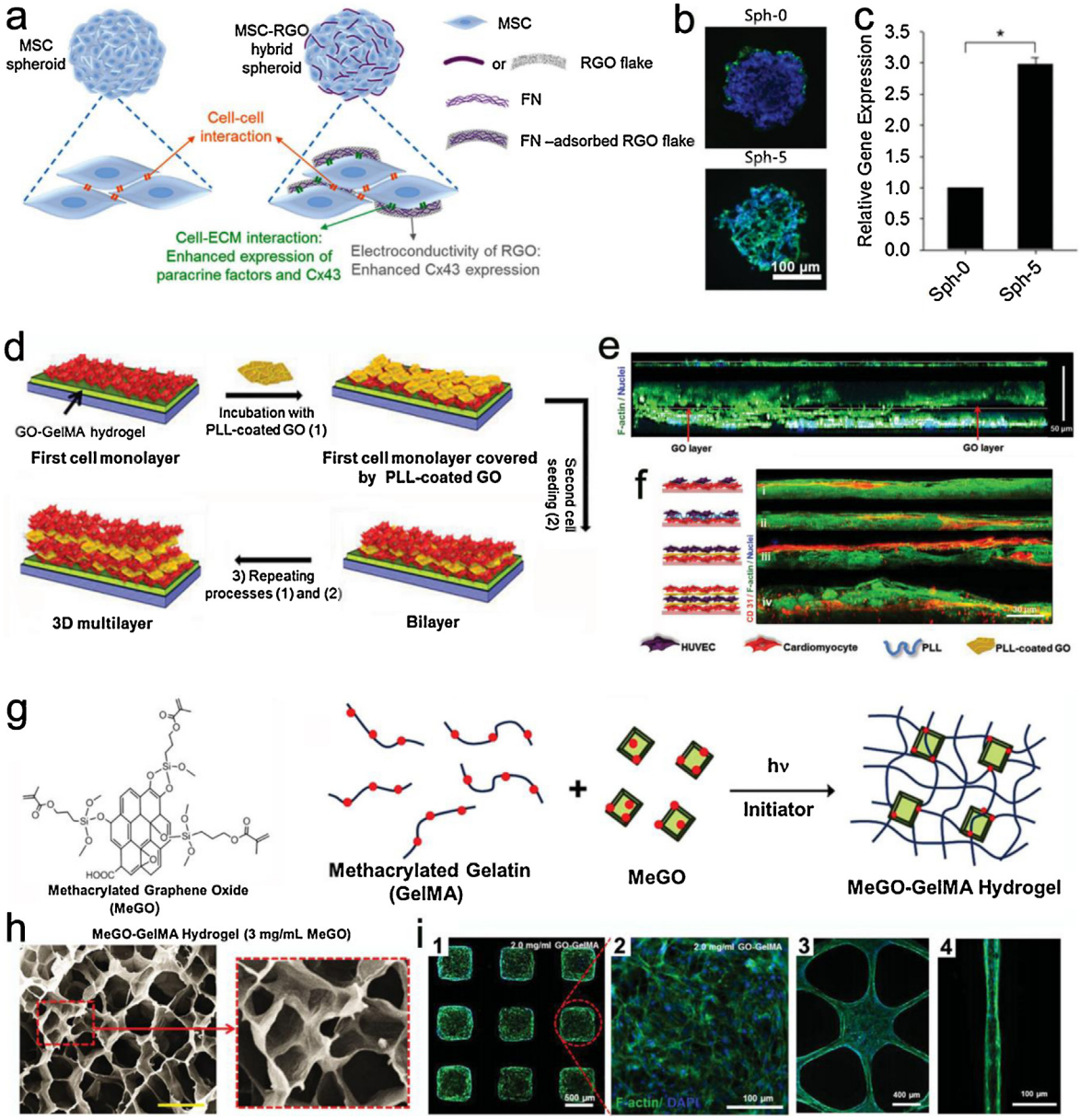

Fig. 17. (a) Schematic image for the FNs-RGO and its influences in MSC spheroids. (b) The immunohistochemistry tests for FN in the FNs-RGO added MSC spheroids. (c) The expression of integrin β1 in the hybrid spheroids tested by western blot analysis. *$p < 0.05$. Reproduced with permission [273]. Copyright 2015, Wiley-VCH. (d) Fabrication of layer-by-layer GNs/cell-based multilayer cardiac tissue. (e) Confocal cross-sectional images of the control group (top) and the 3L tissue constructs (bottom) after 2-days of culture. F-actin and cell nuclei were labeled with green and blue fluorescent dyes respectively. (f) Schematic illustration (left) and 3D reconstructed confocal cross-section images (right) of the twolayer GNs-cardiomyocyte hybrid construct. Reproduced with permission [287]. Copyright 2014, Wiley-VCH. (g) Chemical structure of MeGO and MeGO-GelMA hydrogel formation by photoinitiated crosslinking of GelMA and MeGO. (h) SEM images of freeze-dried MeGO-GelMA hydrogel. Scale bar: 200 μm. Reproduced with permission [286]. Copyright 2014, Wiley-VCH. (i) Cellular behaviors of NIH-3T3 fibroblasts encapsulated in the constructed GO-GelMA hybrid scaffold (1, 2) microfabricated blocks; (3, 4) hexagonal and microchannel patterns. (5) A microfluidic system to fabricate GO-GelMA (1.0 mg/mL) microbeads. Reproduced with permission [288]. Copyright 2013, Wiley-VCH.

would then generate massive heat and cause effective cancer cell death [305].

Due to the week NIR adsorption capability, most of the GO-based nanoagents show limited efficiency in PTT treatment. It was revealed that the reduction of GO could dramatically enhance the optical absorbance for GO in the NIR region, the resulted RGO-based nanoagents showed nearly twice the photo-thermal conversion efficiency of GO-based one [81]. After conjugation with cell-adhesive RGD peptide, such a nanoagent could act as a targeted PTT agent for selective tumor cell ablation. Recently, bioactive polymers decorated GNs have been synthesized for enhancing the targeted tumor therapy. The NGO/hyaluronic acid has been proposed to serve as PTT nanoagents in melanoma treatment, one of the most fatal skin cancers, as shown in Fig. 19a [314]. Hyaluronic acid facilitated the transdermal delivery of NGO, while upon NIR, NGO generated heat for cancer cell ablation. To further enhance the NIR adsorption efficiency of GNs-based nanoagents, the Au nanoparticles are integrated with RGO and DOX together into the liposome as a sequential chemo and photothermal cancer therapy nano-platform, such a nano-system can achieve synergic effects for cancer therapy and also higher efficiency [315].

As another effective light-triggered anticancer strategy, PDT employs a photosensitizer to generate ROS under light irradiation

Table 2
Representative biofunctionalities and potential applications of diverse bio-adaptable and biomimetic GNs.

GNs	Biofunctionalities	Applications	Ref.
Bulk GO, RGO and GQD	1 Absorbing biological molecules, e. g. proteins, RNA and DNA. 2 Attaching to and penetrating the membrane of bacterial and mammalian cells. 3 Generating ROS. 4 Bioimaging and biosensing signals. 5 Guiding neuron differentiation of stem cells. 6 Catalyzing reactions by mimicking enzymes.	Antibacterial/virus materials, biosensing, tissue regeneration, monitoring biosensors etc.	[45,251,255,289,290,291,292]
GO, RGO/hemin, Au, Pt etc.	1 Catalyzing reactions like enzymes, e. g. peroxidase. 2 Detecting biosignals. 3 Generating ROS from H_2O_2.	Biosensing, antibacterial materials.	[132,133,134,135]
GO, RGO, GQD/PEG	1 Minimized non-specific interaction with biological systems. 2 EPR effects of tumor cells. 3 Active targeting after ligand modification. 4 Generating heat by NIR. 5 Loading and delivery of drugs.	Drug delivery, PTT, PDT, bioimaging, tissue regeneration etc.	[24,81,108,285,293,294]
GO, RGO/PG, dPGS	1 Different interactions with cells for different charges and sizes. 2 Guiding neural differentiation of hADMSCs. 3 Binding and inhibition of orthopoxvirus.	Drug delivery, PTT, tissue regeneration, virus inhibition etc.	[44,113,114,115]
GO/Chitosan	1 Promoting adhesion and proliferation of various kinds of cells. 2 Integrated antibacterial activity. 3 Loading and delivery of genes.	Wound dressing, tissue regeneration, drug and gene delivery.	[104,106,107,148]
GO/Heparin, heparin-like polymers	1 Increased affinity to endothelial cells. 2 Increased blood compatibility in terms of prolonging clotting times, inhibiting platelet adhesion and activation, and suppressing coagulate activation. 3 Removal of blood toxins.	Blood purification, tissue engineering, drug delivery.	[144,183,239]
GO/Gelatin	1 Adhesive to various kinds of cells and tissues. 2 Promoting cell growth and tissue regeneration. 3 Loading and delivery of growth factors, drugs, and genes.	Tissue regeneration.	[43,286,287,288]
GO, RGO/Ag	1 Integrated antibacterial activity. 2 Generating heat by NIR.	Antibacterial materials.	[48,295]
GO/Fe_3O_4	1 On-demand manual targeting by magnetic field. 2 Magnetic resonance imaging (MRI). 3 Generating heat by NIR.	Drug delivery, PTT, bioimaging.	[182,296,297]
GO, RGO/Ce6, GNs-ZnO etc.	1 Generating heat and ROS by light/laser. 2 Delivery of drugs and genes. 3 Bioimaging signals.	PTT, PDT.	[292,298,299,300]
GO, RGO/Collagen, HAp etc.	1 Promoting osteoblast proliferation and differentiation. 2 Matching to the nanostructure and mechanically properties of bone.	Bone regeneration.	[129,131,177,301]

to destroy cells. The produced ROS show several detrimental effects toward cells, including a decrease in mitochondrial membrane potential, oxidization of cellular enzymes, and increased malondialdehyde production, eventually inducing cancer cell apoptosis [304]. The developed photosensitizers are mostly hydrophobic and tend to aggregate in water, which leads to a decrease in quantum yield. Thereby, G-BFNs can play as carriers in the delivery of photosensitizers to tumors, for instance the Ce6 and folic acid conjugated GO could selectively kill foliate receptor-positive cancer cells under 633 nm light irradiation [298].

Besides the photosensitive dyes, the intrinsic PDT activity of GQDs has also been reported [251]. GQDs could produce highly reactive $^1O_2$ via a multistate sensitization process with a quantum yield of approximately 1.3, which is higher than any other organic photosensitizers [251]. Although high $^1O_2$ generation was only observed in the visible light region, the GQDs were still satisfactory for the treatment of skin cancers. Moreover, the GQDs exhibited superiority, including good water dispersibility, high pH and photo stability and good biocompatibility. To achieve PDT effects in deep tissues, the GQDs are combined with rare-earth doped upconversion nanoparticles (UCNPs), as shown in Fig. 19b-d [299]. Under NIR, the UCNPs could emit UV–vis light, which further excited GQD to produce $^1O_2$. The functionalization of GQDs/UCNPs using a hydrophilic rhodamine derivative, TRITC, further promoted the mitochondrial-targeting properties. Therefore, mitochondrial-targeted $^1O_2$ generation induced a significant decrease in mitochondrial membrane potential and subsequently initiated irreversible cancer cell apoptosis.

Although considerable progress has been made using PTT or PDT nanoagents for cancer treatment, to date, the sole model ther-

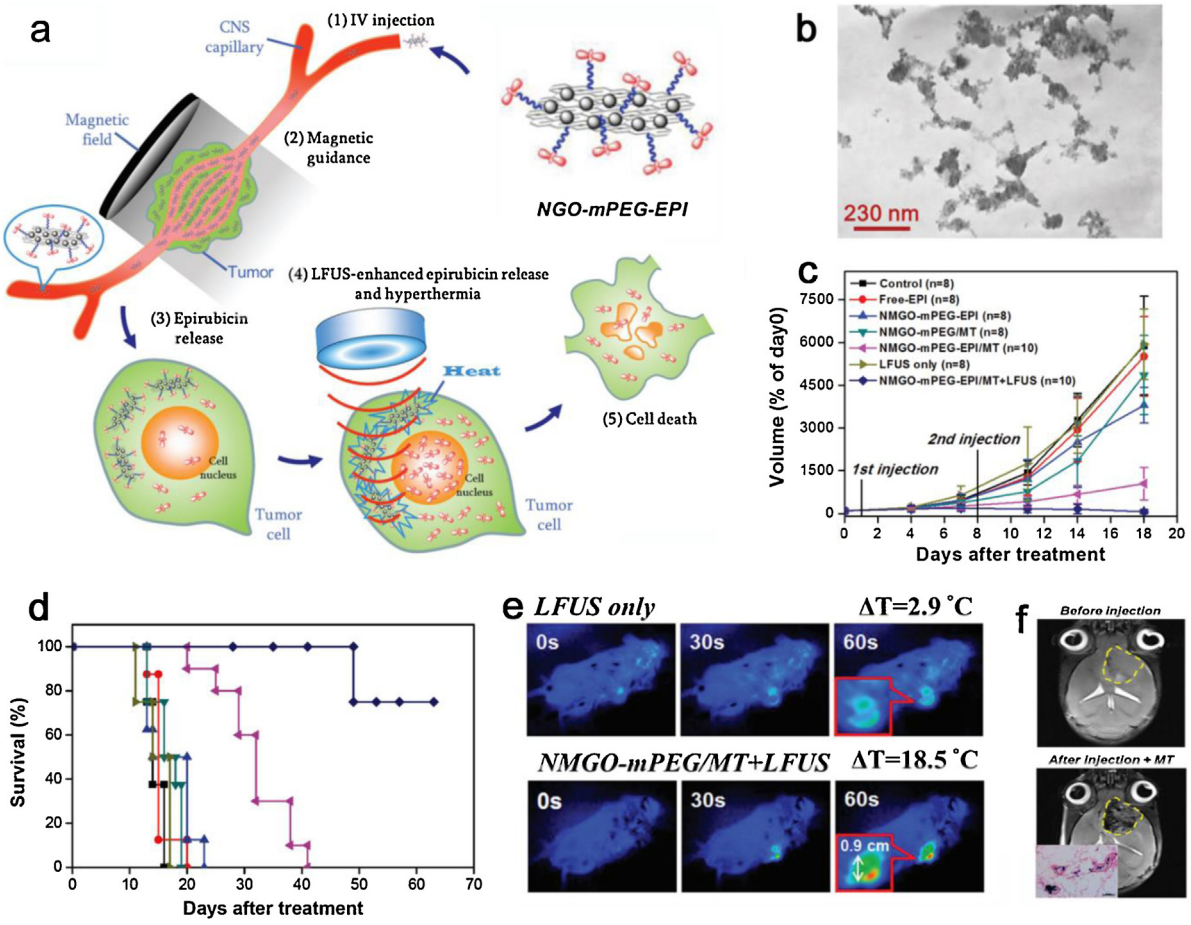

Fig. 18. (a) The mechanism of action of NGO-mPEG-epirubicin (NGO-mPEG-EPI) for magnetic-guided cancer therapy and low-density focused-ultrasound (LUFS)-induced hyperthermia. (b) TEM images of NMGO-mPEG. (c) Tumor sizes and (d) survival curves of mice bearing GL261 tumors after different treatments. (e) Thermal images of tumors in mice after the indicated treatments (LFUS: 2 W; laser: 2 W/cm^2). (f) T_2-weighted MRI for the tissue distribution of NMGO-mPEG-EPI in brain tumors before and after injection and magnetic targeting (0.4 T) for 36 h (inset: Prussian blue staining). Reproduced with permission. [296] Copyright 2013, Wiley-VCH.

Table 3
Summary of mostly studied PTT nanoagents and their remarks, the heating profiles are compared by the increased temperatures after NIR irradiation.

Phototheraml agents	Typical heating profiles	Remarks	Ref.
Gold nanoparticle	Increased 60 °C, 24 mM, 1.20 W/cm^2, 5 min.	1 The size of gold nanoparticle can be easily controlled. 2 Gold shows good biocompatibiolity.	[306]
Gold nanorod	Increased 60 °C, OD_{808} = 1*, 0.8 W/cm^2, 5 min.	1 The gold nanorod is stable in physiological condition and can be readily cleared.	[307]
Pd nanosheet	Increased 24 °C, 26.0 ppm, 2 W/cm^2, 5 min	Pd nanosheet shows good stability under laser irradiation and exhibits potential for image guided PTT.	[308]
Semiconductive copolymer-C60	Increased 30 °C, 15 μg/mL, 0.50 W/cm^2, 5 min.	The nanoparticle shows good structural flexibility and synthetic simplicity.	[309]
Indocyanine green	Increased 30 °C, 200 μg/mL, 1.00 W/cm^2, 5 min.	1 Indocyanine green is approved for clinical usage. 2 Indocyanine green can be rapidly excreted by renal excretion.	[310]
Polyaniline nanoparticles	Increased 50 °C, 500 μg/mL, 2.45 W/cm^2, 3 min.	Functionalized polyaniline nanoparticle is water-dispersible and shows good colloid stability.	[311]
Polypyrrole nanoparticles	Increased 35 °C, 40 μg/mL, 2 W/cm^2, 10 min.	Functionalized polypyrrole nanoparticle exhibits good colloid stability and photostability.	[312]
Carbon nanotube	Increased 40 °C, 140 μg/mL, 3.80 W/cm^2, 3 min.	Functionalized carbon nanotube can serve as multimodal therapeutic platform.	[313]
GO RGO	Increased 15 °C, 10 μg/mL, 0.60 W/cm^2, 5 min. Increased 30 °C, 20 μg/mL, 0.60 W/cm^2, 8 min.	1 RGO shows higher photothermal efficiency than GO. 2 Functionalized RGO is a versatile nanoplatform for drug loading and bioimaging agents.	[81]

* In this study, the concentration of AuNR is expressed at optical density at 808 nm (OD_{808}).

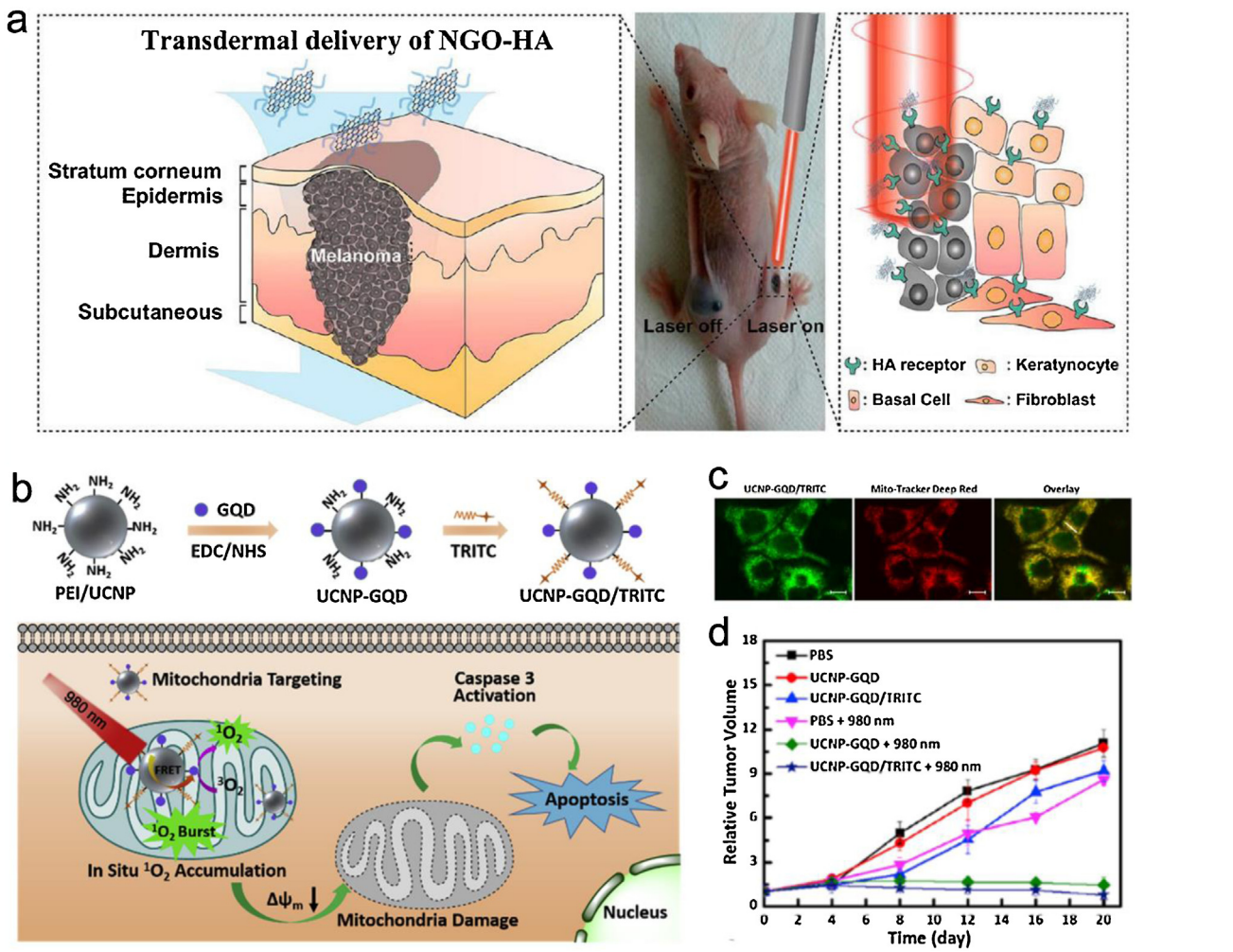

Fig. 19. (a) Schematic of the transdermal delivery of NGO-hyaluronic acid (NGO-HA) into melanoma cells and subsequent PTT therapy using NIR. Reproduced with permission. [314] Copyright 2014, American Chemical Society. (b) Fabrication of mitochondria-targeting UCNP-GQD/TRITC. (c) Mitochondria-targeting efficiency by fluorescence microscopy. (d) Growth curves of 4T1 tumors in each group. Reproduced with permission. [299] Copyright 2018, Elsevier Ltd.

apy still suffers from poor therapeutic efficiency, especially when cancer cells gradually develop resistance to the drugs [316]. One of the most promising coping approaches is to integrate multiple strategies together as a multimodal nanomedicine [26]. Multifunctional nano-systems based on G-BFNs that integrate drug/gene delivery, PTT, and PDT have been developed, in which G-BFNs work as a drug-loading vehicle and PTT/PDT agent. It was demonstrated that the Ce6 loaded GO-PEG nano-platform could generate $^1O_2$ under laser irradiation, thus serve as PTT/PDT dual therapy for cancer cells [24]. Meanwhile, it is interesting to find that the GO-PEG induces mild local heating under NIR irradiation, which thus promotes the uptake of GO-PEG/Ce6 by increasing cellular membrane permeability rather than killing cells, further enhancing the efficiency of PDT against cancer cells in terms of intracellular delivery. Besides the organic dye, the inorganic ZnO nanoparticles had also been integrated with RGO to generate electron-hole pairs upon light illumination and produce ROS, thus yielding a sequential irradiation-activated apoptotic therapy platform [292]. Light was first applied to induce ROS generation by ZnO, and then, NIR was used to induce heat generation by RGO. Such a platform caused much higher cancer cell death than solo treatment. There are many other formulations of multifunctional G-BFNs based on integrated therapy, which has been summarized in Table 2.

Biological imaging nanoagents

Fluorescent species in the NIR and infrared range are very useful for biological applications because cells do not exhibit auto-fluorescence in this region. Owing to the strong photoluminescence (PL) in the NIR and infrared range, GNs have established applications in biomedical imaging, especially luminescent GQDs [317,318]. Compared with conventional metal-based quantum dots with potential harm to health and the environment, GQDs show superior performance in bio-imaging due to their strong PL properties and reduced toxicity. For instance, the one-step solvothermal method has been proposed to synthesize strongly fluorescent GQDs, the resulting GQDs exhibited a quantum yield up to 11.4% and could be dissolved in many kinds of solvents with high stability, such as water, ethanol, THF, acetone, DMF and dimethyl sulfoxide [87]. Owing to the low toxicity and high PL yield, the GQDs could be recognized as a "green" material as well as satisfactory bio-labeling agents. To solve the problem of low production ratio of GQDs in solvothermal method, a deflagrating carbon-rich materials strategy has been developed to produce GQDs on a gram-scale, as shown in Fig. 20a [289]. The prepared GQDs had a diameter of approximately 10 nm and presented strong fluorescence with strong emission at 570 nm with 460 nm excitation, which could be used as an excellent probe for cellular imaging (Fig. 20b-d).

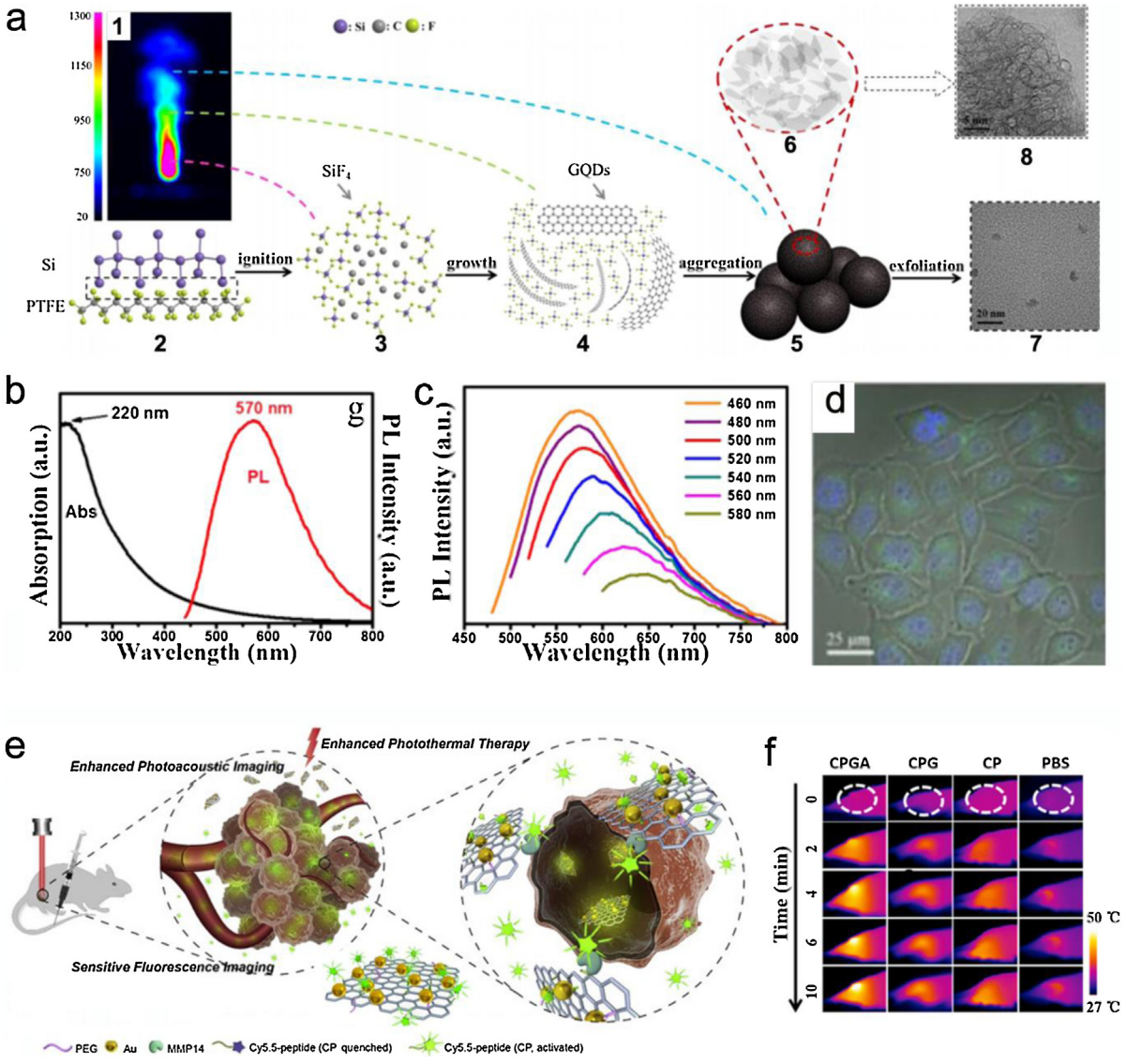

Fig. 20. (a) Synthesis of GQDs on a gram scale by deflagrating carbon-rich materials. (b) UV – vis (black) and PL (excitation: 400 nm, red) spectra of the GQDs. (c) PL spectra of GQDs with different excitations. (d) Fluorescence image of HeLa cells with GQD staining. Reproduced with permission. [289] Copyright 2015, American Chemical Society. (e) Illustration of Cy5.5-labeled matrix metalloproteinase-14 (CP) substrate-conjugated GO/Au (GA) to produce CPGA as a theranostic probe for image-guided PTT. (f) Thermal images of the samples under NIR irradiation. Reproduced with permission. [319] Copyright 2016, Elsevier Ltd.

For the development of MRI nanoagents, superparamaganetic iron oxide nanoparticles (IONPs) have captured extensive interest as a contrast agent. IONPs can induce local magnetic field inhomogeneity and cause a decrease in regional signal intensity by shortening T_2 relaxation, and the GO-IONP nanohybrids have been successfully used for bioimaging applications [320]. It is found that loading IONP on GO platform can significantly prevent the aggregation of IONP *in vivo* and thus prolong the circulation time in blood. After further surface decoration with dextran, the modified IONP/GO nanocomposite was found to possess even better colloidal stability and smaller cytotoxicity [321]. Moreover, the nanoagents showed significantly improved cellular MRI with the ability to detect cells at a Fe concentration of 20 μg/mL and cell density of 2×10^5 cells/mL, or 5 μg/mL and 1000 cells/mL. Under the guidance of imaging, it was noticed that the tumors treated with the nanohybrids were effectively ablated upon NIR irradiation at 0.5 W/cm^2.

The versatile chemical and physical capabilities of graphene and GNs enable the combination of diagnosis with therapy to form clinically adaptable formulations for targeted drug delivery, visualization of drug release, and therapeutic efficacy, namely, "cancer theranostic" [305]. Thus far, imaging modalities that have been incorporated in G-BFNs-based nano-platforms include fluorescence imaging, computed tomography (CT), positron emission tomography (PET), MRI, NIR imaging and photoacoustic imaging. As a representative example, the CdSe/ZnS quantum dot-tagged RGO nanocomposites (RGO/CdSe/ZnS) have been synthesized for combined fluorescent imaging and PTT [294]. In such a system, the heat generation by NIR increased the temperature and decreased the quantum dot brightness, providing a nano-platform for *in situ* sensing heat/temperature and monitoring PTT progress simultaneously. Recently, the photoacoustic imaging, sensitive fluorescence imaging and PTT have been combined together by loading Cy5.5-labeled matrix metalloproteinase-14 substrate on a GO/Au nanocomposite, as shown in Fig. 20e, f [319]. The fluorescence of Cy5.5 was initially quenched by GO/Au, but after degradation by metalloproteinase-14, it was released from GO/Au and boosted strong fluorescence signals. After intravenous administration, strong fluorescence and photoacoustic signals were detected for the tumor, and a peak signal was obtained after 6 h.

Antibacterial and virus inhibition nanoagents

Anti-pathogen materials are gaining increasing interest worldwide due to the growing demand for an effective strategy to fight bacteria and viruses. As a versatile nano-platform for the loading of antibacterial agents, GNs have been developed as efficient nanoagents after the incorporation of antibiotics, cationic polymers and metal nanoparticles. For example, silver nanoparticles (AgNPs) have a long history of use for sterilization, and nanocomposites of AgNPs-GNs provide more robust antibacterial capabilities due the increased colloidal stability and synergistic antibacterial effects [174,295]. However, the fast releasing of Ag^+ ions and high toxicity of AgNPs remain a limitation to their biomedical applications. To overcome this problem, recently, a polymer shell protection strategy has been created to decrease the silver oxidation and ions releasing speed, as shown in Fig. 21a. By coating a mussel-inspired sodium alginate sulfate (SAS) on the GO/AgNPs (Ag@G-SAS), the cellular toxicity of Ag@G-SAS was significantly reduced, while robust antibacterial activity was maintained. The antibacterial activity was further boosted by NIR, the Ag and GO together converted NIR irradiation into heat to ablate the bacteria (Fig. 21a-1, a-2). The prepared Ag@G-SAS could be used as a wound dressing spray or surface antibacterial coating for biomedical devices. Due to the shielding effects of sodium alginate sulfate, a surface that is capable of inactivating bacteria, good cellular and blood compatibility has also been obtained [48].

As mentioned in the section 4.2.1, there are strong interactions between GNs and bacteria, for instance GN-based nanoagents can cut into bacterial membranes and cause the release of intracellular contents due to their blade-like shape [56]. Moreover, the GNs can also increase the ROS level for the microbes, leading to inactivation, which can generate oxygen free radicals with light excitation [56,322,323]. It was noticed that GQDs could act as artificial enzymes to catalyze the conversion of H_2O_2 into more bactericidal HO•, as shown in Fig. 21b. Thus, effective killing of bacteria could be achieved at low H_2O_2 concentrations, avoiding the toxicity of a high H_2O_2 dosage (Fig. 21b-1,b-2) [324]. This GQDs-based antibacterial agents have been examined as coating layer for Band-Aid, as shown in Fig. 21c,c-1,c-2. It was found that these Band-Aid could be used for mouse skin disinfection with very efficient bacterial inhibition and wound healing [324]. Compared with antibiotics that are currently limited by environmental pollution, high production costs and emerging antibiotic resistance, these G-BFNs-based antibacterial nanoagents are considered to be a green antibacterial strategy and have attracted great interest [325].

GNs are also recognized as novel nanoagents for viral inhibition and blocking. Compared with polymeric viral inhibitor, either a linear or hyperbranched polymer, GNs have the advantages of large surface area and flexible nanostructure, which facilitate the interaction and wrapping of the virus at approximately 100 nm. It was reported that GO can capture and inhibit virus, meanwhile, it had been validated that both the surface functional groups and the large surface area are essential for virus binding [326]. In another study, the curcumin loaded β-CD/GO nano-platform was reported for the inhibition of respiratory syncytial virus, of which the CD molecules not only facilitated the loading of anti-viral curcumin but also enhanced the interaction and binding with virus [327]. Recently, the multivalent polymers functionalized GNs-based inhibitors with enriched binding groups on the surface have also been reported by Haag's group [44,115,328]. The grafted dPGS could enhance the binding efficiency to the virus surface via electrostatic interaction. The multivalent presentation of sulfate groups on the RGO surface promoted efficient binding to the virus. When contacting a virus, such as orthopoxvirus, RGO-dPGS wraps the virus surface and inhibits viral infection of normal cells.

Stem cell controlling and tissue regeneration

Stem cell controlling and electrical stimulation

The design of highly bioactive scaffolds to direct stem cell differentiation has become critical in tissue engineering. A major drawback for using nanomaterials for stem cells based scaffolds is their potential cell toxicity and lack of biological cues to induce suitable bioactivities or electronic-cellular interactions [114,329]. In the past years, G-BFNs have emerged as important nanomaterials in the search for ideal scaffolds due to their versatile biointeractions and good compatibility with stem cells, as described section 4.2.2. For instance, in a recent study, a multivalent and bioactive polymer functionalized RGO (HRG-HPGS) was utilized to construct tight, uniform, and ultrathin carbon layers coated nanofibrous scaffolds for the growth, orientation, and differentiation of hADMSC, as shown in Fig. 22a-d [114]. The results of live-dead staining indicated that the HRG-HPGS-coated nanofibers showed good cytocompatibility, which was even comparable to the TCPS surface. The stem-cell orientation activity of the bare and GNs coated aligned poly(ε-caprolactone) (PCL) nanofiber (PCL-A) was investigated (Fig. 22c,d). The PCL-A-HRG-HPGS nanofibers exhibited uniform cell alignment along with the fiber direction with an orientation angles within ±10°, and cells showed much larger cell extending length compared to the other surfaces [114]. Thus, the HRG-HPGS is able to serve as exclusively biocompatible and bioactive coating reagents for G-BFNs-based nerve, cardiac, and tendon scaffolds.

Besides the polymer functionalized GNs, the nanoparticles-GO co-assembled substrate had also been systemically investigated for the effects on the differentiation of NSCs [330]. As shown in Fig. 22e-g, the differentiated NSCs exhibited well-aligned and well-extended axons on GO-coated surfaces, but not on glass and bare silica nanoparticles. It was demonstrated that the engineered nano-topographical GO surface showed instructive physical cues to enhance neuronal differentiation of NSCs with obviously aligned axons, which presented tremendous potential for neural tissue regeneration. Besides the orientation activity of the GNs coated substrates, the GO-decorated nanofibrous scaffolds have also been reported for the oligodendrocytes induction activity of human NSCs (hNSCs) due to the synergistic effects of 3D nanostructures mimicking the physical conditions of neurons and bioactivity of GO, this induction can be achieved even in the absence of chemical inducers [45].

GNs have revealed tremendous potential for use as neurointerfacial substrates not only because their favorable adhesion, growth, proliferation, spreading, and differentiation induction activity of immobilized stem cells, but also their good conductivity in electrical stimuli for the cultured stem cells [278]. For example, it was noticed that hydrazine-RGO and ginseng-RGO films could direct the differentiation of NSCs into neurons due to the electric conductivity of the RGO substrate [331]. In a recent study, the RGO coated nanofiber scaffolds (G-NFs) exhibited good neural induction capability and show high potential as neural implants due to the integrated recoverable electrical conductivity and soft physical characteristics (Fig. 23a-d) [290]. The G-NF scaffolds could unprecedentedly accelerate the growth and maturation of primary motor neurons, because of the long-term electrical stimulation period via the conductive scaffolds. Compared with the widely applied chemical cues, electrical stimulation using G-NFs allowed greater possibilities to regulate therapeutic parameters to cope with neurologic diseases.

Another powerful effects of electrical stimuli is that it can also induce the neural differentiation potential of some other types of stem cells, especially MSCs [332]. It has been reported that the MSC can differentiate into Schwann cell (SC)-like phenotypes

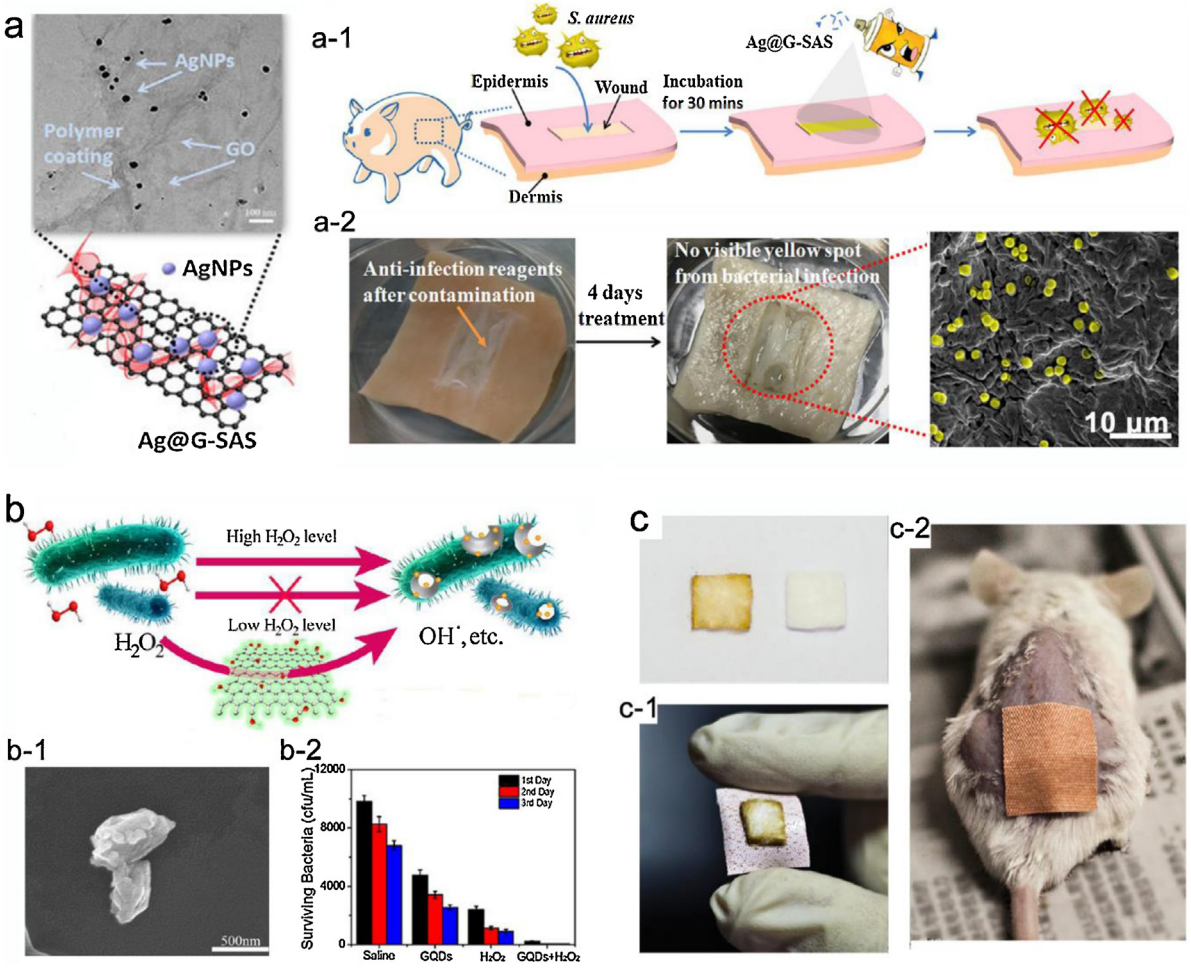

Fig. 21. (a) TEM and schematic image of Ag@G-SAS. (a-1) Application of Ag@G-SAS as a wound disinfection spray. (a-2) Optical and SEM images of a wound infected by *S. aureus*. Scale bar: 10 μm. Reproduced with permission. [48] Copyright 2018, American Chemical Society. (b) Schematic diagram of GQD-induced bacterial death in the presence of H_2O_2. (**b-**1) SEM image of *S. aureus* treated with GQD and H_2O_2. (**b-**2) Surviving number bacteria in the wound treated with GQD and H_2O_2. (c) Images of cotton fabric absorbed with and without GQD. (c-1) Images of GQDs Band-Aid and (c-2) a bacteria infected mouse treated with GQDs Band-Aid. Reproduced with permission. [324] Copyright 2014, American Chemical Society.

via the utilization of electrical stimuli on a GNs-based electrode (Fig. 23e,f) [333]. First, the flexible, inkjet-printed graphene interdigitated electrode circuit has been made via a postprint pulse-laser annealing process. Then, the electrically induced differentiation of MSCs into SC-like phenotypes is carried out, the results show that the MSC differentiation and paracrine activity are all higher than the conventional chemical treatment strategies [333]. Besides, the electrical stimuli, the electromagnetic fields can also modulate the differentiation of MSCs (Fig. 23g-i) [334]. After RGO is adsorbed onto glass, it has been demonstrated that the combination of RGO and pulsed electromagnetic fields can enhances both the osteogenic and neurogenic differentiation of MSCs [334]. These results help pave the way for in vivo applications of GNs based electrodes or substrates for stem cells differentiation, especially in electrical simulation for nerve regeneration.

Bone is a rigid, dynamic, highly vascularized tissue, which has unique abilities to remodel and heal without leaving any scar. To regenerate bones *in vitro* or *in vivo*, the key is to guide and promote the proliferation and differentiation of MSCs in a controlled manner. Compared with many other traditional materials, GNs show better matched mechanical properties and physical characteristics to native bones [42]. The recent experiments demonstrated that the GN-based hydrogels showed obviously positive effects on the adhesion, spreading, and growth of rat bone marrow stromal stem cells (rBMSCs) [335]. They noticed that RGO-based hydrogels in the absence of any chemical inducer, could induce the osteogenic differentiation of rBMSCs. After being implanted in a subcutaneous position, there was only slight generation of a fibrous capsule, the *in vivo* tissue response was low, and the formation of blood vessels was noticed. Furthermore, it had also been demonstrated that the covalent incorporation of GO in a 3D collagen scaffold could not only increase the mechanical strength but also promote the osteogenic differentiation [301]. It was suggested that the adhesion and signaling molecules of MSCs would be activated or up-regulated after adhering to a stiff interface, which thus promoted osteogenic differentiation on GO-collagen.

Implantable tissue scaffolds

With these great achievements, it was expected that GNs-based/decorated scaffold would facilitate a beneficial platform for the regeneration treatments of many human tissues, such as bone, cardiac, nerve and muscle system. There are already a large amount of successes have been achieved by using the G-BFNs-based composites to serve as tissue scaffolds, the *in vivo* animal tests have validated their potential applications in the future applications as discussed in many recent review articles [4,54]. Here, we will focus on discussing currently emerged topics in the G-BFNs-based tissue scaffolds.

After being implanted, bacterial contamination could be a potential threaten for patients. Normally, people received with

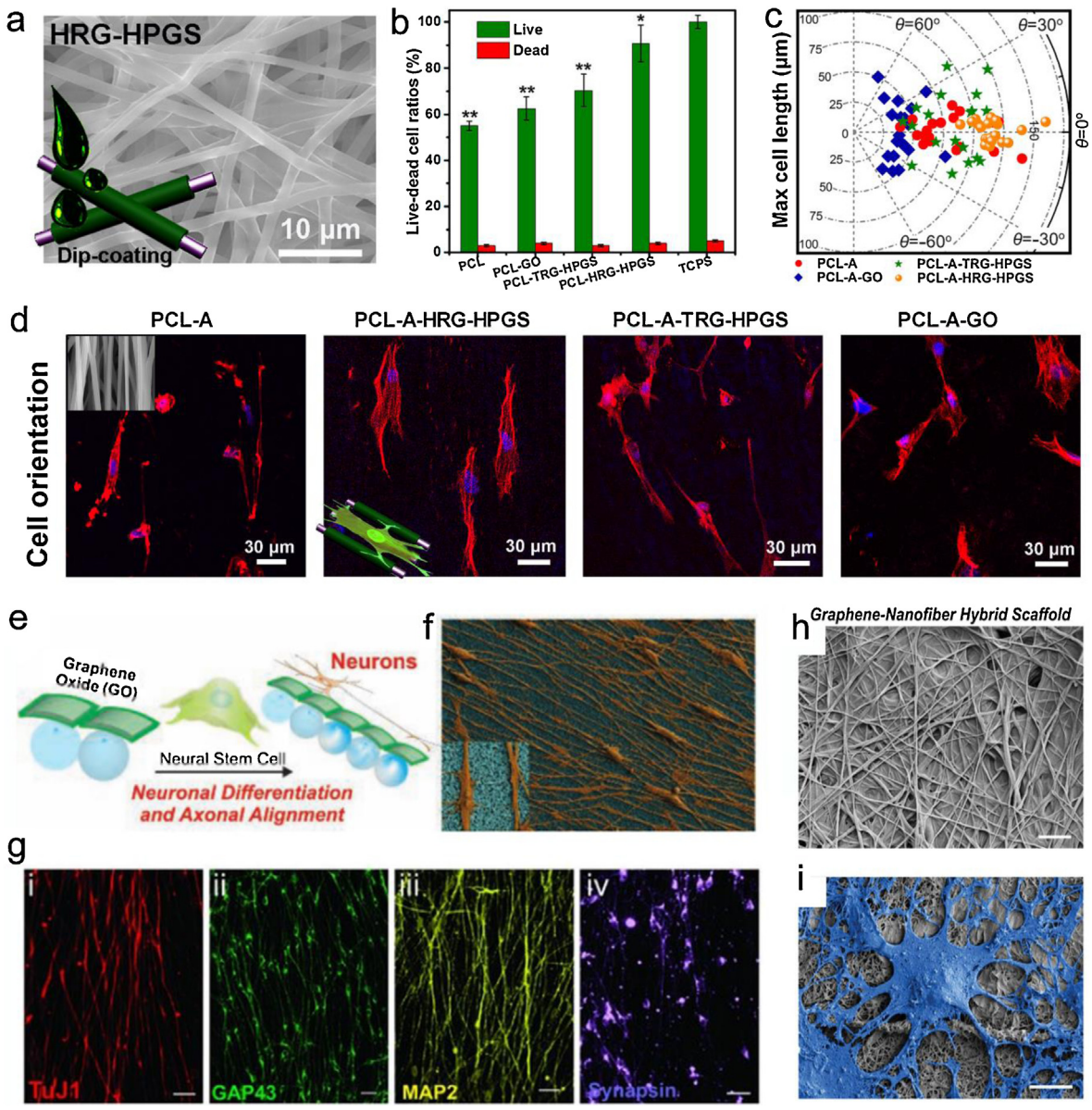

Fig. 22. (a) The surface SEM images of the PCL-HRG-HPGS nanofibers. (b) Live-dead cell ratios of hADMSC on different GNs coated nanofibers. *P < 0.05 and **P < 0.005 versus bare TCPS. (c) The cellular orientation distribution on the engineered GNs coated nanofibers. (d) Typical CLSM images of hADMSC on bare and GNs coated aligned PCL nanofibers. Reproduced with permission. [114] Copyright 2018, Wiley-VCH. (e) Behaviors of hNSCs on GO-silica assembled substrates. (f) SEM images of hNSCs cultured on GO-silica assembled substrates. (g) CLSM images of hNSCs after differentiation by staining with the early stage neuronal marker TuJ1, late stage neuronal markers MAP2, and synapsin and axonal marker GAP43 (green). Scale bar: 10 μm. Reproduced with permission. [330] Copyright 2013, Wiley-VCH. SEM images of (h) PCL/GO composite nanofibers and (i) hNSCs on PCL/GO nanofibers. Scale bars: 2 μm (top) and 10 μm (bottom). Reproduced with permission [45]. Copyright 2014, Wiley-VCH.

bone implants will take antibiotics to resist bacterial contamination, but antibiotics can affect bone regeneration and even induce drug resistance in bacteria. Recently, it was reported that the G-BFNs-based coating was able to not only promote bond regeneration but also inhibit bacterial film formation in a contact-killing manner, as shown in Fig. 24a-f [176]. Using a RGO-PDA coating, the Ti alloy substrate could significantly resist bacterial adhesion and growth since that RGO can damage bacterial membrane and induce oxidative stress. Since mammalian cells have a much larger surface area than bacteria and superior endurance towards ROS, therefore, the toxic effects of RGO to the bone cells were minimized. In addition to the bioadhesiveness of PDA, the substrate could promote bone cell adhesion on Ti surfaces as well as osteo-differentiation.

For the fabrication of G-BFNs-based tissue scaffolds, most of the conventional approaches, such as hydrothermal treatment, polymerization, and *in situ* crosslinking, are limited for the generation of stochastic and random porous structures, for which the biofunctionalities are rather limited due to the lack of adaptiveness to the biological system; especially for the development of implantable devices, a shape matching the desired area is highly required. To enable G-BFNs-based tissue scaffolds with more precisely controlled morphology and structures, a series of arbitrarily scaffolds by 3D printing of graphene/PLG nano-inks have been constructed recently, as shown in Fig. 24g-I [233]. In addition to the high conductivity, the printed microstructured scaffolds also showed high flexibility, good compatibility for tissue cell growth and stem cell induction. The *in vivo* results also suggested the printed devices were quite stable and compatible with tissues, since no GNs flakes were detected in kidney, liver, or spleen even after 30 days of implantation. More recently, the graphene/gelatin nanocomposites have also been printed into well-ordered grids and found that the graphene could increase the protein adsorption of the scaffold

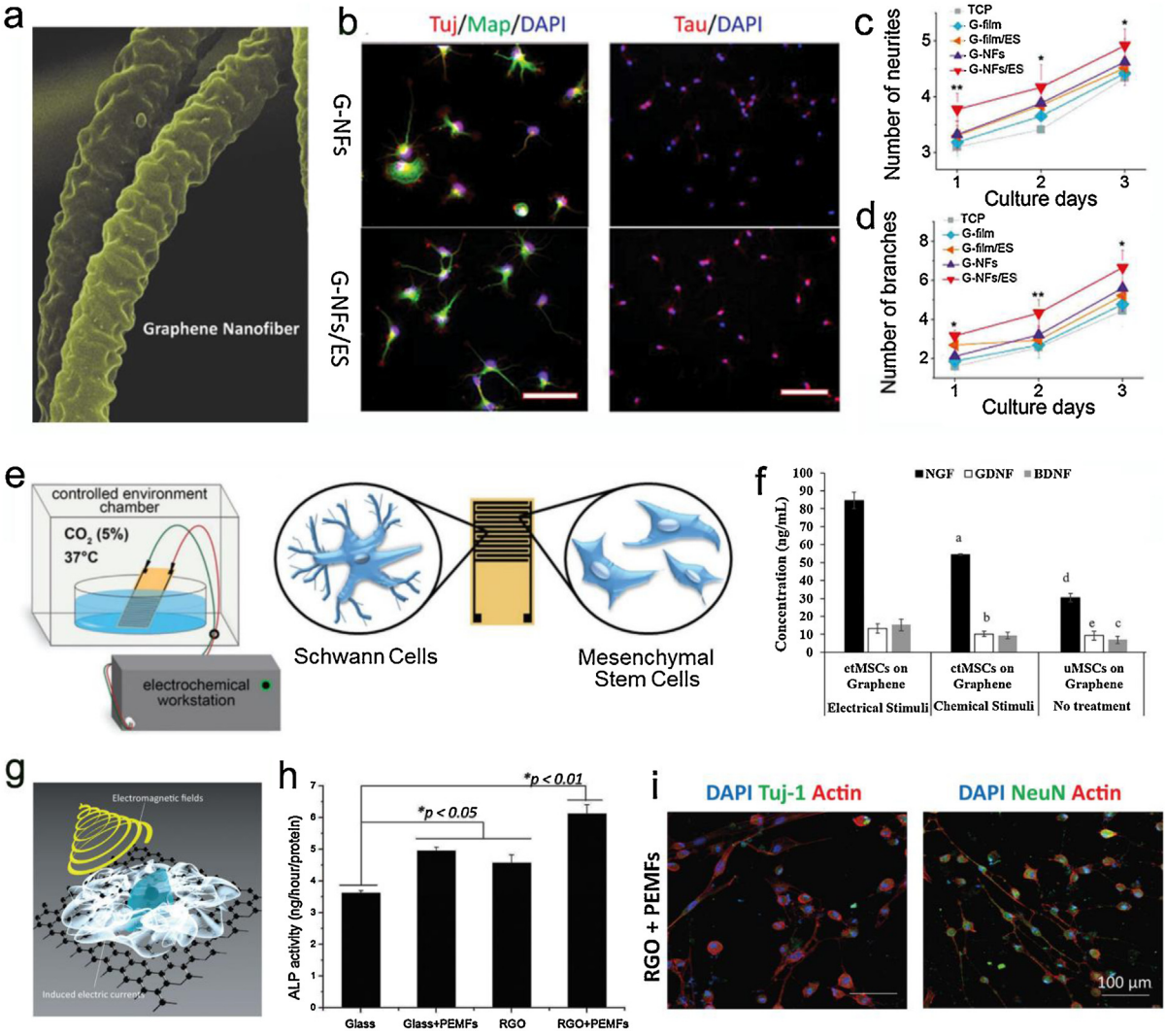

Fig. 23. (a) SEM images of graphene-coated nanofibers. (b) Growth of motor neuron cells stained with differentiation markers on different substrates, scale bar left): 80 μm; right) 200 μm. The mean numbers (c) and branches (d) of neurites, respectively. Reproduced with permission. [290] Copyright 2015, Wiley-VCH. (e) Schematic image for using IDE circuit to provide electrical stimulation to MSCs and the resulted postelectrical stimulated differentiated SCs. (f) Paracrine activity for the released concentration of NGF, GDNF, and BDNF from the cultured MSCs. Reproduced with permission [333]. Copyright 2017, Wiley-VCH. (g) Schematic image for the pulsed EMFs stimulated MSC differentiation when exposed on RGO substrates. (h) ALP activity results at week one. (i) CLSM images of RGO + pulsed EMFs group, the expression of Tuj-1 and NeuN neural markers. Reproduced with permission. [334] Copyright 2016, Wiley-VCH.

and promote glycosaminoglycan, total protein, and collagen levels for the chondrogenic differentiation of MSCs [336]. Besides the bare scaffolds, the 3D printing techniques has also been utilized to construct multi-drug eluting intravascular stent by using GNs incorporated PCL as the matrix [337]. GNs not only increased the tensile strength of the PCL stent to be more satisfactory for coronary artery implantation but also allowed the stent to carry drugs to inhibit restenosis, a scenario faced by most metal stents.

G-BFNs-based monitoring biosensors

Recent years have witnessed the rapid development of monitoring biosensors or bioelectronics for flexible, implantable and minimally invasive biomedical devices endowed with diagnostic function and controllable therapeutic capabilities for customized medicine [338,339]. These biosensors not only detect biological signals for clinical treatment, but they may also be able to release therapeutics accordingly. Among diverse nanomaterials, two dimensional nanostructures are especially favored because they can address the challenges of mechanical disparity between rigid/planar devices and soft/curvilinear interfaces and incorporate therapeutic functional nanomaterials [340,341]. Due to the good flexibility and extraordinary conductivity, graphene and GNs have been processed into textiles, thin films, papers, foams and stretchable conductors as flexible biosensors and bioelectronics for monitoring applications [342–344].

Direct interfacing and immobilization of biosensors onto biomaterial interfaces could achieve highly sensitive health quality monitoring. The graphene layer has been printed onto the water-soluble silk. This in turn enable intimate biotransfer of graphene biosensors onto different substrates, including tooth enamel. The resulted biointerfaced sensing platform with antibacterial peptides shows highly selective detection of bacteria at single-cell levels, as shown in Fig. 25a,a-1 [345]. Besides sensing of bacteria, GNs-based flexible sensors can also be used for calcium imaging on neurons with single-cell spatial resolution in the brain, as shown in Fig. 25b,b-1. It was demonstrated that the transparent and flexible neural electrode can image hippocampal slices by both confocal and two-photon microscopy without inducing any light-caused artefacts during electrical recordings (Fig. 25b-2, b-3) [346].

Skin monitoring is another important application fields of these GNs-based biosensors, it was found that the graphene-based

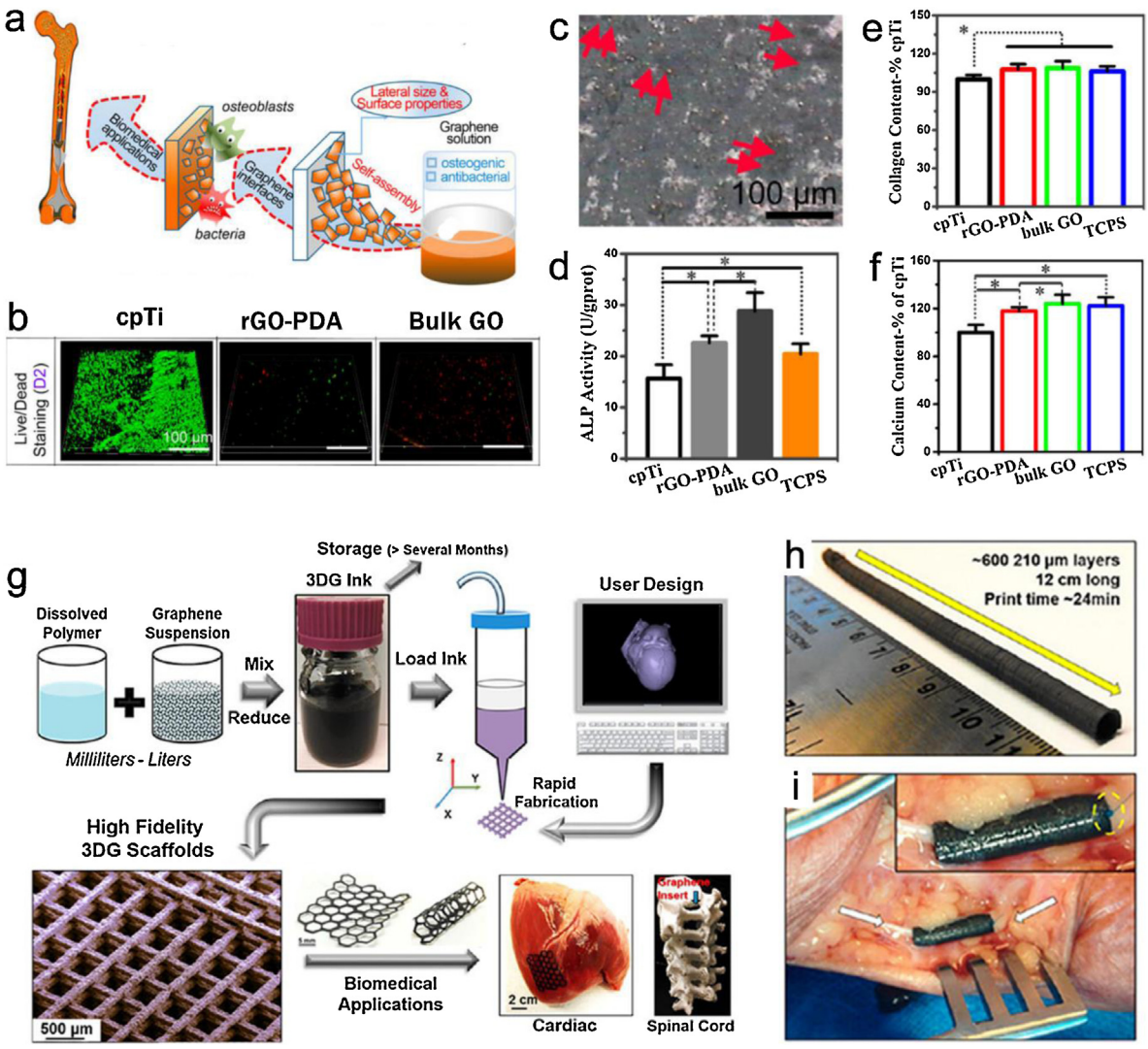

Fig. 24. (a) Illustration of the construction of multifunctional graphene biointerfaces for bone regeneration. cpTi: commercially available pure titanium. (b) Live (green)/dead (red) staining images for *S. aureus* adhered on the surface. (c) Alkaline phosphatase staining and (d) alkaline phosphatase activity during osteo-differentiation. Quantification of (e) collagen and (f) calcium contents during osteo-differentiation. *$p < 0.05$. Reproduced with permission. [176] Copyright 2016, American Chemical Society. (g) Schematic illustration of a 3D printable graphene based nano-ink for tissue scaffolds. 3DG: 3D printable graphene. (h) A 3D printed hollow tube of graphene/PLG. (i) Photograph of the hollow tube-based nerve conduit implanted into a human cadaver. Reproduced with permission [233]. Copyright 2015, American Chemical Society.

electronic nano-tattoo biosensor can fabricated and customized according to the skin, and it is able to tightly attach to skin for several hours without fracture or delamination [347]. Currently, noninvasive glucose monitoring has been widely established due to its high sensitivity, weak blood glucose correlation, and inability to detect hyperglycemia/hypoglycemia during sleep [338]. GN-based biosensors that integrated with thermo-responsive microneedles have been designed for diabetes monitoring and therapy, as shown in Fig. 26a-c [348]. The devices contain two units: a sensing device featuring a bilayer of Au mesh and GO-Au forming the electrochemical interface to transfer signals; and a therapy unit made up of a heater, multiple sensors (glucose, humidity, temperature and pH) and polymeric microneedles that can deliver drugs (metformin) transcutaneously in a thermally activated manner. The two sensing and therapy devices have been validated as effective for the regulation of glucose levels in diabetic mice [348].

In another noninvasive, *in situ*, and highly accurate intravascular blood glucose monitoring system, an ultrathin skin-like biosensor with paper battery–powered electrochemical twin channels have been designed (Fig. 26d,e) [349]. The fabricated biosensors can drive intravascular blood glucose out of the vessel and transport it to the skin surface for glucose detection with high sensitivity (130.4 μA/mM). Owing to its extreme conformability, this sensor can be directly applied for *in vivo* human clinical trials. The data obtained from noninvasive blood glucose exhibited a high correlation (>0.9) compared to the clinically measured blood glucose levels, which thus provided up new pathway for clinically noninvasive continuous glucose sensing (Fig. 26f) [349].

Besides skins, the GNs-based biosensors can also be integrated with wearable contact lenses for direct detection of biomarkers contained in body fluids [350]. For instance, a GNs based multifunctional contact lens biosensor has been developed to monitor glucose within tears and also the intraocular pressure by utilizing the resistance and capacitance of the sensor, as shown in Fig. 26g,h [351]. Both the live rabbit and bovine eyeball tests suggested that this biosensor provide reliable and robust sensing capability to the glucose level in tear fluid and intraocular pressure simultaneously (Fig. 26i,j). Such a multiplexed contact lens sensor indicates substantial potential for future ocular diagnostics, which not only detects disease-related biomarkers but also monitors ocular and overall health conditions of our body.

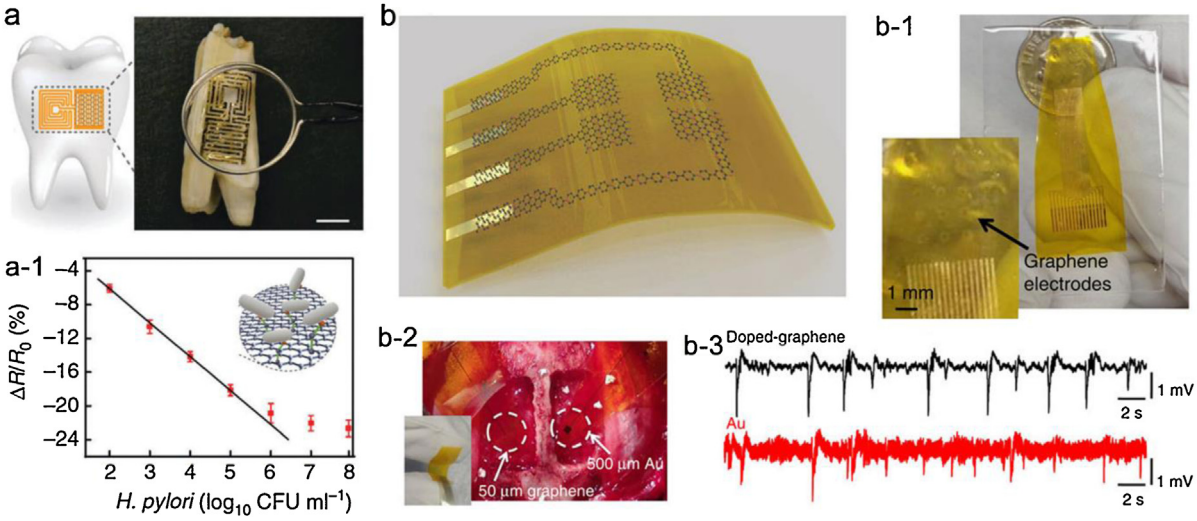

Fig. 25. (a) Flexible graphene-based nanosensors for bacteria sensing on tooth enamel. (a-1) Bacteria detection and quantification via the electrical resistance variation. Reproduced with permission. [345] Copyright 2012, Nature Publishing Group. (b) Schematic image for the graphene based flexible neural electrode. (**b-**1) Photograph for a graphene based neural electrodes with 16 array. (**b-**2) The flexible neural electrode and neural recordings in rat brain. (**b-**3) Interictal-like spiking activity recorded by graphene-based or **gold-**based electrode. Reproduced with permission [346]. Copyright 2014, Nature Publishing Group.

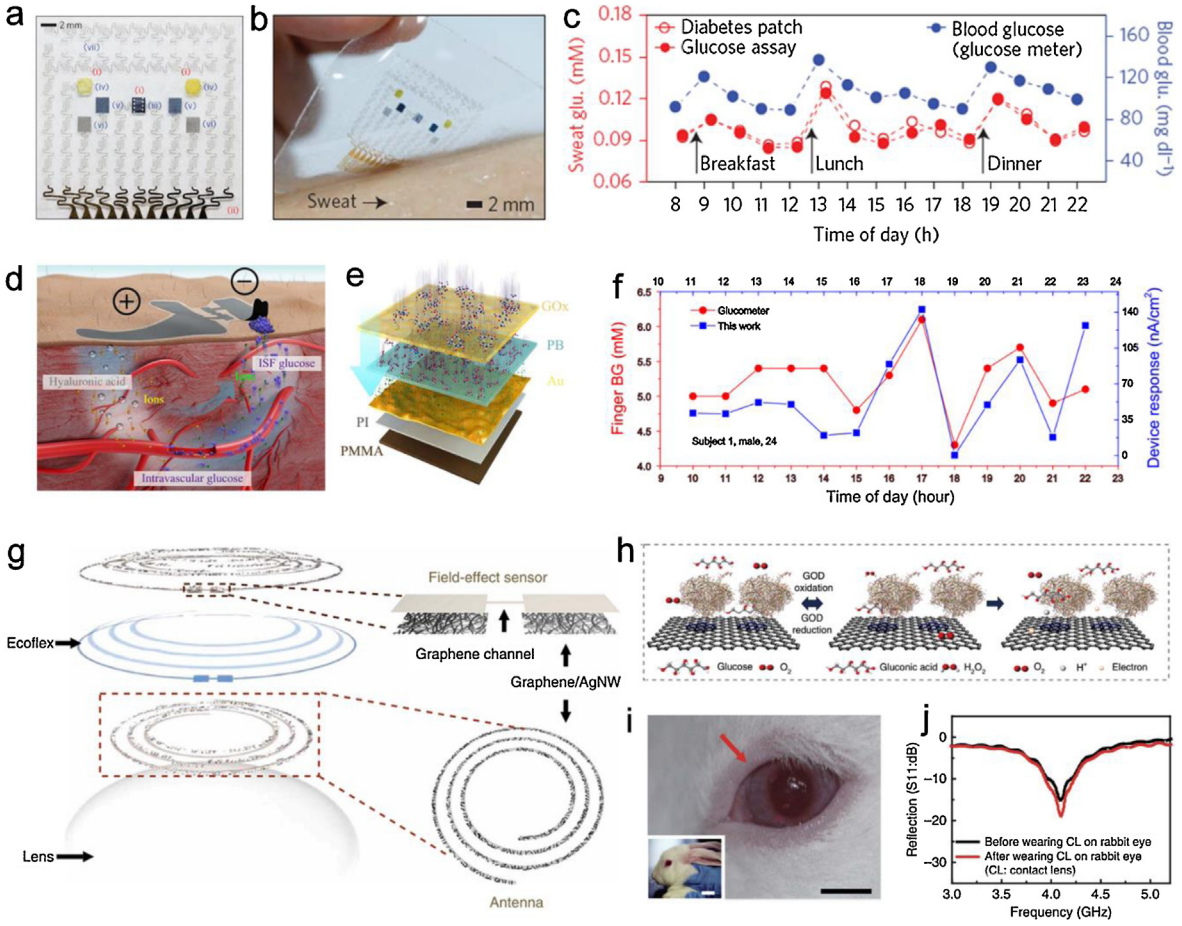

Fig. 26. (a) Optical image of the electrochemical sensor array (left) and therapeutic array (right). (b) Image of the device array on the human skin with perspiration. (c) One-day monitoring of glucose concentrations in the sweat and blood of a human. Reproduced with permission. [348] Copyright 2016, Nature Publishing Group. (d) Schematic image of the glucose sensors. (e) The structure of the ultrathin skin-like biosensor multilayers. (f) The mornitoring data for the hourly glucose monitoring in 1-day period. Reproduced with permission [349]. Copyright 2017, AAAS. (g) Schematic image for the contact lens sensor. (h) Illustration and principle of the glucose detection by using the GOD-pyrene decorated GNs biosensors. (i) Photographs of biosensor attached onto the eyes of a live rabbit. Scale bars, 1 cm **(black)** and 5 cm **(white)**. (j) Wireless sensing data for the glucose concentration for the live rabbit with contact lens sensors. Reproduced with permission. CL: contact lens. [351] Copyright 2017, Nature Publishing Group.

Summaries and perspectives

Due to the unique physicochemical, electronic and biological properties of graphene and GNs, great efforts have already been devoted on the decoration, fabrication, and utilization of G-BFNs in diverse biological and biomedical fields. With the rapid progresses and developments of graphene and GNs in biological systems, there is increased interests to investigate and fabricate more advanced G-BFNs to bridge the gap between the fundamental advantages of GNs and the application requirements of biomaterials and biomedical devices.

Here, the new horizons and recent achievements in fabricating G-BFNs for advanced biological and cellular interfaces have been clearly outlined and summarized. We have discussed the general protocols for synthesis of G-BFNs, especially diverse facile and eco-friendly synthetic and decorating strategies. The current developed G-BFNs-based on their nanostructures and biofunctionalities have also been carefully discussed. Moreover, biointeractions at the interfaces of G-BFNs with viruses, bacteria and stem cells, and the relevant biocompatibilities are also highlighted. In the end, the emerging applications and future perspectives on G-BFNs in nanotherapeutics, anti-pathogens, regenerative medicine, and monitoring biosensors are carefully discussed.

For the fabrication of G-BFNs, despite there are already abundant successful developments in using graphene and GNs for nanomedicines, biocomposites, and biomedical devices, a large number of challenges still exist. There is urgent need to explore more conventional and green methods for the fabrication of micro/meso-structured GNs-based platforms favorable interfaces that can match well with biological and human-systems on both physical, chemical and biological aspects. To achieve this goal, the functionalization of GNs via green chemistry avenues and methodologies should be widely explored and many of current systems needed to be further improved. The stabilities of many non-covalently modified GNs in physiological solutions still need to be verified both in long-term and *in vivo*.

Though, the covalent approaches can achieve higher stability, but the complicated reactions and purification processes for some systems may limit their biological applications. Other efficient green chemistry systems with high-yield and byproduct-free may also be introduced to synthesize the G-BFNs-based nanomedicines, such as copper (I)-catalyzed azide-alkene cyclo-addition, photo-induced thiol-ene reaction, Diels-Alder reaction etc [352,353]. Meanwhile, as an important green method and reversible chemical bond, the dynamic covalent bonds are also critical important for the graphene and GNs' surface modification to tune the interface properties via external stimuli and facilitate the design of smart and bio-adaptable G-BFNs [354–356].

In respect to the synthesis of biomimetic G-BFNs, the nature has provided endless inspiration on the design of biomimetic materials both on structure and function. By learning from nature, researchers have already constructed many advanced biomimetic G-BFNs composites with excellent physical, chemical and biological properties and good biological adaptability. Because of the combination of easiness, convenience and efficiency, further investigations on mussel inspired chemistry will push forward the fabrication of G-BFNs for diverse biomedical applications. Besides the mussel inspired chemistry, heparin-mimetic interface, biomineralization, and nacre-like layered composites, there are many other types of nature inspired systems that are suitable for the modifications of graphene and GNs, such as the autonomous shape-changing systems [123], dynamic capsules [357], virus-like and cell membrane-mimetic structures [180,358,359], and so on.

For the inorganic nanomaterials integrated G-BFNs, the current application areas are biosensors, theranostic nanoplatforms, tissue scaffolds and monitoring electronic devices and so on. On one hand, their interactions with biological systems, including biomolecules, cells and tissues, should be carefully studied to achieve advanced nanomedicines or bioelectronic devices. On the other hand, more works are requested to integrate graphene with emerged inorganic semiconductors, such as black phosphorus and MoS_2, to extend their functionalities in bioelectronic and optical devices. Although it seems unlikely that commercial biosensors or bioelectronic devices can be available in the next few years, significantly progresses are being achieved. As noticed, the complex integration of emerged inorganic semiconductors with graphene/GNs has been gradually overcome in many application areas. And a growing range of field for future applications has also been established steadily, for instance the catalytic nanozymes for antibacterial or anti-tumor therapies.

For the interfacial biointeractions and toxicity studies of graphene and GNs, one of the most serious issues is the accumulated toxic concern against living cells and human beings. Based on the current understandings, it is believed that the interfacial interactions between graphene/GNs and biomacromolecules are critical for its undesired toxicity. Further optimization of surface chemistry for G-BFNs still needs a lot of efforts and tests both *in vitro* and *in vivo*. For the macro-scale biocomposites and devices, the long-term biological responses (at least for 6 months) should be carefully concerned after implantation, such as the inflammation and carcinogenicity potentials.

On the designing of G-BFNs-based regenerative composites, it has been validated that G-BFNs modified conventional matrices, such as the polymeric films, membranes, electro-spun nanofibers, hydrogels and 3D foams, exhibit tailored interfacial chemical and physical properties. The micro/nano structured and interface properties tailored G-BFNs-based scaffolds may lead to well-tuned physiological properties for targeted tissues regeneration. Attributed to their distinguished mechanical performance and intrinsic bioactivity, G-BFNs incorporated biocomposites have been recognized as one of the most promising candidates for designing next generation multifunctional tissue scaffolds, especially for the bone, cardiac and neural regeneration. However, the detailed signaling pathways and underlying mechanisms for promoting stem cell differentiations on G-BFNs-based scaffolds still haven't been clearly revealed. Further investigations on the clarification of these mechanisms at the cellular or subcellular level are needed for using G-BFNs in guiding stem cell differentiations. Meanwhile, G-BFNs-based scaffolds constructed by the automatic 3D printing or other advanced microfabrication technologies that interfaced with beneficial nano-morphologies, tunable mechanics, and good electrical conductivity are extremely important, which have gradually become the intriguing future trends in the exploration of nano/stem cells interactions.

Last, the recent years have experienced fast developments and successes on construction of graphene and GNs-based bioelectronics or biosensors for future clinical diagnose. However, much effort is still needed to improve detection performances, especially for the sensitivities on diagnosis of specific biomarkers, molecules or diseases. On one hand, future explorations should focus more on the fabrication of G-BFNs sensing platforms with more specific cell/pathogen interactions or highly sensitive detection limits on targeted cells or pathogens, thus bringing these techniques to markets and clinical usages. Construction of more flexible, conductive and electrochemically-active G-BFNs-based electronics or implantable probes by microfabrication or 3D printing technologies for on-line recording and monitoring human or tissue signals/activities is also of great importance, especially for the *in situ* signals' recording of pulse, cardiac and brain.

Conflict of interest

The authors declare no conflict of interest.

Acknowledgements

This work was financially sponsored by the National Natural Science Foundation of China (Grant Nos. 51503125, 51673125, and 51773127), the State Key Research Development Programme of China (2016YFC1103000 and 2016YFC1103001), and the Youth Science and Technology Innovation Team of Sichuan Province (Grant No. 2015TD0001). C. Nie acknowledges the financial support of China Scholarship Council (CSC) for PhD study in Freie Universität Berlin. Dr. L. Ma acknowledges the National Natural Science Foundation of China (No. 51703141), China Postdoctoral Science Foundation (No. 2017M623039) and the Full-time Postdoctoral Research and Development Fund Project of Sichuan University (No. 2018SCU12031). Prof. C. Cheng acknowledges the financial support from the DRS POINT Fellowship of Freie Universität Berlin, the Alexander von Humboldt Fellowship, and the Thousand Youth Talents Plan. Dr. Chao He and Yi Xia are acknowledged for their generous help in manuscript preparation.

References

[1] V. Georgakilas, J.A. Perman, J. Tucek, R. Zboril, Chem. Rev. 115 (2015) 4744–4822.
[2] K.S. Novoselov, V.I. Fal'ko, L. Colombo, P.R. Gellert, M.G. Schwab, K. Kim, Nature 490 (2012) 192–200.
[3] L. Gao, G.-X. Ni, Y. Liu, B. Liu, A.H. Castro Neto, K.P. Loh, Nature 505 (2014) 190–194.
[4] C. Cheng, S. Li, A. Thomas, N.A. Kotov, R. Haag, Chem. Rev. 117 (2017) 1826–1914.
[5] H.Y. Mao, S. Laurent, W. Chen, O. Akhavan, M. Imani, A.A. Ashkarran, M. Mahmoudi, Chem. Rev. 113 (2013) 3407–3424.
[6] F. Yuan, S. Li, Z. Fan, X. Meng, L. Fan, S. Yang, Nano Today 11 (2016) 565–586.
[7] K. Hu, D.D. Kulkarni, I. Choi, V.V. Tsukruk, Prog. Polym. Sci. 39 (2014) 1934–1972.
[8] P.T. Yin, S. Shah, M. Chhowalla, K.-B. Lee, Chem. Rev. 115 (2015) 2483–2531.
[9] A. Dasgupta, L.P. Rajukumar, C. Rotella, Y. Lei, M. Terrones, Nano Today 12 (2017) 116–135.
[10] C. Xie, Y. Wang, Z.-X. Zhang, D. Wang, L.-B. Luo, Nano Today 19 (2018) 41–83.
[11] S. Li, C. Cheng, X. Zhao, J. Schmidt, A. Thomas, Angew. Chem. Int. Ed. 130 (2018) 1874–1880.
[12] S. Li, C. Cheng, H.W. Liang, X. Feng, A. Thomas, Adv. Mater. 29 (2017) 1700707.
[13] H.J. Cui, Z. Zhou, D.Z. Jia, Mater. Horiz. 4 (2017) 7–19.
[14] T.T. Tung, M.J. Nine, M. Krebsz, T. Pasinszki, C.J. Coghlan, D.N.H. Tran, D. Losic, Adv. Funct. Mater. 27 (2017) 1702891.
[15] D. Bischoff, M. Eich, A. Varlet, P. Simonet, H.C. Overweg, K. Ensslin, T. Ihn, Mater. Today 19 (2016) 375–381.
[16] N. Kurra, Q. Jiang, P. Nayak, H.N. Alshareef, Nano Today 24 (2019) 81–102.
[17] F. Perreault, A.F. de Faria, M. Elimelech, Chem. Soc. Rev. 44 (2015) 5861–5896.
[18] S. Li, C. Cheng, A. Thomas, Adv. Mater. 29 (2017) 1602547.
[19] Z. Tu, V. Wycisk, C. Cheng, W. Chen, M. Adeli, R. Haag, Nanoscale 9 (2017) 18931–18939.
[20] C. Dai, S.J. Zhang, Z. Liu, R. Wu, Y. Chen, ACS Nano 11 (2017) 9467–9480.
[21] T.J. Yin, J.Y. Liu, Z.K. Zhao, Y.Y. Zhao, L.H. Dong, M. Yang, J.P. Zhou, M.R. Huo, Adv. Funct. Mater. 27 (2017) 1604620.
[22] S. Gai, G. Yang, P. Yang, F. He, J. Lin, D. Jin, B. Xing, Nano Today 19 (2018) 146–187.
[23] J. Liu, Q. Chen, L. Feng, Z. Liu, Nano Today 21 (2018) 55–73.
[24] B. Tian, C. Wang, S. Zhang, L. Feng, Z. Liu, ACS Nano 5 (2011) 7000–7009.
[25] Y. Yang, L. Ma, C. Cheng, Y. Deng, J. Huang, X. Fan, C. Nie, W. Zhao, C. Zhao,Adv. Funct. Mater. 28 (2018), 1705708.
[26] M. Zhang, F. Wu, W. Wang, J. Shen, N. Zhou, C. Wu, Chem. Mater. (2018), http://dx.doi.org/10.1021/acs.chemmater.1028b00934.
[27] J. Zhu, M. Xu, M. Gao, Z. Zhang, Y. Xu, T. Xia, S. Liu, ACS Nano 11 (2017) 2637–2651.
[28] C. Choi, M.K. Choi, S. Liu, M.S. Kim, O.K. Park, C. Im, J. Kim, X. Qin, G.J. Lee, K.W. Cho, M. Kim, E. Joh, J. Lee, D. Son, S.H. Kwon, N.L. Jeon, Y.M. Song, N. Lu, D.H. Kim, Nat. Commun. 8 (2017) 1664.
[29] K. Kostarelos, M. Vincent, C. Hebert, J.A. Garrido,Adv. Mater. 29 (2017), 1700909.
[30] Y. Qian, X. Zhao, Q. Han, W. Chen, H. Li, W. Yuan, Nat. Commun. 9 (2018) 323.
[31] K. Yang, L. Feng, X. Shi, Z. Liu, Chem. Soc. Rev. 42 (2013) 530–547.
[32] L. Feng, L. Wu, X. Qu, Adv. Mater. 25 (2013) 168–186.
[33] S.K. Rastogi, G. Raghavan, G. Yang, T. Cohen-Karni, Nano Lett. 17 (2017) 3297–3301.
[34] N.N. Luo, J.K. Weber, S. Wang, B.Q. Luan, H. Yue, X.B. Xi, J. Du, Z.X. Yang, W. Wei, R.H. Zhou, G.H. Ma, Nat. Commun. 8 (2017) 14537.
[35] M. Orecchioni, D. Bedognetti, L. Newman, C. Fuoco, F. Spada, W. Hendrickx, F.M. Marincola, F. Sgarrella, A.F. Rodrigues, C. Menard-Moyon, G. Cesareni, K. Kostarelos, A. Bianco, L.G. Delogu, Nat. Commun. 8 (2017) 1109.
[36] X. Tian, Z. Yang, G. Duan, A. Wu, Z. Gu, L. Zhang, C. Chen, Z. Chai, C. Ge, R. Zhou, Small 13 (2017) 1602133.
[37] S. Lee, I. Jo, S. Kang, B. Jang, J. Moon, J.B. Park, S. Lee, S. Rho, Y. Kim, B.H. Hong, ACS Nano 11 (2017) 5318–5324.
[38] N. Cheeveewattanagul, E. Morales-Narvaez, A.R.H.A. Hassan, J.F. Bergua, W. Surareungchai, M. Somasundrum, A. Merkoci, Adv. Funct. Mater. 27 (2017) 1702741.
[39] H.H. Cheng, Y.X. Huang, Q.L. Cheng, G.Q. Shi, L. Jiang, L.T. Qu, Adv. Funct. Mater. 27 (2017) 1703096.
[40] Y.B. Yang, X.D. Yang, X.M. Zou, S.T. Wu, D. Wan, A.Y. Cao, L. Liao, Q. Yuan, X.F. Duan, Adv. Funct. Mater. 27 (2017) 1604096.
[41] S.S. Gong, H. Ni, L. Jiang, Q.F. Cheng, Mater. Today 20 (2017) 210–219.
[42] T.-H. Kim, S. Shah, L. Yang, P.T. Yin, M.K. Hossain, B. Conley, J.-W. Choi, K.-B. Lee, ACS Nano 9 (2015) 3780–3790.
[43] A. Paul, A. Hasan, H.A. Kindi, A.K. Gaharwar, V.T.S. Rao, M. Nikkhah, S.R. Shin, D. Krafft, M.R. Dokmeci, D. Shum-Tim, A. Khademhosseini, ACS Nano 8 (2014) 8050–8062.
[44] B. Ziem, H. Thien, K. Achazi, C. Yue, D. Stern, K. Silberreis, M.F. Gholami, F. Beckert, D. Groger, R. Mulhaupt, J.P. Rabe, A. Nitsche, R. Haag, Adv. Healthc. Mater. 5 (2016) 2922–2930.
[45] S. Shah, P.T. Yin, T.M. Uehara, S.-T.D. Chueng, L. Yang, K.-B. Lee, Adv. Mater. 26 (2014) 3673–3680.
[46] S.M. Kang, S. Park, D. Kim, S.Y. Park, R.S. Ruoff, H. Lee, Adv. Funct. Mater. 21 (2011) 108–112.
[47] L. Ma, C. Cheng, C. He, C. Nie, J. Deng, S. Sun, C. Zhao, ACS Appl. Mater. Interfaces 7 (2015) 26050–26062.
[48] X. Fan, F. Yang, C. Nie, Y. Yang, H. Ji, C. He, C. Cheng, C. Zhao, ACS Appl. Mater. Interfaces 10 (2018) 296–307.
[49] K. Chen, B. Shi, Y. Yue, J. Qi, L. Guo, ACS Nano 9 (2015) 8165–8175.
[50] W. Cui, M. Li, J. Liu, B. Wang, C. Zhang, L. Jiang, Q. Cheng, ACS Nano 8 (2014) 9511–9517.
[51] S. Wang, R. Cazelles, W.-C. Liao, M. Vázquez-González, A. Zoabi, R. Abu-Reziq, I. Willner, Nano Lett. 17 (2017) 2043–2048.
[52] P. Cai, W.R. Leow, X. Wang, Y.L. Wu, X. Chen, Adv. Mater. 29 (2017) 1605529.
[53] L. Cheng, C. Wang, L. Feng, K. Yang, Z. Liu, Chem. Rev. 114 (2014) 10869–10939.
[54] R. Geetha Bai, N. Ninan, K. Muthoosamy, S. Manickam, Prog. Mater. Sci. 91 (2018) 24–69.
[55] W.C. Kenry, K.P. Lee, C.T.Lim Loh, Biomaterials 155 (2018) 236–250.
[56] X.F. Zou, L. Zhang, Z.J. Wang, Y. Luo, J. Am. Chem. Soc. 138 (2016) 2064–2077.
[57] B.T. Liu, J. Xie, H. Ma, X. Zhang, Y. Pan, J.W. Lv, H. Ge, N. Ren, H.Q. Su, X.J. Xie, L. Huang, W. Huang, Small 13 (2017) 1601001.
[58] Y.J. Yun, J. Ju, J.H. Lee, S.H. Moon, S.J. Park, Y.H. Kim, W.G. Hong, D.H. Ha, H. Jang, G.H. Lee, H.M. Chung, J. Choi, S.W. Nam, S.H. Lee, Y. Jun, Adv. Funct. Mater. 27 (2017) 1701513.
[59] S.K. Deng, V. Berry, Mater. Today 19 (2016) 197–212.
[60] P.C. Sherrell, C. Mattevi, Mater. Today 19 (2016) 428–436.
[61] T.P. Dasari Shareena, D. McShan, A.K. Dasmahapatra, P.B. Tchounwou, Nano-Micro Lett. 10 (2018) 53.
[62] L. Peng, Z. Xu, Z. Liu, Y. Wei, H. Sun, Z. Li, X. Zhao, C. Gao, Nat. Commun. 6 (2015) 5716.
[63] S. Pei, Q. Wei, K. Huang, H.-M. Cheng, W. Ren, Nat. Commun. 9 (2018) 145.
[64] J. Zhang, H. Yang, G. Shen, P. Cheng, J. Zhang, S. Guo, Chem. Commun. (Camb.) 46 (2010) 1112–1114.
[65] J. Liu, S. Fu, B. Yuan, Y. Li, Z. Deng, J. Am. Chem. Soc. 132 (2010) 7279–7281.
[66] D. Mhamane, W. Ramadan, M. Fawzy, A. Rana, M. Dubey, C. Rode, B. Lefez, B. Hannoyer, S. Ogale, Green Chem. 13 (2011) 1990.
[67] K. Liu, J.-J. Zhang, F.-F. Cheng, T.-T. Zheng, C. Wang, J.-J. Zhu, J. Mater. Chem. 21 (2011) 12034–12040.
[68] C. Zhu, S. Guo, Y. Fang, S. Dong, ACS Nano 4 (2010) 2429–2437.
[69] Y. Wang, Z. Shi, J. Yin, ACS Appl. Mater. Interfaces 3 (2011) 1127–1133.
[70] A.G. Nandgaonkar, Q. Wang, K. Fu, W.E. Krause, Q. Wei, R. Gorga, L.A. Lucia, Green Chem. 16 (2014) 3195.
[71] V. Georgakilas, M. Otyepka, A.B. Bourlinos, V. Chandra, N. Kim, K.C. Kemp, P. Hobza, R. Zboril, K.S. Kim, Chem. Rev. 112 (2012) 6156–6214.
[72] S. Yang, R. Lohe Martin, K. Müllen, X. Feng, Adv. Mater. 28 (2016) 6213–6221.
[73] S. Yang, G. Ricciardulli Antonio, S. Liu, R. Dong, R. Lohe Martin, A. Becker, A. Squillaci Marco, P. Samorì, K. Müllen, X. Feng, Angew. Chem. Int. Ed. 56 (2017) 6669–6675.
[74] F. Liu, J.Y. Choi, T.S. Seo, Chem. Commun. (Camb.) 46 (2010) 2844–2846.
[75] S. Ahadian, M. Estili, V.J. Surya, J. Ramon-Azcon, X. Liang, H. Shiku, M. Ramalingam, T. Matsue, Y. Sakka, H. Bae, K. Nakajima, Y. Kawazoe, A. Khademhosseini, Nanoscale 7 (2015) 6436–6443.
[76] K. Yang, J. Wan, S. Zhang, B. Tian, Y. Zhang, Z. Liu, Biomaterials 33 (2012) 2206–2214.
[77] X. Wang, H. Bai, G. Shi, J. Am. Chem. Soc. 133 (2011) 6338–6342.
[78] X. Sun, Z. Liu, K. Welsher, J.T. Robinson, A. Goodwin, S. Zaric, H. Dai, Nano Res. 1 (2008) 203–212.

[79] H. Zhang, C. Peng, J. Yang, M. Lv, R. Liu, D. He, C. Fan, Q. Huang, ACS Appl. Mater. Interfaces 5 (2013) 1761–1767.
[80] O. Akhavan, E. Ghaderi, A. Akhavan, Biomaterials 33 (2012) 8017–8025.
[81] J.T. Robinson, S.M. Tabakman, Y. Liang, H. Wang, H. Sanchez Casalongue, D. Vinh, H. Dai, J. Am. Chem. Soc. 133 (2011) 6825–6831.
[82] J. Shen, Y. Zhu, X. Yang, C. Li, Chem. Commun. (Camb.) 48 (2012) 3686–3699.
[83] H.A. Lin, Y. Sato, Y. Segawa, T. Nishihara, N. Sugimoto, L.T. Scott, T. Higashiyama, K. Itami, Angew. Chem. Int. Ed. 57 (2018) 2874–2878.
[84] Y. Zhang, P. Han, H. Zhou, N. Wu, Y. Wei, X. Yao, J. Zhou, Y. Song, Adv. Funct. Mater. 28 (2018) 1802585.
[85] S. Zhu, Y. Song, J. Wang, H. Wan, Y. Zhang, Y. Ning, B. Yang, Nano Today 13 (2017) 10–14.
[86] X.T. Zheng, A. Ananthanarayanan, K.Q. Luo, P. Chen, Small 11 (2015) 1620–1636.
[87] S. Zhu, J. Zhang, C. Qiao, S. Tang, Y. Li, W. Yuan, B. Li, L. Tian, F. Liu, R. Hu, H. Gao, H. Wei, H. Zhang, H. Sun, B. Yang, Chem. Commun. (Camb.) 47 (2011) 6858–6860.
[88] X. Li, M. Rui, J. Song, Z. Shen, H. Zeng, Adv. Funct. Mater. 25 (2015) 4929–4947.
[89] G. Shim, J.Y. Kim, J. Han, S.W. Chung, S. Lee, Y. Byun, Y.K. Oh, J. Control. Release 189 (2014) 80–89.
[90] Y.S. Ye, H. Zeng, J. Wu, L. Dong, J. Zhu, Z.-G. Xue, X.-P. Zhou, X. Xie, Y.-W. Mai, Green Chem. 18 (2016) 1674–1683.
[91] Y. Chong, C. Ge, Z. Yang, J.A. Garate, Z. Gu, J.K. Weber, J. Liu, R. Zhou, ACS Nano 9 (2015) 5713–5724.
[92] C. Cheng, S. Nie, S. Li, H. Peng, H. Yang, L. Ma, S. Sun, C. Zhao, J. Mater. Chem. B Mater. Biol. Med. 1 (2013) 265–275.
[93] C. Cheng, S. Li, J. Zhao, X. Li, Z. Liu, L. Ma, X. Zhang, S. Sun, C. Zhao, Chem. Eng. J. 228 (2013) 468–481.
[94] W. Li, J. Wang, J. Ren, X. Qu, Angew. Chem. Int. Ed. 52 (2013) 6726–6730.
[95] T. Premkumar, K.E. Geckeler, Prog. Polym. Sci. 37 (2012) 515–529.
[96] J.N. Tiwari, K. Nath, S. Kumar, R.N. Tiwari, K.C. Kemp, N.H. Le, D.H. Youn, J.S. Lee, K.S. Kim, Nat. Commun. 4 (2013) 2221.
[97] L. Tang, Y. Wang, Y. Liu, J. Li, ACS Nano 5 (2011) 3817–3822.
[98] R. Mo, T. Jiang, W. Sun, Z. Gu, Biomaterials 50 (2015) 67–74.
[99] F. Zhao, H. Li, Y. Jiang, X. Wang, X. Mu, Green Chem. 16 (2014) 2558.
[100] Y. Guo, L. Deng, J. Li, S. Guo, E. Wang, S. Dong, ACS Nano 5 (2011) 1282–1290.
[101] Q. Zeng, J. Cheng, L. Tang, X. Liu, Y. Liu, J. Li, J. Jiang, Adv. Funct. Mater. 20 (2010) 3366–3372.
[102] J. Zhang, F. Zhang, H. Yang, X. Huang, H. Liu, J. Zhang, S. Guo, Langmuir 26 (2010) 6083–6085.
[103] Y. Zhang, J. Zhang, X. Huang, X. Zhou, H. Wu, S. Guo, Small 8 (2012) 154–159.
[104] H. Bao, Y. Pan, Y. Ping, N.G. Sahoo, T. Wu, L. Li, J. Li, L.H. Gan, Small 7 (2011) 1569–1578.
[105] D. Han, L. Yan, W. Chen, W. Li, Carbohydr. Polym. 83 (2011) 653–658.
[106] D. Depan, B. Girase, J.S. Shah, R.D.K. Misra, Acta Biomater. 7 (2011) 3432–3445.
[107] S. Wan, J. Peng, Y. Li, H. Hu, L. Jiang, Q. Cheng, ACS Nano 9 (2015) 9830–9836.
[108] W. Zhang, Z. Guo, D. Huang, Z. Liu, X. Guo, H. Zhong, Biomaterials 32 (2011) 8555–8561.
[109] K. Yang, J. Wan, S. Zhang, Y. Zhang, S.-T. Lee, Z. Liu, ACS Nano 5 (2010) 516–522.
[110] S. Zhang, S. Tang, J. Lei, H. Dong, H. Ju, J. Electroanal. Chem. Lausanne (Lausanne) 656 (2011) 285–288.
[111] B. Genorio, A. Znidarsic, J. Phys. D Appl. Phys. 47 (2014) 094012.
[112] H. Zhang, Y. Han, Y. Guo, C. Dong, J. Mater. Chem. 22 (2012) 23900–23905.
[113] Z. Tu, K. Achazi, A. Schulz, R. Mulhaupt, S. Thierbach, E. Ruhl, M. Adeli, R. Haag, Adv. Funct. Mater. 27 (2017) 1701837.
[114] C. Cheng, J. Zhang, S. Li, Y. Xia, C. Nie, Z. Shi, J.L. Cuellar-Camacho, N. Ma, R. Haag, Adv. Mater. 30 (2018) 1705452.
[115] M.F. Gholami, D. Lauster, K. Ludwig, J. Storm, B. Ziem, N. Severin, C. Böttcher, J.P. Rabe, A. Herrmann, M. Adeli, Adv. Funct. Mater. 27 (2017) 1606477.
[116] H. Kim, R. Namgung, K. Singha, I.-K. Oh, W.J. Kim, Bioconjug. Chem. 22 (2011) 2558–2567.
[117] T. Ren, L. Li, X. Cai, H. Dong, S. Liu, Y. Li, Polym. Chem. 3 (2012) 2561–2569.
[118] C.M. Santos, M.C.R. Tria, R.A.M.V. Vergara, F. Ahmed, R.C. Advincula, D.F. Rodrigues, Chem. Commun. (Camb.) 47 (2011) 8892–8894.
[119] W. Li, J. Wang, J. Ren, X. Qu, Adv. Mater. 25 (2013) 6737–6743.
[120] C.H. Zhu, Y. Lu, J. Peng, J.F. Chen, S.H. Yu, Adv. Funct. Mater. 22 (2012) 4017–4022.
[121] Y. Pan, H. Bao, N.G. Sahoo, T. Wu, L. Li, Adv. Funct. Mater. 21 (2011) 2754–2763.
[122] A. Sahu, W.I. Choi, G. Tae, Chem. Commun. (Camb.) 48 (2012) 5820–5822.
[123] J. Mu, C. Hou, H. Wang, Y. Li, Q. Zhang, M. Zhu, Sci. Adv. 1 (2015) e1500533.
[124] M. Nurunnabi, Z. Khatun, M. Nafiujjaman, D.-g. Lee, Y.-k. Lee, ACS Appl. Mater. Interfaces 5 (2013) 8246–8253.
[125] W. Jiang, F. Mo, X. Jin, L. Chen, L.J. Xu, L. Guo, F. Fu, Adv. Mater. Interfaces 4 (2017) 1700425.
[126] Y. Xu, K. Sheng, C. Li, G. Shi, ACS Nano 4 (2010) 4324–4330.
[127] S. Kim, S.H. Ku, S.Y. Lim, J.H. Kim, C.B. Park, Adv. Mater. 23 (2011) 2009–2014.
[128] S. Kumar, K. Chatterjee, Nanoscale 7 (2015) 2023–2033.
[129] M. Li, Q. Liu, Z. Jia, X. Xu, Y. Cheng, Y. Zheng, T. Xi, S. Wei, Carbon 67 (2014) 185–197.
[130] H. Liu, P. Xi, G. Xie, Y. Shi, F. Hou, L. Huang, F. Chen, Z. Zeng, C. Shao, J. Wang, J. Phys. Chem. C 116 (2012) 3334–3341.
[131] H. Liu, J. Cheng, F. Chen, F. Hou, D. Bai, P. Xi, Z. Zeng, ACS Appl. Mater. Interfaces 6 (2014) 3132–3140.
[132] Y. Tao, Y. Lin, Z. Huang, J. Ren, X. Qu, Adv. Mater. 25 (2013) 2594–2599.
[133] L. Shang, T. Bian, B. Zhang, D. Zhang, L.Z. Wu, C.H. Tung, Y. Yin, T. Zhang, Angew. Chem. Int. Ed. 126 (2014) 254–258.
[134] M.I. Kim, M.S. Kim, M.-A. Woo, Y. Ye, K.S. Kang, J. Lee, H.G. Park, Nanoscale 6 (2014) 1529–1536.
[135] S. Dutta, C. Ray, S. Mallick, S. Sarkar, R. Sahoo, Y. Negishi, T. Pal, J. Phys. Chem. C 119 (2015) 23790–23800.
[136] W. Zhang, C. Chen, D. Yang, G. Dong, S. Jia, B. Zhao, L. Yan, Q. Yao, A. Sunna, Y. Liu, Adv. Mater. Interfaces 3 (2016) 1600590.
[137] Y. Fang, E. Wang, Chem. Commun. (Camb.) 49 (2013) 9526–9539.
[138] T.N.N. Dau, V.H. Vu, T.T. Cao, V.C. Nguyen, C.T. Ly, D.L. Tran, T.T.N. Pham, N.T. Loc, B. Piro, T.T. Vu, Sens. Actuators B Chem. 283 (2019) 52–60.
[139] M. Garrido, J. Calbo, L. Rodriguez-Perez, J. Arago, E. Orti, M.A. Herranz, N. Martin, Chem. Commun. (Camb.) 53 (2017) 12402–12405.
[140] P. He, J. Sun, S. Tian, S. Yang, S. Ding, G. Ding, X. Xie, M. Jiang, Chem. Mater. 27 (2015) 218–226.
[141] A.J. Patil, J.L. Vickery, T.B. Scott, S. Mann, Adv. Mater. 21 (2009) 3159–3164.
[142] Y. Xu, Q. Wu, Y. Sun, H. Bai, G. Shi, ACS Nano 4 (2010) 7358–7362.
[143] W. Miao, G. Shim, C.M. Kang, S. Lee, Y.S. Choe, H.G. Choi, Y.K. Oh, Biomaterials 34 (2013) 9638–9647.
[144] D.Y. Lee, Z. Khatun, J.H. Lee, Y.K. Lee, I. In, Biomacromolecules 12 (2011) 336–341.
[145] N. Kundu, A. Roy, D. Banik, J. Kuchlyan, N. Sarkar, J. Phys. Chem. C 119 (2015) 25023–25035.
[146] R. Xiong, H.S. Kim, L. Zhang, V.F. Korolovych, S. Zhang, Y.G. Yingling, V.V. Tsukruk, Angew. Chem. Int. Ed. 57 (2018) 8508–8513.
[147] M. Ionita, L.E. Crica, H. Tiainen, H.J. Haugen, E. Vasile, S. Dinescu, M. Costache, H. Iovu, J. Mater. Chem. B Mater. Biol. Med. 4 (2016) 282–291.
[148] H.L. Fan, L.L. Wang, K.K. Zhao, N. Li, Z.J. Shi, Z.G. Ge, Z.X. Jin, Biomacromolecules 11 (2010) 2345–2351.
[149] T. Sangfai, F. Dong, V. Tantishaiyakul, K.D. Jandt, C. Lüdecke, O. Boonrat, N. Hirun, Express Polym. Lett. 11 (2017) 73–82.
[150] X.H. Liu, D.M. Ma, H. Tang, L. Tan, Q.J. Xie, Y.Y. Zhang, M. Ma, S.Z. Yao, ACS Appl. Mater. Interfaces 6 (2014) 8173–8183.
[151] L. Feng, S. Zhang, Z. Liu, Nanoscale 3 (2011) 1252–1257.
[152] N.V. Medhekar, A. Ramasubramaniam, R.S. Ruoff, V.B. Shenoy, ACS Nano 4 (2010) 2300–2306.
[153] Y. Tan, Y. Song, Q. Zheng, Nanoscale 4 (2012) 6997–7005.
[154] Z. Liu, J.T. Robinson, X. Sun, H. Dai, J. Am. Chem. Soc. 130 (2008) 10876–10877.
[155] Y. Lin, J. Jin, M. Song, J. Mater. Chem. 21 (2011) 3455–3461.
[156] L. Feng, X. Yang, X. Shi, X. Tan, R. Peng, J. Wang, Z. Liu, Small 9 (2013) 1989–1997.
[157] C. Shan, H. Yang, D. Han, Q. Zhang, A. Ivaska, L. Niu, Langmuir 25 (2009) 12030–12033.
[158] M. Li, Y. Wang, Q. Liu, Q. Li, Y. Cheng, Y. Zheng, T. Xi, S. Wei, J. Mater. Chem. B Mater. Biol. Med. 1 (2013) 475–484.
[159] N. Luo, D. Ni, H. Yue, W. Wei, G. Ma, ACS Appl. Mater. Interfaces 7 (2015) 5239–5247.
[160] C. Nie, L. Ma, Y. Xia, C. He, J. Deng, L. Wang, C. Cheng, S. Sun, C. Zhao, J. Membr. Sci. 475 (2015) 455–468.
[161] S.H. Lee, D.R. Dreyer, J. An, A. Velamakanni, R.D. Piner, S. Park, Y. Zhu, S.O. Kim, C.W. Bielawski, R.S. Ruoff, Macromol. Rapid Commun. 31 (2010) 281–288.
[162] L. Kan, Z. Xu, C. Gao, Macromolecules 44 (2011) 444–452.
[163] A. Faghani, I.S. Donskyi, M. Fardin Gholami, B. Ziem, A. Lippitz, W.E. Unger, C. Böttcher, J.P. Rabe, R. Haag, M. Adeli, Angew. Chem. Int. Ed. 56 (2017) 2675–2679.
[164] C. He, Z.-Q. Shi, C. Cheng, H.-Q. Lu, M. Zhou, S.-D. Sun, C.-S. Zhao, Biomater. Sci. 4 (2016) 1431–1440.
[165] C. He, C. Cheng, S.-Q. Nie, L.-R. Wang, C.-X. Nie, S.-D. Sun, C.-S. Zhao, J. Mater. Chem. B Mater. Biol. Med. 4 (2016) 6143–6153.
[166] J.R. Lomeda, C.D. Doyle, D.V. Kosynkin, W.-F. Hwang, J.M. Tour, J. Am. Chem. Soc. 130 (2008) 16201–16206.
[167] L.-H. Liu, M.M. Lerner, M. Yan, Nano Lett. 10 (2010) 3754–3756.
[168] H. Lee, S.M. Dellatore, W.M. Miller, P.B. Messersmith, Science 318 (2007) 426–430.
[169] W. Qiang, A. Katharina, L. Hendrik, S. Andrea, N.P.L. Michael, G. Ingo, H. Rainer, Angew. Chem. Int. Ed. 53 (2014) 11650–11655.
[170] W. Qiang, B. Tobias, N.P.L. Michael, G. Ingo, H. Rainer, Adv. Mater. 26 (2014) 2688–2693.
[171] Z. Zhang, J. Zhang, B. Zhang, J. Tang, Nanoscale 5 (2013) 118–123.
[172] L.Q. Xu, W.J. Yang, K.-G. Neoh, E.-T. Kang, G.D. Fu, Macromolecules 43 (2010) 8336–8339.
[173] L. Yu, C. Cheng, Q. Ran, C. Schlaich, P.-L.M. Noeske, W. Li, Q. Wei, R. Haag, ACS Appl. Mater. Interfaces 9 (2017) 6624–6633.
[174] C. Nie, Y. Yang, C. Cheng, L. Ma, J. Deng, L. Wang, C. Zhao, Acta Biomater. 51 (2017) 479–494.
[175] C. Nie, C. Cheng, Z. Peng, L. Ma, C. He, Y. Xia, C. Zhao, J. Mater. Chem. B Mater. Biol. Med. 4 (2016) 2749–2756.
[176] Z. Jia, Y. Shi, P. Xiong, W. Zhou, Y. Cheng, Y. Zheng, T. Xi, S. Wei, ACS Appl. Mater. Interfaces 8 (2016) 17151–17165.
[177] Z. Fan, J. Wang, Z. Wang, H. Ran, Y. Li, L. Niu, P. Gong, B. Liu, S. Yang, Carbon 66 (2014) 407–416.

[178] S. Li, D. Wu, C. Cheng, J. Wang, F. Zhang, Y. Su, X. Feng, Angew. Chem. Int. Ed. 52 (2013) 12105–12109.
[179] M. Mahmoudi, I. Lynch, M.R. Ejtehadi, M.P. Monopoli, F.B. Bombelli, S. Laurent, Chem. Rev. 111 (2011) 5610–5637.
[180] C.G. Palivan, R. Goers, A. Najer, X. Zhang, A. Car, W. Meier, Chem. Soc. Rev. 45 (2016) 377–411.
[181] C. Marcelo, Q.M. Abdul, S.S. Kumar, H. Rainer, Adv. Mater. 22 (2010) 190–218.
[182] C. Cheng, S. Li, S. Nie, W. Zhao, H. Yang, S. Sun, C. Zhao, Biomacromolecules 13 (2012) 4236–4246.
[183] H. Zhou, C. Cheng, H. Qin, L. Ma, C. He, S. Nie, X. Zhang, Q. Fu, C. Zhao, Polym. Chem. 5 (2014) 3563.
[184] T.H. Nguyen, S.H. Kim, C.G. Decker, D.Y. Wong, J.A. Loo, H.D. Maynard, Nat. Chem. 5 (2013) 221–227.
[185] O. Arlov, F.L. Aachmann, A. Sundan, T. Espevik, G. Skjak-Braek, Biomacromolecules 15 (2014) 2744–2750.
[186] L.R. Wang, H. Qin, S.Q. Nie, S.D. Sun, F. Ran, C.S. Zhao, Acta Biomater. 9 (2013) 8851–8863.
[187] N. Willems, A. Urtizberea, A.F. Verre, M. Iliut, M. Lelimousin, M. Hirtz, A. Vijayaraghavan, M.S.P. Sansom, ACS Nano 11 (2017) 1613–1625.
[188] S.Y. Lee, S.H. Kim, S.M. Kim, H. Lee, G. Lee, S.Y. Park, New J. Chem. 38 (2014) 2225–2228.
[189] J. Liao, Y. Qu, B. Chu, X. Zhang, Z. Qian, Sci. Rep. 5 (2015) 9879.
[190] S. Myung, A. Solanki, C. Kim, J. Park, K.S. Kim, K.-B. Lee, Adv. Mater. 23 (2011) 2221–2225.
[191] W. Zhang, X. Yu, Y. Li, Z. Su, K.D. Jandt, G. Wei, Prog. Polym. Sci. 80 (2018) 94–124.
[192] M. Mahmoudi, O. Akhavan, M. Ghavami, F. Rezaee, S.M.A. Ghiasi, Nanoscale 4 (2012) 7322–7325.
[193] J. Liu, Y. Li, Y. Li, J. Li, Z. Deng, J. Mater. Chem. 20 (2010) 900–906.
[194] S. Mura, J. Nicolas, P. Couvreur, Nat. Mater. 12 (2013) 991–1003.
[195] J. Deng, X. Liu, L. Ma, C. Cheng, S. Sun, C. Zhao, J. Mater. Chem. B Mater. Biol. Med. 4 (2016) 694–703.
[196] F. Dong, I. Firkowska-Boden, M.M.L. Arras, K.D. Jandt, RSC Adv. 7 (2017) 3720–3726.
[197] Y. Tang, H. Hu, M.G. Zhang, J. Song, L. Nie, S. Wang, G. Niu, P. Huang, G. Lu, X. Chen, Nanoscale 7 (2015) 6304–6310.
[198] I. Firkowska-Boden, X. Zhang, K.D. Jandt, Adv. Healthc. Mater. 7 (2017) 1700995.
[199] K. Paek, H. Yang, J. Lee, J. Park, B.J. Kim, ACS Nano 8 (2014) 2848–2856.
[200] L. Feng, K. Li, X. Shi, M. Gao, J. Liu, Z. Liu, Adv. Healthc. Mater. 3 (2014) 1261–1271.
[201] J. Liu, G. Chen, M. Jiang, Macromolecules 44 (2011) 7682–7691.
[202] H. Moon, D. Kumar, H. Kim, C. Sim, J.-H. Chang, J.-M. Kim, H. Kim, D.-K. Lim, ACS Nano 9 (2015) 2711–2719.
[203] H. Huang, W. Bai, C. Dong, R. Guo, Z. Liu, Biosens. Bioelectron. 68 (2015) 442–446.
[204] H. Chen, Y. Li, F. Zhang, G. Zhang, X. Fan, J. Mater. Chem. 21 (2011) 17658–17661.
[205] M. Liu, H. Zhao, S. Chen, H. Yu, X. Quan, ACS Nano 6 (2012) 3142–3151.
[206] Y.-l. Dong, H.-g. Zhang, Z.U. Rahman, L. Su, X.-j. Chen, J. Hu, X.-g. Chen, Nanoscale 4 (2012) 3969–3976.
[207] Y. Cheng, Y. Chang, Y. Feng, N. Liu, X. Sun, Y. Feng, X. Li, H. Zhang, Small 13 (2017) 1603935.
[208] J.W. Jeon, S.Y. Cho, Y.J. Jeong, D.S. Shin, N.R. Kim, Y.S. Yun, H.-T. Kim, S.B. Choi, W.G. Hong, H.J. Kim, H.-J. Jin, B.H. Kim, Adv. Mater. 29 (2017) 1605479.
[209] F. Bonaccorso, A. Bartolotta, J.N. Coleman, C. Backes, Adv. Mater. 28 (2016) 6136–6166.
[210] E.B. Secor, B.Y. Ahn, T.Z. Gao, J.A. Lewis, M.C. Hersam, Adv. Mater. 27 (2015) 6683–6688.
[211] K. Arapov, E. Rubingh, R. Abbel, J. Laven, G. de With, H. Friedrich, Adv. Funct. Mater. 26 (2015) 586–593.
[212] Y.Q. Li, T. Yu, T.Y. Yang, L.X. Zheng, K. Liao, Adv. Mater. 24 (2012) 3426–3431.
[213] M. Wu, J. Chen, Y. Wen, H. Chen, Y. Li, C. Li, G. Shi, ACS Appl. Mater. Interfaces 10 (2018) 5812–5818.
[214] M. Zhang, Y. Wang, L. Huang, Z. Xu, C. Li, G. Shi, Adv. Mater. 27 (2015) 6708–6713.
[215] X. Yang, J. Zhu, L. Qiu, D. Li, Adv. Mater. 23 (2011) 2833–2838.
[216] J. Qiao, J. Di, S. Zhou, K. Jin, S. Zeng, N. Li, S. Fang, Y. Song, M. Li, R.H. Baughman, Q. Li, Small 14 (2018) 1801883.
[217] Y. Wen, M. Wu, M. Zhang, C. Li, G. Shi, Adv. Mater. 29 (2017) 1702831.
[218] M. Zhang, L. Huang, J. Chen, C. Li, G. Shi, Adv. Mater. 26 (2014) 7588–7592.
[219] S. Wan, S. Fang, L. Jiang, Q. Cheng, R.H. Baughman, Adv. Mater. 0 (2018) 1802733.
[220] K. Hu, L.S. Tolentino, D.D. Kulkarni, C. Ye, S. Kumar, V.V. Tsukruk, Angew. Chem. Int. Ed. 52 (2013) 13784–13788.
[221] S. Wan, Q. Zhang, X. Zhou, D. Li, B. Ji, L. Jiang, Q. Cheng, ACS Nano 11 (2017) 7074–7083.
[222] T. Ma, H.L. Gao, H.P. Cong, H.B. Yao, L. Wu, Z.Y. Yu, S.M. Chen, S.H. Yu, Adv. Mater. 30 (2018) 1706435.
[223] I.H. Kim, T. Yun, J.-E. Kim, H. Yu, S.P. Sasikala, K.E. Lee, S.H. Koo, H. Hwang, H.J. Jung, J.Y. Park, H.S. Jeong, S.O. Kim, Adv. Mater. 0 (2018) 1803267.
[224] H.-P. Cong, X.-C. Ren, P. Wang, S.-H. Yu, ACS Nano 6 (2012) 2693–2703.
[225] H. Gao, Y. Sun, J. Zhou, R. Xu, H. Duan, ACS Appl. Mater. Interfaces 5 (2013) 425–432.
[226] Y. Yue, N. Liu, Y. Ma, S. Wang, W. Liu, C. Luo, H. Zhang, F. Cheng, J. Rao, X. Hu, J. Su, Y. Gao, ACS Nano 12 (2018) 4224–4232.
[227] E. Singh, Z. Chen, F. Houshmand, W. Ren, Y. Peles, H.-M. Cheng, N. Koratkar, Small 9 (2012) 75–80.
[228] X. Du, H.-Y. Liu, Y.-W. Mai, ACS Nano 10 (2016) 453–462.
[229] K. Li, Z. Zhang, D. Li, W. Zhang, X. Yu, W. Liu, C. Gong, G. Wei, Z. Su, Adv. Funct. Mater. 28 (2018) 1801056.
[230] Q. Zhang, F. Zhang, S.P. Medarametla, H. Li, C. Zhou, D. Lin, Small 12 (2016) 1702–1708.
[231] C. Zhu, T.Y.-J. Han, E.B. Duoss, A.M. Golobic, J.D. Kuntz, C.M. Spadaccini, M.A. Worsley, Nat. Commun. 6 (2015) 6962.
[232] Y. Jiang, Z. Xu, T. Huang, Y. Liu, F. Guo, J. Xi, W. Gao, C. Gao, Adv. Funct. Mater. 28 (2018) 1707024.
[233] A.E. Jakus, E.B. Secor, A.L. Rutz, S.W. Jordan, M.C. Hersam, R.N. Shah, ACS Nano 9 (2015) 4636–4648.
[234] X. Tang, H. Zhou, Z. Cai, D. Cheng, P. He, P. Xie, D. Zhang, T. Fan, ACS Nano 12 (2018) 3502–3511.
[235] L. Zhang, Z. Wang, C. Xu, Y. Li, J. Gao, W. Wang, Y. Liu, J. Mater. Chem. 21 (2011) 10399–10406.
[236] G. Du, L. Nie, G. Gao, Y. Sun, R. Hou, H. Zhang, T. Chen, J. Fu, ACS Appl. Mater. Interfaces 7 (2015) 3003–3008.
[237] N. Annabi, S.R. Shin, A. Tamayol, M. Miscuglio, M.A. Bakooshli, A. Assmann, P. Mostafalu, J.-Y. Sun, S. Mithieux, L. Cheung, X. Tang, A.S. Weiss, A. Khademhosseini, Adv. Mater. 28 (2016) 40–49.
[238] C. He, Z.-Q. Shi, L. Ma, C. Cheng, C.-X. Nie, M. Zhou, C.-S. Zhao, J. Mater. Chem. B Mater. Biol. Med. 3 (2015) 592–602.
[239] C. He, C. Cheng, H.-F. Ji, Z.-Q. Shi, L. Ma, M. Zhou, C.-S. Zhao, Polym. Chem. 6 (2015) 7893–7901.
[240] J. Wu, A. Chen, M. Qin, R. Huang, G. Zhang, B. Xue, J. Wei, Y. Li, Y. Cao, W. Wang, Nanoscale 7 (2015) 1655–1660.
[241] S.F. Kiew, L.V. Kiew, H.B. Lee, T. Imae, L.Y. Chung, J. Control. Release 226 (2016) 217–228.
[242] G. Lalwani, M. D'Agati, A.M. Khan, B. Sitharaman, Adv. Drug Delivery Rev. 105 (2016) 109–144.
[243] R. Li, L.M. Guiney, C.H. Chang, N.D. Mansukhani, Z. Ji, X. Wang, Y.-P. Liao, W. Jiang, B. Sun, M.C. Hersam, A.E. Nel, T. Xia, ACS Nano 12 (2018) 1390–1402.
[244] A. Sasidharan, L.S. Panchakarla, A.R. Sadanandan, A. Ashokan, P. Chandran, C.M. Girish, D. Menon, S.V. Nair, C.N. Rao, M. Koyakutty, Small 8 (2012) 1251–1263.
[245] L. Kovbasyuk, A. Mokhir, Toxicity studies and biomedical applications of graphene oxide, in: A.M. Dimiev, E. S (Eds.), Graphene Oxide: Fundamentals and Applications, John Wiley & Sons, Ltd, 2016, pp. 364–381.
[246] S.K. Singh, M.K. Singh, M.K. Nayak, S. Kumari, S. Shrivastava, J.J.A. Grácio, D. Dash, ACS Nano 5 (2011) 4987–4996.
[247] H. Zhou, K. Zhao, W. Li, N. Yang, Y. Liu, C. Chen, T. Wei, Biomaterials 33 (2012) 6933–6942.
[248] D.A. Jasim, S. Murphy, L. Newman, A. Mironov, E. Prestat, J. McCaffrey, C. Ménard-Moyon, A.F. Rodrigues, A. Bianco, S. Haigh, R. Lennon, K. Kostarelos, ACS Nano 10 (2016) 10753–10767.
[249] C. Kinnear, T.L. Moore, L. Rodriguez-Lorenzo, B. Rothen-Rutishauser, A. Petri-Fink, Chem. Rev. 117 (2017) 11476–11521.
[250] K.-H. Liao, Y.-S. Lin, C.W. Macosko, C.L. Haynes, ACS Appl. Mater. Interfaces 3 (2011) 2607–2615.
[251] J. Ge, M. Lan, B. Zhou, W. Liu, L. Guo, H. Wang, Q. Jia, G. Niu, X. Huang, H. Zhou, X. Meng, P. Wang, C.-S. Lee, W. Zhang, X. Han, Nat. Commun. 5 (2014) 4596.
[252] S.A. Sydlik, S. Jhunjhunwala, M.J. Webber, D.G. Anderson, R. Langer, ACS Nano 9 (2015) 3866–3874.
[253] X. Wang, P. Li, C. Luedecke, Q. Zhang, Z. Wang, K.D. Jandt, J. Nano Res. 45 (2017) 199–207.
[254] A.R. Rafieerad, A.R. Bushroa, A. Amiri, K. Kalaiselvam, K.M. Vellasamy, J. Vadivelu, J. Hazard. Mater. 360 (2018) 132–140.
[255] Y. Tu, M. Lv, P. Xiu, T. Huynh, M. Zhang, M. Castelli, Z. Liu, Q. Huang, C. Fan, H. Fang, R. Zhou, Nat. Nanotechnol. 8 (2013) 594–601.
[256] F. Perreault, A.F. de Faria, S. Nejati, M. Elimelech, ACS Nano 9 (2015) 7226–7236.
[257] M.-C. Wu, A.R. Deokar, J.-H. Liao, P.-Y. Shih, Y.-C. Ling, ACS Nano 7 (2013) 1281–1290.
[258] Z. Qi, P. Bharate, C.H. Lai, B. Ziem, C. Bottcher, A. Schulz, F. Beckert, B. Hatting, R. Mulhaupt, P.H. Seeberger, R. Haag, Nano Lett. 15 (2015) 6051–6057.
[259] S. Bhatia, L.C. Camacho, R. Haag, J. Am. Chem. Soc. 138 (2016) 8654–8666.
[260] C. Fasting, C.A. Schalley, M. Weber, O. Seitz, S. Hecht, B. Koksch, J. Dernedde, C. Graf, E.W. Knapp, R. Haag, Angew. Chem. Int. Ed. 51 (2012) 10472–10498.
[261] B.N.S. Thota, L.H. Urner, R. Haag, Chem. Rev. 116 (2016) 2079–2102.
[262] Y. Wang, X. Bai, W. Wen, X. Zhang, S. Wang, ACS Appl. Mater. Interfaces 7 (2015) 18872–18879.
[263] J. Wen, W. Li, J. Li, B. Tao, Y. Xu, H. Li, A. Lu, S. Sun, Sens. Actuators B Chem. 227 (2016) 655–659.
[264] Y.N. Chen, Y.H. Hsueh, C.T. Hsieh, D.Y. Tzou, P.L. Chang, Int. J. Environ. Res. Public Health 13 (2016) 430.
[265] M. Sametband, I. Kalt, A. Gedanken, R. Sarid, ACS Appl. Mater. Interfaces 6 (2014) 1228–1235.
[266] Y. Li, H. Yuan, A. von dem Bussche, M. Creighton, R.H. Hurt, A.B. Kane, H. Gao, Proc. Natl. Acad. Sci. U S A 110 (2013) 12295–12300.
[267] J. Mao, R. Guo, L.-T. Yan, Biomaterials 35 (2014) 6069–6077.

[268] H. Pieper, S. Chercheja, S. Eigler, C.E. Halbig, M.R. Filipovic, A. Mokhir, Angew. Chem. Int. Ed. 55 (2016) 405–407.
[269] Q. Mu, G. Su, L. Li, B.O. Gilbertson, L.H. Yu, Q. Zhang, Y.P. Sun, B. Yan, ACS Appl. Mater. Interfaces 4 (2012) 2259–2266.
[270] H.-K. Na, M.-H. Kim, J. Lee, Y.-K. Kim, H. Jang, K.E. Lee, H. Park, W. Do Heo, H. Jeon, I.S. Choi, Y. Lee, D.-H. Min, Nanoscale 5 (2013) 1669–1677.
[271] J. Park, B. Kim, J. Han, J. Oh, S. Park, S. Ryu, S. Jung, J.-Y. Shin, B.S. Lee, B.H. Hong, D. Choi, B.-S. Kim, ACS Nano 9 (2015) 4987–4999.
[272] Q. Tu, L. Pang, Y. Chen, Y. Zhang, R. Zhang, B. Lu, J. Wang, Analyst 139 (2014) 105–115.
[273] J. Park, Y.S. Kim, S. Ryu, W.S. Kang, S. Park, J. Han, H.C. Jeong, B.H. Hong, Y. Ahn, B.-S. Kim, Adv. Funct. Mater. 25 (2015) 2590–2600.
[274] P. Ertl, D. Sticker, V. Charwat, C. Kasper, G. Lepperdinger, Trends Biotechnol. 32 (2014) 245–253.
[275] X. Ding, H. Liu, Y. Fan, Adv. Healthc. Mater. 4 (2015) 1451–1468.
[276] T.R. Nayak, H. Andersen, V.S. Makam, C. Khaw, S. Bae, X. Xu, P.L. Ee, J.H. Ahn, B.H. Hong, G. Pastorin, B. Ozyilmaz, ACS Nano 5 (2011) 4670–4678.
[277] S.Y. Park, J. Park, S.H. Sim, M.G. Sung, K.S. Kim, B.H. Hong, S. Hong, Adv. Mater. 23 (2011) H263–H267.
[278] Z. Zhang, L.H. Klausen, M. Chen, M. Dong, Small 14 (2018) 1801983.
[279] O. Akhavan, E. Ghaderi, Nanoscale 5 (2013) 10316–10326.
[280] O. Akhavan, E. Ghaderi, J. Mater. Chem. B Mater. Biol. Med. 1 (2013) 6291–6301.
[281] O. Akhavan, E. Ghaderi, J. Mater. Chem. B Mater. Biol. Med. 2 (2014) 5602–5611.
[282] Z. Zhang, R. Xu, Z. Wang, M. Dong, B. Cui, M. Chen, ACS Appl. Mater. Interfaces 9 (2017) 34736–34743.
[283] O. Akhavan, E. Ghaderi, Small 9 (2013) 3593–3601.
[284] C.X. Guo, S.R. Ng, S.Y. Khoo, X. Zheng, P. Chen, C.M. Li, ACS Nano 6 (2012) 6944–6951.
[285] Y. Lee, J.W. Bae, T.T. Hoang Thi, K.M. Park, K.D. Park, Chem. Commun. (Camb.) 51 (2015) 8876–8879.
[286] C. Cha, S.R. Shin, X. Gao, N. Annabi, M.R. Dokmeci, X.S. Tang, A. Khademhosseini, Small 10 (2014) 514–523.
[287] S.R. Shin, B. Aghaei-Ghareh-Bolagh, X. Gao, M. Nikkhah, S.M. Jung, A. Dolatshahi-Pirouz, S.B. Kim, S.M. Kim, M.R. Dokmeci, X. Tang, A. Khademhosseini, Adv. Funct. Mater. 24 (2014) 6136–6144.
[288] S.R. Shin, B. Aghaei-Ghareh-Bolagh, T.T. Dang, S.N. Topkaya, X. Gao, S.Y. Yang, S.M. Jung, J.H. Oh, M.R. Dokmeci, X.S. Tang, Adv. Mater. 25 (2013) 6385–6391.
[289] Y. Liu, B. Gao, Z. Qiao, Y. Hu, W. Zheng, L. Zhang, Y. Zhou, G. Ji, G. Yang, Chem. Mater. 27 (2015) 4319–4327.
[290] Z.-Q. Feng, T. Wang, B. Zhao, J. Li, L. Jin, Adv. Mater. 27 (2015) 6462–6468.
[291] X. Wu, F. Tian, W. Wang, J. Chen, M. Wu, J.X. Zhao, J. Mater. Chem. C Mater. Opt. Electron. Devices 1 (2013) 4676–4684.
[292] Z. Chen, Z. Li, J. Wang, E. Ju, L. Zhou, J. Ren, X. Qu, Adv. Funct. Mater. 24 (2014) 522–529.
[293] X. Yang, G. Niu, X. Cao, Y. Wen, R. Xiang, H. Duan, Y. Chen, J. Mater. Chem. 22 (2012) 6649–6654.
[294] S.H. Hu, Y.W. Chen, W.T. Hung, I.W. Chen, S.Y. Chen, Adv. Mater. 24 (2012) 1748–1754.
[295] T. Tian, X. Shi, L. Cheng, Y. Luo, Z. Dong, H. Gong, L. Xu, Z. Zhong, R. Peng, Z. Liu, ACS Appl. Mater. Interfaces 6 (2014) 8542–8548.
[296] H.-W. Yang, M.-Y. Hua, T.-L. Hwang, K.-J. Lin, C.-Y. Huang, R.-Y. Tsai, C.-C.M. Ma, P.-H. Hsu, S.-P. Wey, P.-W. Hsu, P.-Y. Chen, Y.-C. Huang, Y.-J. Lu, T.-C. Yen, L.-Y. Feng, C.-W. Lin, H.-L. Liu, K.-C. Wei, Adv. Mater. 25 (2013) 3605–3611.
[297] G. Gollavelli, Y.-C. Ling, Biomaterials 35 (2014) 4499–4507.
[298] P. Huang, C. Xu, J. Lin, C. Wang, X. Wang, C. Zhang, X. Zhou, S. Guo, D. Cui, Theranostics 1 (2011) 240.
[299] D. Zhang, L. Wen, R. Huang, H. Wang, X. Hu, D. Xing, Biomaterials 153 (2018) 14–26.
[300] A. Sahu, W.I. Choi, J.H. Lee, G. Tae, Biomaterials 34 (2013) 6239–6248.
[301] S. Kang, J.B. Park, T.-J. Lee, S. Ryu, S.H. Bhang, W.-G. La, M.-K. Noh, B.H. Hong, B.-S. Kim, Carbon 83 (2015) 162–172.
[302] W. Huiyun, D. Chunyan, D. Haiqing, S. Aijun, X. Wenjuan, C. Xiaojun, S. Yanyan, L. Xuequan, L. Yongyong, S. Donglu, Small 8 (2012) 760–769.
[303] C.L. Weaver, J.M. LaRosa, X. Luo, X.T. Cui, ACS Nano 8 (2014) 1834–1843.
[304] J. Saleem, L. Wang, C. Chen, Adv. Healthc. Mater. 0 (2018) 1800525.
[305] K. Yang, S. Zhang, G. Zhang, X. Sun, S.-T. Lee, Z. Liu, Nano Lett. 10 (2010) 3318–3323.
[306] J. Li, Y. Hu, J. Yang, P. Wei, W. Sun, M. Shen, G. Zhang, X. Shi, Biomaterials 38 (2015) 10–21.
[307] J. Song, X. Yang, O. Jacobson, P. Huang, X. Sun, L. Lin, X. Yan, G. Niu, Q. Ma, X. Chen, Adv. Mater. 27 (2015) 4910–4917.
[308] X. Huang, S. Tang, B. Liu, B. Ren, N. Zheng, Adv. Mater. 23 (2011) 3420–3425.
[309] Y. Lyu, Y. Fang, Q. Miao, X. Zhen, D. Ding, K. Pu, ACS Nano 10 (2016) 4472–4481.
[310] Z. Sheng, D. Hu, M. Zheng, P. Zhao, H. Liu, D. Gao, P. Gong, G. Gao, P. Zhang, Y. Ma, L. Cai, ACS Nano 8 (2014) 12310–12322.
[311] J. Yang, J. Choi, D. Bang, E. Kim, E.-K. Lim, H. Park, J.-S. Suh, K. Lee, K.-H. Yoo, E.-K. Kim, Y.-M. Huh, S. Haam, Angew. Chem. Int. Ed. 50 (2010) 441–444.
[312] Z. Zha, X. Yue, Q. Ren, Z. Dai, Adv. Mater. 25 (2012) 777–782.
[313] H.K. Moon, S.H. Lee, H.C. Choi, ACS Nano 3 (2009) 3707–3713.
[314] H.S. Jung, W.H. Kong, D.K. Sung, M.-Y. Lee, S.E. Beack, D.H. Keum, K.S. Kim, S.H. Yun, S.K. Hahn, ACS Nano 8 (2014) 260–268.
[315] J. Song, X. Yang, O. Jacobson, L. Lin, P. Huang, G. Niu, Q. Ma, X. Chen, ACS Nano 9 (2015) 9199–9209.
[316] M. Zhang, W. Wang, F. Wu, K. Graveran, J. Zhang, C. Wu, Chem. Eur. J. 24 (2018) 12890–12901.
[317] Q. Liu, B. Guo, Z. Rao, B. Zhang, J.R. Gong, Nano Lett. 13 (2013) 2436–2441.
[318] P. Roy, P.-C. Chen, A.P. Periasamy, Y.-N. Chen, H.-T. Chang, Mater. Today 18 (2015) 447–458.
[319] S. Gao, L. Zhang, G. Wang, K. Yang, M. Chen, R. Tian, Q. Ma, L. Zhu, Biomaterials 79 (2016) 36–45.
[320] Y. Kai, H. Lilei, M. Xingxing, Y. Shuoqi, C. Liang, S. Xiaoze, L. Changhui, L. Yonggang, L. Zhuang, Adv. Mater. 24 (2012) 1868–1872.
[321] W. Chen, P. Yi, Y. Zhang, L. Zhang, Z. Deng, Z. Zhang, ACS Appl. Mater. Interfaces 3 (2011) 4085–4091.
[322] S. Panda, T.K. Rout, A.D. Prusty, P.M. Ajayan, S. Nayak, Adv. Mater. 30 (2018) 1702149.
[323] W.-S. Kuo, H.-H. Chen, S.-Y. Chen, C.-Y. Chang, P.-C. Chen, Y.-I. Hou, Y.-T. Shao, H.-F. Kao, C.-L. Lilian Hsu, Y.-C. Chen, S.-J. Chen, S.-R. Wu, J.-Y. Wang, Biomaterials 120 (2017) 185–194.
[324] H. Sun, N. Gao, K. Dong, J. Ren, X. Qu, ACS Nano 8 (2014) 6202–6210.
[325] H.E. Karahan, C. Wiraja, C. Xu, J. Wei, Y. Wang, L. Wang, F. Liu, Y. Chen, Adv. Healthc. Mater. 7 (2018) 1701406.
[326] Z. Song, X. Wang, G. Zhu, Q. Nian, H. Zhou, D. Yang, C. Qin, R. Tang, Small 11 (2015) 1171–1176.
[327] X.X. Yang, C.M. Li, Y.F. Li, J. Wang, C.Z. Huang, Nanoscale 9 (2017) 16086–16092.
[328] B. Ziem, W. Azab, M.F. Gholami, J.P. Rabe, N. Osterrieder, R. Haag, Nanoscale 9 (2017) 3774–3783.
[329] C. Cheng, S. Li, Y. Xia, L. Ma, C. Nie, C. Roth, A. Thomas, R. Haag, Adv. Mater. 30 (2018) 1802669.
[330] A. Solanki, S.T. Chueng, P.T. Yin, R. Kappera, M. Chhowalla, K.B. Lee, Adv. Mater. 25 (2013) 5477–5482.
[331] O. Akhavan, E. Ghaderi, E. Abouei, S. Hatamie, E. Ghasemi, Carbon 66 (2014) 395–406.
[332] W. Guo, X. Zhang, X. Yu, S. Wang, J. Qiu, W. Tang, L. Li, H. Liu, Z.L. Wang, ACS Nano 10 (2016) 5086–5095.
[333] S.R. Das, M. Uz, S. Ding, M.T. Lentner, J.A. Hondred, A.A. Cargill, D.S. Sakaguchi, S. Mallapragada, J.C. Claussen, Adv. Healthc. Mater. 6 (2017) 1601087.
[334] K.-T. Lim, H. Seonwoo, K.S. Choi, H. Jin, K.-J. Jang, J. Kim, J.-W. Kim, S.Y. Kim, P.-H. Choung, J.H. Chung, Adv. Healthc. Mater. 5 (2016) 2069–2079.
[335] J. Lu, Y.-S. He, C. Cheng, Y. Wang, L. Qiu, D. Li, D. Zou, Adv. Funct. Mater. 23 (2013) 3494–3502.
[336] X. Zhou, M. Nowicki, H. Cui, W. Zhu, X. Fang, S. Miao, S.-J. Lee, M. Keidar, L.G. Zhang, Carbon 116 (2017) 615–624.
[337] S.K. Misra, F. Ostadhossein, R. Babu, J. Kus, D. Tankasala, A. Sutrisno, K.A. Walsh, C.R. Bromfield, D. Pan, Adv. Healthc. Mater. 6 (2017) 1700008.
[338] Y. Yang, W. Gao, Chem. Soc. Rev. (2019), http://dx.doi.org/10.1039/C7CS00730B.
[339] P. Wang, Z. Peng, M. Li, Y. Wang, Small 14 (2018) 1802625.
[340] J.A. Rogers, M.G. Lagally, R.G. Nuzzo, Nature 477 (2011) 45.
[341] Y. Ma, P.M. Ajayan, S. Yang, Y. Gong, Small 14 (2018) 1801606.
[342] N. Karim, S. Afroj, S. Tan, P. He, A. Fernando, C. Carr, K.S. Novoselov, ACS Nano 11 (2017) 12266–12275.
[343] G. Wu, P.F. Tan, X.J. Wu, L. Peng, H.Y. Cheng, C.F. Wang, W. Chen, Z.Y. Yu, S. Chen, Adv. Funct. Mater. 27 (2017) 1702493.
[344] L. Liu, Y. Yu, C. Yan, K. Li, Z. Zheng, Nat. Commun. 6 (2015) 7260.
[345] M.S. Mannoor, H. Tao, J.D. Clayton, A. Sengupta, D.L. Kaplan, R.R. Naik, N. Verma, F.G. Omenetto, M.C. McAlpine, Nat. Commun. 3 (2012) 763.
[346] D. Kuzum, H. Takano, E. Shim, J.C. Reed, H. Juul, A.G. Richardson, J. de Vries, H. Bink, M.A. Dichter, T.H. Lucas, D.A. Coulter, E. Cubukcu, B. Litt, Nat. Commun. 5 (2014) 5259.
[347] S. Kabiri Ameri, R. Ho, H. Jang, L. Tao, Y. Wang, L. Wang, D.M. Schnyer, D. Akinwande, N. Lu, ACS Nano 11 (2017) 7634–7641.
[348] H. Lee, T.K. Choi, Y.B. Lee, H.R. Cho, R. Ghaffari, L. Wang, H.J. Choi, T.D. Chung, N. Lu, T. Hyeon, Nat. Nanotechnol. 11 (2016) 566.
[349] Y. Chen, S. Lu, S. Zhang, Y. Li, Z. Qu, Y. Chen, B. Lu, X. Wang, X. Feng, Sci. Adv. 3 (2017) e1701629.
[350] R. Yin, Z. Xu, M. Mei, Z. Chen, K. Wang, Y. Liu, T. Tang, M.K. Priydarshi, X. Meng, S. Zhao, B. Deng, H. Peng, Z. Liu, X. Duan, Nat. Commun. 9 (2018) 2334.
[351] J. Kim, M. Kim, M.-S. Lee, K. Kim, S. Ji, Y.-T. Kim, J. Park, K. Na, K.-H. Bae, H. Kyun Kim, F. Bien, C. Young Lee, J.-U. Park, Nat. Commun. 8 (2017) 14997.
[352] J.E. Moses, A.D. Moorhouse, Chem. Soc. Rev. 36 (2007) 1249–1262.
[353] J.M. Baskin, J.A. Prescher, S.T. Laughlin, N.J. Agard, P.V. Chang, I.A. Miller, A. Lo, J.A. Codelli, C.R. Bertozzi, Proc. Natl. Acad. Sci. U S A 104 (2007) 16793–16797.
[354] A.P. Blum, J.K. Kammeyer, A.M. Rush, C.E. Callmann, M.E. Hahn, N.C. Gianneschi, J. Am. Chem. Soc. 137 (2015) 2140–2154.
[355] T. Maeda, H. Otsuka, A. Takahara, Prog. Polym. Sci. 34 (2009) 581–604.
[356] X. Du, J. Li, A. Welle, L. Li, W. Feng, P.A. Levkin, Adv. Mater. 27 (2015) 4997–5001.
[357] Z. He, J. Zhou, X. Lu, B. Corry, ACS Nano 7 (2013) 10148–10157.
[358] A.R. Studart, Angew. Chem. Int. Ed. 54 (2015) 3400–3416.
[359] Z. Zhang, X. Zhang, X. Xu, Y. Li, Y. Li, D. Zhong, Y. He, Z. Gu, Adv. Funct. Mater. 25 (2015) 5250–5260.

Chuanxiong Nie received his B.S. and M.Sc. degree in College of Polymer Science and Engineering, Sichuan University, China, under the supervision of Prof. Changsheng Zhao in 2017. Afterwards, he has been doing PhD study at the group of Prof. Rainer Haag in Department of Chemistry, Freie Universität Berlin, Germany. His research interests cover the synthesis of functional carbon and 2D nanomaterials for biological applications, including anticoagulant materials, antibacterial materials, virus inhibitors and tissue regeneration scaffolds.

Lang Ma obtained his B.S. and Ph.D. degrees from College of Polymer Science and Engineering, Sichuan University, China in 2012 and 2016, respectively. He has been doing postdoctoral research work at West China Hospital, Sichuan University, China since 2016. His current research interests include the design and fabrication of biopolymers functionalized nanomedical materials and their applications in diagnosis and therapies for the biomedical field, such as wound healing, skin tumor, and rheumatoid arthritis.

Shuang Li is currently a postdoc in functional materials at Technische Universität Berlin. She received her Master's degree at Shanghai Jiao Tong University in 2013 under the supervision of Prof. Yuezeng Su and Prof. Xinliang Feng. During Master period, she took part in the ERC grant 2DMATER at the Max Planck Institute for Polymer Research in Mainz in 2013. After a research scholar from 2014 at University of Michigan, Ann Arbor in the group of Prof. Nicolas A. Kotov, she started her Ph.D studies in the group of Prof. Arne Thomas in 2015 at Technische Universität Berlin. Her current research focuses on synthesis of porous carbon and graphene based nanocomposites from coordination polymers and their applications as advanced electrode materials.

Xin Fan was born in Fujian, China, in 1994. He received his B.S. degrees from Hefei University of Technology, China in 2016. After graduation, he joined the group of Prof. Changsheng Zhao in College of Polymer Science and Engineering, Sichuan University, China for his Master degree. His research mainly focuses on the design and fabrication of functional 2D carbon nanomaterials with augmented anti-infective and bacterial eradication capabilities.

Ye Yang was born in Nantong, China in 1994. He received his B.S. degree at College of Polymer Science and Engineering, Sichuan University, China in 2017. After graduation, he joined the group of Prof. Changsheng Zhao in College of Polymer Science and Engineering, Sichuan University, China for his Mater degree. His research focuses on stimuli-responsive carbon nanomaterials and their applications in biomedical field.

Chong Cheng is currently a subgroup leader for advanced 2D materials in Department of Chemistry, Freie Universität Berlin, and he has just been appointed as a full professor in Sichuan University. He received his Ph.D in 2015 for polymer science and biomedical researches from Sichuan University, China. After a research stay (2013-2015) for carbon nanomaterials at University of Michigan, Ann Arbor, USA, he joined the group of Prof. Rainer Haag in Freie Universität Berlin as a DRS POINT and an AvH research fellow from 2015. His current scientific interests include low-dimensional carbon nanomaterials for nanomedicines, stem cell scaffolds, bioelectronics, catalysts and energy-related applications.

Weifeng Zhao received his B.S. and Ph.D degrees in Biomedical Engineering from Sichuan University in 2009 and 2014, respectively. He received another Ph.D degree in Fibre and Polymer Science at KTH Royal Institute Technology in 2015 with Prof. Ann-Christine Albertsson. Afterward, he joined College of Polymer Science and Engineering, Sichuan University as an associate professor since 2016. His research interests are mostly focused on the development of bioactive and blood-compatible polymers, multifunctional hydrogels, and environmental sensitive biomaterials.

Changsheng Zhao obtained the Ph.D degree in Biomedical Engineering from Sichuan University, China, in 1998. From 2001 to 2003, he was doing the research work in Hokkaido University (Japan) as a postdoctoral research fellow. Currently, he is the Chair and Leading Professor at Department of Biomedical Engineering in Sichuan University. His research interests focused on the development of environmental sensitive, blood compatible and biological active polymers, and the regarding functional membranes, polymer-nanomaterial composites and biomimetic nanosystems for applications in biomedical fields.